DISSERTATION FOR THE DEGREE OF DOCTOR OF PHILOSOPHY (PHD)

Characterization of scorpion peptide toxins that target voltage-gated potassium channels

by Kashmala Shakeel

UNIVERSITY OF DEBRECEN
DOCTORAL SCHOOL OF MOLECULAR MEDICINE

DEBRECEN, 2025

DISSERTATION FOR THE DEGREE OF DOCTOR OF PHILOSOPHY (PHD)

Characterization of scorpion peptide toxins that target voltage-gated potassium channels

by Kashmala Shakeel

Supervisor: Prof. György Panyi

UNIVERSITY OF DEBRECEN
DOCTORAL SCHOOL OF MOLECULAR MEDICINE

DEBRECEN, 2025

TABLE OF CONTENTS

LIST OF ABBREVIATIONS

AIS: Axon initial segment

BBB: Blood-brain barrier

BLASTP: Basic Local Alignment Search Tool for Proteins

BSA: Bovine serum albumin

CaM: Calmodulin

CHO: Chinese hamster ovary

ChTx: Charybdotoxin

CNS: Central nervous system

CPPs: Cell-penetrating peptides

CRAC: Calcium release-activated channel

DMEM: Dulbecco's Modified Eagle Medium

EE: Epileptic encephalopathy

FBS: Fetal bovine serum

FUS: Focused ultrasound

GFP: Green fluorescent protein

GOF: Gain of function

HEK: Human embryonic kidney

HgTx-1: Hongotoxin-1

HPLC: High-performance liquid chromatography

ICV: Intracerebroventricular

ID: Intellectual disability/global developmental delay

IEC: Ion exchange chromatography

K_d: Dissociation constant

KCa: Calcium-activated potassium ion channel

Kv: Voltage-gated potassium ion channel

KTxs: Potassium channel inhibitor toxins

LOF: Loss of function

MAFFT: Multiple alignment using fast Fourier transform

MgTx: Margatoxin

MS: Multiple sclerosis

MTfp: Melanotransferrin protein

MW: Molecular weight

Nav: Voltage-gated sodium channel

PBMC: Peripheral blood mononuclear cell

PD: Parkinson's disease

PHA: Phytohemagglutinin A

RA: Rheumatoid arthritis

RCF: Remaining current fraction

SEM: Standard error of the mean

SKCa: Small conductance calcium-activated K^+ channels

T1: Tetramerization Domain 1

TIDM: Type-1 diabetes mellitus

TEA^+: Tetraethylammonium ion,

TM: Transmembrane

4-AP: 4-Aminopyridine

1. PREFACE

Potassium ion channels are present in cell membrane, allow the passage of K^+ ions in and out of cell and regulate diverse physiological functions in both excitable and non-excitable cells. The voltage-gated potassium Kv1.2 ion channel is widely localized in the CNS and plays a crucial role in maintaining neuronal excitability, synaptic function and the generation of action potential. *KCNA2* gene encodes Kv1.2 channel. A decade ago, *de novo* mutations in *KCNA2* gene were identified in patients with epileptic encephalopathy (EE), a severe neurological disorder characterized with seizures, intellectual and development disability in patients. The mutations caused gain of function (GOF) of the channel activity which corresponds to the progression of EE. Emerging evidence demonstrates that inhibiting Kv1.2 ion channels could be a potential approach to cure Kv1.2 GOF related channelopathies.

Scorpion venom contains a complex mixture of peptide toxins which can modulate the Kv channel currents. A few peptide toxins have been derived from scorpion venom which inhibit Kv1.2 with pico-nanomolar affinity for example, Margatoxin (MgTx, K_d = 6 pM),) and Hongotoxin-1 (HgTx-1, K_d = 170 pM) though selectivity is a major hindrance in the utilization of these peptides as these toxins also impede Kv1.3 with similar potencies (11 pM and 86 pM, respectively). The high affinity of peptide toxins makes them an attractive candidate to be utilized for drug development. In general toxins that target K^+ channels are composed of 23 to 40 amino acid residues and share a common structural framework (an α-helix and β-sheet) stabilized by 3 to 4 disulfide bridges. A typical feature called functional dyad is present, usually consisting of lysine and tyrosine where lysine is essential for blocking the current as it protrudes into the selectivity filter of the ion channel. The diverse features of toxins encourage the exploration of scorpion venoms from different geographic regions to identify high potency inhibitor for Kv1.2 ion channel.

In this work, to pursuit the quest for Kv1.2 potent inhibitor, we describe the pharmacological characterization of seven novel peptide toxins isolated from the venom of scorpion *Centruroides bonito*, two new toxins from venom of *Centruroides villegasi* and a peptide toxin isolated from *Centruroides* margaritas. We further extended our studies by investigating the mechanism of block and the binding kinetics of the potential Kv1.2 inhibitors.

2. INTRODUCTION

2.1 Ion channels

Ion channels are integral membrane proteins, made up of multiple subunits that form a hydrophilic pore, enabling specific inorganic ions to pass through the plasma membrane according to their electrochemical gradients. Ion channels are efficient transporters with a transfer rate of one million ions/second [1]. They are essential for cellular functions such as regulating membrane potential, muscle excitation, action potential generation, maintaining cell shape and volume, sensory transduction, blood pressure control, hormone secretion, and more [2]. Apart from plasma membrane, they also exists in intracellular organelle membranes, including mitochondria, lysosomes, the nucleus, vesicles, and the endoplasmic/sarcoplasmic reticulum [3, 4]. Ion channels exhibit ion selectivity, allowing certain inorganic ions to pass while restricting others and contain a selectivity filter that aids in limiting the passage of ions. The classification of ion channels is done based on: their ion selectivity (K^+, Na^+, H^+, Cl^- etc.), gating mechanisms (such as voltage, signal, ligand, etc.), and the direction of ionic current (outward-, inward- or non-rectifier) [5]. From a functional point of view, ion channels can be in two states depending on whether the pore is permeable to ions or not, i.e. they are present in a conducting state (open) and a non-conducting state (closed or inactivated) [6].

2.1.1 Potassium ion channels

Potassium ion channels are the biggest family and most widely distributed family of ion channels. They are multimers of alpha (α) subunits with a conserved pore loop (P) containing the selectivity filter (SF), enabling selective K^+ transport. Despite this shared core, their sensing domains vary significantly, allowing gating in response to diverse signals. K^+ channels are classified into five distinct categories based on the similarity of their amino acid sequences and the number of transmembrane alpha helices (TMs) within each α-subunit, varying from 2, 4, 6 or 7, as shown in Fig. 1. [7, 8]. (i) The inward rectifier K^+ channels (Kir) are formed through the tetramerization of individual subunits where each subunit is comprised of two transmembrane (TM) segments (denominated by S1 and S2) with a pore loop (P) in the middle of two segments. The four pore loops from the tetrameric assembly together create a single functional pore. They are further categorized into 7 subfamilies (Kir1–7) and are encoded by 15 distinct genes [7, 9]. (ii) K2P channels are made up by the dimerization of two subunits where each subunit is composed of 4TM and two pore loops. The first pore loop (P1) exists

between S1-S2, and the second pore loop (P2) is between S3-S4. They are also termed as leak or background channels and are encoded by 15 genes [10, 11]. (iii) Voltage-gated potassium channels (Kv) where each α-subunit has six TM (S1-S6) and one pore loop between S5 and S6. Segment S1-S4 make up the voltage sensing domain (VSD) with S4 rich in positively charged residues and S5-S6 make up the pore domain (PD). The whole functional channel is made by the tetramerization of four α-subunits. Kv channels is the largest family with >32 known genes and classified into several subfamilies as discussed in next section 2.1.2. [6, 12]. (iv) Small conductance calcium (Ca^{2+}) -activated K^+ channels (SKCa), also composed of six TM segments (S1-S6), however, unlike Kv channels S4 segment contains two arginines only, making this subfamily voltage-insensitive. These channels are regulated by the concentration of the intracellular free calcium and are classified into two subgroups KCa2.x and KCa3.1 as discussed in detail in section 2.1.3 [13, 14]. (v) Voltage- and Ca^{2+}-activated big-conductance (BK, Slo) channel family has four members; Slo1, Slo2.1, Slo2.2 and Slo3. These also have six TM segments (S1-S6) except Slo1 and Slo3 which have an additional S0 segment with extracellular N-terminus, making a total of 7TM segments with 1P between S5-S6 [15]. Like Kv channel family, S4 in VSD of BK channels has multiple positively charged residues.

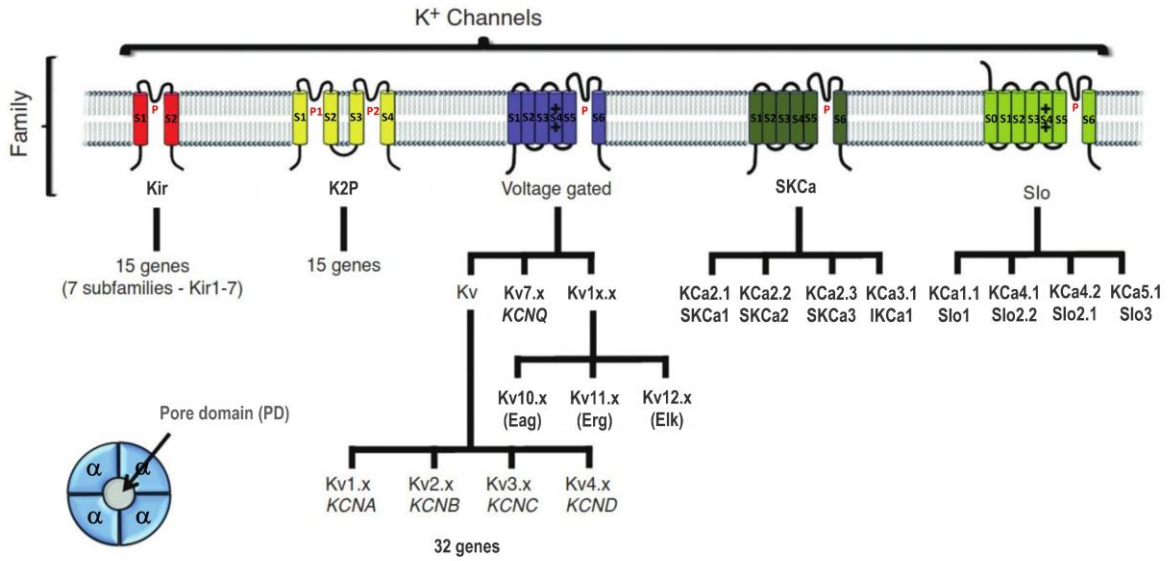

Figure 1: **Potassium channel families classification based on their subunit composition** [7]. Kir: Inward rectifier K^+ channels (2TM and 1P); K2P: Background or leak K^+ channel (4TM and 2P); Voltage-gated K^+ channels (6TM and 1P); SKCa: Ca^{2+}-activated K^+ channels (6M and 1P); and Slo: Voltage- and Ca^{2+}-gated K^+ channels (6 or 7 TM and 1P). The inset (on the left bottom) represents how four α-subunits assemble into a tetramer that forms a functional K^+-conducting pore.

2.1.2 Voltage-gated potassium channels (Kv)

Kv channels is the largest, evolutionary conseved and diverse family in the potassium channel group, possessing high K^+ selectivity. As mentioned briefly above, Kv channels are formed by the assembling of four α-subunits which are arranged in circumference to form a VSD from the first 4 helices (S1-S4) and a central pore domain (PD) from S5-S6 helices with connecting pore loop of each α-subunit of tetramer. The PD is responsible for conduction of K^+ ions (Fig. 1.) [16]. Kv channels are encoded by 40 genes in humans and are divided into 12 subfamilies (Kv1–Kv12) [7]. Each subfamily exhibits significant diversity due to variations in subunit composition, associated beta subunits, regulatory modifiers, and post-translational modifications [17]. Based on the conduction Kv channels are divided into two groups: (i) the conductive group which includes; Kv1.x–Kv4.x (*KCNA* to *KCND*), Kv7.x (*KCNQ*), Kv10.x (Eag), Kv11.x (Erg), and Kv12.x (Elk) subfamilies; and (ii) the non-conductive group, which functions as gating modulators and includes Kv5 (*KCNF*), Kv6 (*KCNG*), Kv8 (*KCNV*), and Kv9 (*KCNS*) subfamilies [7]. Based on their biophysical properties of conductive group, we distinguish between slow or non-inactivating channels called as delayed rectifiers (Kv1.1, Kv1.2, Kv1.3, Kv1.5, Kv1.6, Kv1.7, Kv1.8, Kv2.x and Kv7.x) and rapidly inactivating channels that create type A currents (Kv1.4, Kv3.3, Kv3.4, Kv4.1, Kv4.2 and Kv4.3) [12, 18]. Moreover, several other factors also contribute in the functional diversity of Kv channels; 1) expression of subsets of Kv genes in different cell types, 2) heteromultimerization of members of same subfamily or with the silent subunits of the Kv family and 3) interactions with accessory β-subunits [17, 18].

The Kv1 is a Shaker-related family of K^+ channels and composed of 8 members Kv1.1–Kv1.8. The Kv1 family have characteristic low threshold voltage-gated K^+ currents which are ideal for regulating the duration of frequency of action potential, excitability of neurons, maintaining the pattern and timing of neuron spikes and synaptic and axonal transmissions [6, 19, 20]. Kv1 ion channels are widely localized in brain and the diversity and complexity arises due to the formation of heterotetrametric channels which leads to distinct functional features of ion channels [21, 22]. Kv1.2/Kv1.6 heterotetramers present in somatodendritic region and play a key role in regulating action potential whereas, in hippocampal pyramidal neurons Kv1.1/Kv1.2 heteromeric channels exist and are involved in integrating synaptic inputs [23]. Table 1 summarizes the expression, function and involvement in channelopathies of all Kv channels studied in this work.

Table 1: **Functional role and disease relevance of different channels involved in this study**

Channel	Gene	Expression and function	Involvement in channelopathy
Kv1.1	*KCNA1*	Kv1.1 express in CNS (hippocampus, cerebellum, neocortex) kidney and heart. It plays a major role in nerve signaling and regulating neuronal excitability in CNS [24]	Missense mutations in *KCNA1* gene lead to neurological disorders such as episodic ataxia and a rare genetic disorder primary hypomagnesemia. [25]
Kv1.2	*KCNA2*	Majorly distributed in CNS (axons, neurons, and presynaptic sites), β-pancreatic cells and smooth muscles. Kv1.2 is involved in maintaining the membrane potential neuronal excitability [26]	Mutations in *the KCNA2* gene lead to gain and loss of function of Kv1.2 ion channels which are related to epileptic encephalopathy [27, 28]
Kv1.3	*KCNA3*	Primarily expressed in the immune and central nervous systems, with additional presence in lymphocytes, microglia, lungs, and spleen. It is vital for the activation of T lymphocytes and microglia thus plays role in the development of immunity [29, 30]	Upregulation of Kv1.3 caused autoimmune diseases such as psoriasis, type I diabetes mellitus and arthritis [31, 32] and plays a role in development of neurodegenerative disorders such as Parkinson's diseases and Alzheimer's disease [33, 34]
Kv1.5	*KCNA5*	Mainly express in pulmonary arteries, aorta, smooth muscle cells, and brain tissue responsible for underlying the cardiac ultra-rapid delayed rectifier currents (IKur) in humans [35].	Mutations in *KCNA5* gene caused loss of function of Kv1.5 ion channel and is a novel genetic causes for atrial fibrillation [36]
Kv11.1	*KCNH2*	Kv11.1 is widely distributed in heart, neuroblastoma, brain, liver, lung, ovary and testis. It plays a vital role in the repolarization of cardiac action potentials due to its unique kinetics [37]	Mutations in Kv11.1 causes Type 2 long QT syndrome (LQTS type2) as deficiency of Kv11.1 decreases the repolarization and increases the ventricular fibrillation leading to sudden death [38, 39]

2.1.3 Ca^{2+}-activated potassium channels (KCa)

Ca^{2+}-activated K^+ channels (KCa) are activated by a rise in the intracellular calcium levels. They are categorized into two groups; the first group contains small- and intermediate-conductance K^+ channels also called SKCa, respectively, whereas the second group contains the large conductance channels also known as Slo (BK) (Fig. 1.) [7, 14]. The unitary potassium conductance of SKCa channels is 10-40 pS, and in contrast, Slo channels have high conductance ranges between 200-300 pS [40, 41].

The SKCa channel family consists of two subfamilies KCa2.x and IKCa1. The first subfamily (KCa2) has three subtypes; KCa2.1 (SKCa1), KCa2.2 (SKCa2), and KCa2.3 (SKCa3) and are encoded by encoded by *KCNN1*, *KCNN2* and *KCNN3* genes, respectively [7]. These channels share a high degree of similarity in their transmembrane domains ranging from 80% to 90% but differ significantly in their N- and C-terminal regions. KCa2 channels are predominantly found in the nervous system and therefore, mainly contribute in the regulation of neuronal excitability [40, 42]. In contrast, the IKCa1 subfamily includes a single member, KCa3.1 and is encoded by *KCNN4* gene. KCa3.1 channels are majorly express in lymphocytes, red blood cells, smooth muscle and fibroblasts. In lymphocyte, in addition to Kv1.3 channels, KCa3.1 is also involved in activation and proliferation by maintaining a negative membrane potential [2, 14]. This channel shares only about 40% sequence similarity with the KCa2.x subtypes and is predominantly expressed in non-neuronal peripheral tissues [2]. Both KCa2.x and KCa3.1 channels are structurally similar to voltage-gates K^+ channels, but they contain relatively fewer positive charges in S4 segment of α-helix (VSD), making them insensitive to voltage changes in the transmembrane. These channels are activated by intracellular Ca^{2+} through calmodulin (CaM) that constitutively bound to intracellular C-terminus of channel [43, 44].

Slo channel family differ from Kv and KCa2 channels as they have 7TM segments, an extra segment in the TM α-helix termed as S_0, causing the N-terminus of the channel to be localized extracellularly [5]. These channels are activated by both changes in the membrane potential or by an increase in intracellular Ca^{2+} levels. This channel has two high affinity Ca^{2+} binding sites in each subunit of tetramer and these sites contribute to the formation of a structural component known as the gating ring, which plays a crucial role in channel activation [44]. Slo1 is a member of Slo family and is also called KCa1.1 (encoded by *KCNMA1* gene) and is widely expressed across various tissues including smooth and skeletal muscles, mitochondria, kidney, brain and cochlear hair cells. The functional properties vary depending on factors such as alternative splicing, phosphorylation, and interaction with auxiliary subunits. Physiologically, it is involved in processes like smooth muscle cell hyperpolarization and the triggering of neurotransmitter release [14, 45].

2.2 Structural Insights into the Kv1.2 Potassium Channel

In 1998, a breakthrough in structural biology was achieved with the determination of the first high-resolution crystal structure of a potassium channel KcsA from *Streptomyces*

lividans, solved by Roderick MacKinnon and his team. This structure, resolved at 3.2 Å and it provided crucial atomic-level insight into how potassium ions (K^+) are selectively conducted through the channel, advancing our understanding of ion channel function [16]. Regarding the Kv1.2 ion channel, in 2005, a 2.9 Å crystal structure of the channel obtained by Long *et al*. that revealed the overall architecture of the channel. However, VSD domain had relatively weak densities [46]. To improve this, a study in 2007 introduced the structure of Kv1.2–2.1 paddle chimera, in which a part of the voltage-sensor domain (residues 267-302 from S3–S4 paddle), was substituted with the equivalent sequence from Kv2.1 K^+ channel (residues 274-305). The 2.4 Å X-ray structure of Kv1.2-Kv2.1 paddle chimera provided high-resolution insight into the VSDs and became a key reference for structural and computational studies [47]. In 2022, Reddi *et al*. reported the crystal structure of the Kv1.2 channel (by using Kv1.2-2.1 chimera) in a C-type inactivated state (details of channel inactivation below in this chapter). To determine the structure, three mutations W362F, S367T and V377T in Kv1.2-2.1 chimera have been introduced to enhance the cell surface expression of protein and to increase the rate of C-type inactivation. A very recent study in 2024 presented near-atomic-resolution structures of Kv1.2, obtained via cryoEM, in open, C-type inactivated and toxin-blocked states. These are very similar the previously reported structures of Kv1.2-2.1 chimeric channel. [48].

Kv1.2 channel shares high similarity in structural features with other members of Kv1.x family and possesses up to 82% homology with the *Drosophila Shaker* channel. A functional Kv1.2 ion channel is formed by assembling of four non-covalently linked α-subunits, which are arranged in circumference to make up the pore domain through which potassium ions move [16, 49]. Each α-subunit consists of 6 TM helical segments (S1-S6) as represented in Fig. 2A., and the intra- and extracellular loops connecting them and one cytoplasmic tetramerization domain (T1) (indicated in Fig. 2B.). S1 to S4 segments forms the VSD of the channel (indicated in Fig. 2B.) where S3 has an overall negative charge whereas S4 contains positively charged amino acid residues in RXXR motif (RVIR residues in Kv1.2). S4 plays a major role in the sensing of voltage changes across the cell membrane leading to the opening and closing of channels [47, 50]. S5 and S6 from each α-subunit contribute to the formation of the PD of the channel (Fig. 2B.). The overall architecture of Kv1.2 ion channel with top and side views are shown in Fig. 2C. An extracellular loop, called as pore loop (P, Fig. 2A.), comprised of almost 20 residues, is present between segment S5 and S6 which contribute to the formation of the selectivity filter of the channel [48, 51]. A highly conserved TVGYGD motif is present in the selectivity filter (SF) of Kv channels, commonly referred to as the Kv signature sequence

(shown in Fig. 2D.), which selectively allows the conduction of only K^+ ions across cell membrane [52-54]. The SF typically contains four K^+ binding sites and at any given moment, two of these sites are occupied by K^+ ions, while the other two remain vacant. This alternating occupancy facilitates the movement of dehydrated K^+ ions through the pore via sequential binding and ion-ion repulsion, enabling rapid and selective conduction [16, 46, 47, 55]. The S6 TM α-helix from each α-subunit of tetrameric channel joins together in the intracellular region of the cell membrane and makes the internal activation gate referred as A-gate. At resting (negative) membrane potentials the channel is in the closed state: the S4 helix, which is a positively charged segment as mentioned earlier [46, 50], is stabilized in the downward position by electrostatic interactions, whereas the A-gate is closed (the bundle crossing of the S6 segments of the four pore domains, which line the inner pore, forms a tight seal preventing the K^+ flow). However, when the membrane depolarizes, the electrical field changes, and pushes the S4 helices outward (upward movement). The motion of S4 is transmitted via the S4–S5 linker to the S6 helices, which bend or rotate at a conserved glycine hinge, thereby opening the A-gate and allow K^+ ions to flow through the SF [56-59].

The exposure to prolonged depolarization leads to confirmational changes in Kv channels causing them to enter into a functionally non-conductive inactive state. Two types of inactivation are observed in Kv channels depending upon the type of channel: (i) N-type and (ii) C-type [7]. N-type inactivation (fast-inactivation) occurs in a range of ms, when a 22-residue-long segment at the end of the N-terminus of the channel protein occludes the pore intracellularly in the open state. Such inactivation is present in the Kv1.4 ion channel [60, 61]. On the other hand, C-type inactivation takes a few 100 ms or even seconds and is observed in other Kv1 family members [62-64]. In this process conformational alterations occur in the selectivity filter of the channel that lead to diminishing the K^+ ions permeation [65, 66]. The structural studies of the *Shaker* channel and the Kv1.2–2.1 chimera have revealed that C-type inactivation involves the disruption of two hydrogen bonds in the pore region specifically between Asp and Trp, or Tyr and Thr/Ser [62, 65]. These studies also demonstrate that the outer portion of the selectivity filter expands, leading to partial loss of ion coordination and a subsequent reduction in ion flow. Additionally, molecular dynamics simulations support this view, suggesting that conformational changes within the selectivity filter hinder ion permeation [65, 66]. Recently Suárez-Delgado at el., has demonstrated that the slow inactivation in Kv1.2 channels follows the similar mechanism of C-type inactivation as described for *Shaker* channel [67].

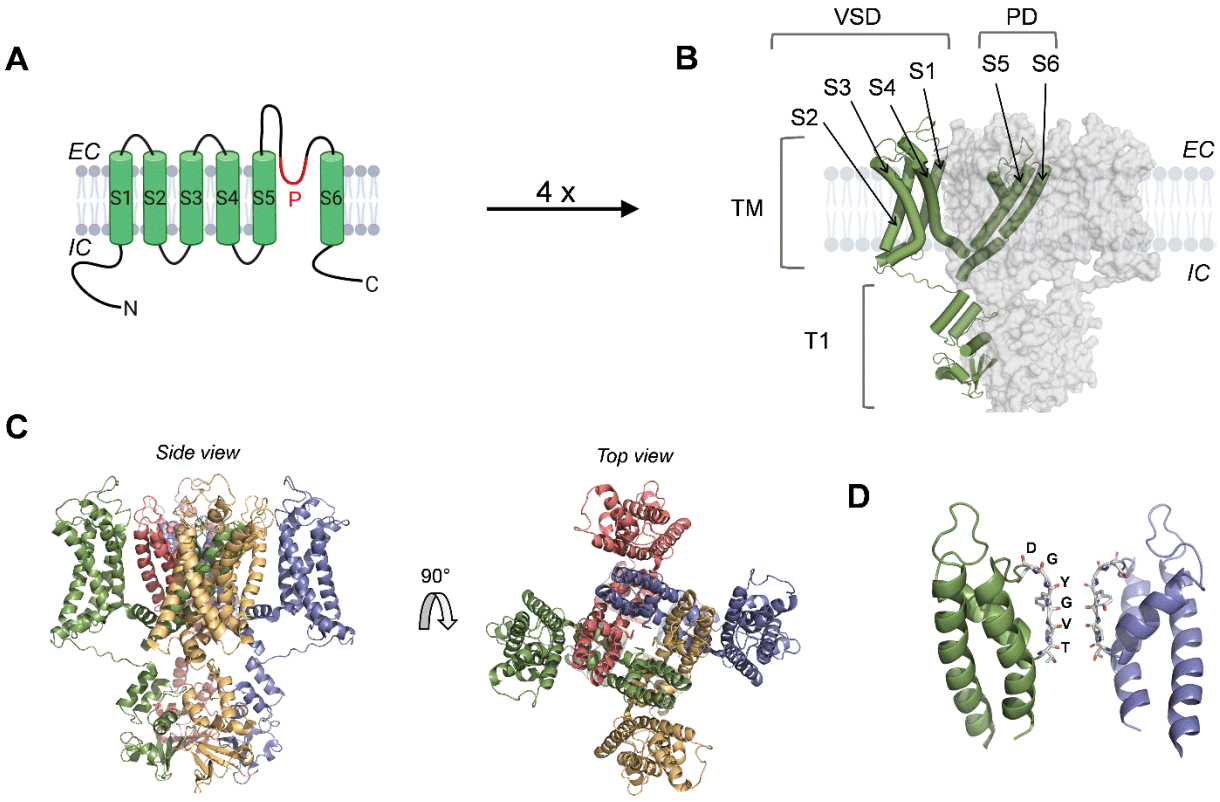

Figure 2: **Structure of human Kv1.2. (A)** The pictogram illustrates the S1-S6 segments of α-subunit in the membrane. **(B)** 4 α-subunits assemble to create one functional Kv1.2 channel as represented by cryoEM structural model of Kv1.2-Kv2.1 paddle chimera (PDB: 6EBK). TM and T1 indicated the transmembrane helices and the cytoplasmic tetramerization domains. Voltage sensing domains (VSDs, S1-S4) and Pore domain (PD, S5-P-S6) are indicated in highlighted α-subunit (α-helices in smudge green cylinders), other three α-subunits are shown in transparent light gray color for better visualization. **(C)** The cartoon representation of tetrameric assembly of Kv1.2-Kv2.1 paddle chimera as side view (left) and top view (right). Each α-subunit is shown in a different color. **(D)** The close-up view of the selectivity filter of Kv1.2 (only 2 α-subunits are shown here for a better representation). The signature sequence (TVGYGD) is indicated with letters. Adopted and presented from Matthies et al [68].

2.2.1 Biophysical characteristics of Kv1.2

Kv1.2 belongs to the delayed-rectifiers class of ion channels. The conductance of a single Kv1.2 channel ranges between 14-18 pS [69, 70]. For the determination of biophysical parameters of Kv1.2 ion channels patch-clamp electrophysiology is used both in whole-cell and cell-attached patch configurations. Kv1.2, unlike other Kv1 channels, has variable activation gating kinetics as represented in Fig. 3. Most studies report that Kv1.2 channels activate rapidly as represented in Fig. 3A., with a half-activation voltage ($V_{1/2}$) between −15 mV and −43 mV

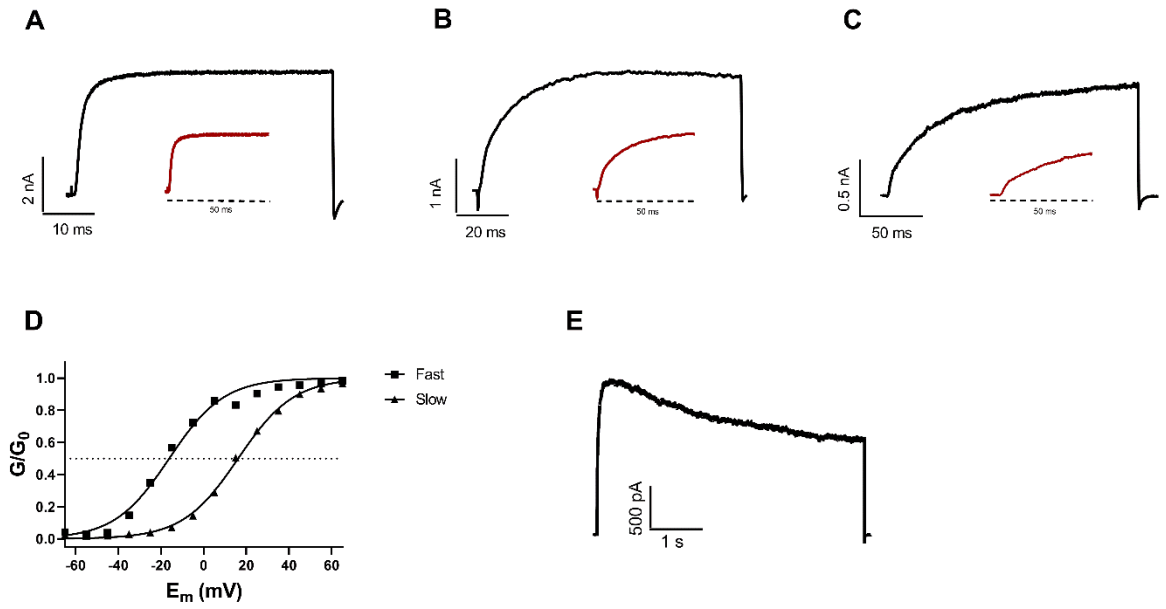

Figure 3: **Biophysical characteristics of Kv1.2 ion channel. (A-C)** Kv1.2 current traces elicited by depolarizing steps from −120 mV of holding potential (V_h) to +50mV (own original records). The gating kinetics of Kv1.2 showed three clear phenotypes. The insets illustrate 50-ms-long segment of current trance for comparison of inactivation variability). **(A)** example of a Kv1.2 current with very fast activation kinetics; **(B)** example of a Kv1.2 current that displays intermediate (mixture of fast and slow activating channels) activation kinetics; **(C)** example of a Kv1.2 current that that exhibited slow activation kinetics **(D)** The mean isochronal activation $V_{1/2}$ was −18.8 ± 2.3mV for fast activating channels (■) and 16.6 ± 1.1mV for slowly activating channels (▲), the conductance-voltage (G-V) relationships were adopted from Rezazadeh *et al*. [71]. **(E)** An example of an original Kv1.2 current trace recorded with a 5-s-long voltage step to +50mV from a V_h of −120mV, to demonstrate the inactivation of Kv1.2 current.

[72-74]. Half activation voltage ($V_{1/2}$) is the membrane potential where the whole-cell K^+ conductance reaches half of its maximal value. However, another study showed a much slower activation kinetics (Fig. 3B. and C, $\tau \approx 25$ ms at +40 mV, where τ is the activation time constant of the current, the time required to reach 67.3% of the peak current) and a more depolarized $V_{1/2}$ of +27 mV [75]. This variability in activation kinetics was further investigated by Rezazadeh *et al*. who observed significant differences in the activation gating kinetics of Kv1.2. At +35 mV, 27% of the cells expressing Kv1.2 channels showed rapid activation time course ($\tau = 4.5 \pm 1.7$ ms), 25% of cells showed mixed (biphasic, a mix of fast and slow components) and 48% cells demonstrate slow activation kinetics ($\tau = 90 \pm 6$ ms) [71]. Analysis of the voltage-dependence of steady-state activation revealed that cells with fast kinetics exhibited activation threshold potentials at negative voltages with $V_{1/2} = -18.8 \pm 2.3$ mV, while cells with slow and mixed kinetics had more positive $V_{1/2}$ values (16.6 ± 1.1 mV; and 14.5 ± 1.6 mV, respectively)

[71] as shown in Fig. 3D. On the other hand, regarding inactivation of Kv1.2, it displays C-type inactivation however with a very slow rate: development of inactivation requires several seconds [67] as represented in Fig. 3E. by a current trace recorded under long depolarization pulse from CHO cells expressing human Kv1.2.

2.2.2 Expression and functions of Kv1.2

Kv1.2 is predominantly present in the CNS mainly in the pons, medulla oblongata, hippocampus, spinal cord and thalamus. They are abundantly present in the axon initial segment (AIS) of human cortical pyramidal neurons [76]. Studies showed that the expression of Kv1.2 channels varies across different brain regions such as the medial layer II neurons, cerebellar cortex, Purkinje cells and corpus callosum have high levels of Kv1.2 mRNA [77, 78]. Kv1.2 channels are crucial for maintaining neuronal excitability and proper synaptic function. They regulate subthreshold excitability and spike timing, particularly in dendrites and axon terminals, influencing action potential initiation and synaptic transmission [79]. Generally, a neuronal action potential begins with depolarization, when the membrane reaches a threshold voltage, triggering voltage-gated sodium channels (Nav) to open and allow Na^+ influx, rapidly depolarizing the membrane potential. After about 1 ms, Nav channels become inactivated. Then, repolarization occurs as slower-opening Kv channels activate, allowing efflux of K^+ ions and restoring the membrane potential. Kv channels remain open slightly longer than necessary, causing the membrane potential to briefly fall below the resting level, a phase called hyperpolarizing afterpotential, before returning to the resting potential [80]. Kv1.2 contribute to the voltage-dependent delayed K^+ current known as the D-type current. This current plays a crucial role by activating at subthreshold membrane potentials, thereby delaying action potential initiation and suppressing repetitive firing [75, 81]. In presynaptic terminals, Kv1.2 channels suppress hyperexcitability following action potential and preserve synaptic fidelity [82-84]. In myelinated axons, Kv1.2 channels help in maintaining the conduction, nevertheless their overactivity during demyelination can suppress action potential propagation [85].

Kv1.2 channels exist as both homo- or heterotetramers in the CNS [86]. Kv1.1/Kv1.2 heterotetramers are widely distributed in neuronal compartments and modulate neuronal excitability and neurotransmitter release [85]. Kv1.2 also interact with auxiliary subunits specifically Kvβ in brain regions that affects the Kv1.2 subcellular localization and protein expression [87-89]. Moreover, other proteins such as PSD-95, RhoA and lipid molecules have

been observed to interact with Kv1.2 and aids in the regulation of expression and gating mechanism of Kv1.2 [70, 90].

2.3 Kv1.3 channel: expression and function

Kv1.3 is also a member of *Shaker* related Kv channel family and bears a high degree of similarity in basic structural organization with other members of Kv1 family. It is broadly expressed in T lymphocytes and thus plays a vital role in the development of immunity. Upon antigen stimulation, T-cell activates and initiates calcium signaling via endoplasmic calcium release, which is followed by extracellular calcium entry through calcium release activated channel (CRAC). Kv1.3 restores the membrane potential that was depolarized by Ca^{2+} entry, thereby maintaining the persistent calcium signaling which regulates the T cell proliferation [91, 92]. Upregulation of Kv1.3 in T-cells has been proven to be a major cause of autoimmune diseases such as multiple sclerosis (MS), type 1 diabetes mellitus (T1DM) and rheumatoid arthritis (RA) [31, 93]. Moreover, Kv1.3 are also expressed in microglia, brain immune cells, and its upregulation is a hallmark of neurodegenerative disorders like Parkinson's disease [34]. Since Kv1.3 is involved in multiple channelopathies, specific inhibition of Kv1.3 holds a great potential to cure such diseases.

Several studies showed the applicability of Kv1.3 inhibitors to target autoimmune and neurodegenerative disorder. For example, ShK-186, a selective peptide inhibitor of Kv1.3, has demonstrated therapeutic potential in animal models of multiple sclerosis and rheumatoid arthritis [94]. Moreover, a recent study found that inhibiting Kv1.3 with PAP-1, (small molecule based Kv1.3 inhibitor) reduced inflammation in a primary microglial *in vitro* model and ameliorated disease symptoms in mouse models of Parkinson's disease (PD) [34].

2.4 Comparison of pore and selectivity filter of Kv1.2 with Kv1.3

The Kv1.2 and Kv1.3 ion channels possess a high similarity in selectivity filter and pore regions. As discussed above (Chapter 2.2) the K^+ selectivity determining signature sequence TVGYGD is highly conserved but subtle differences are present in the remaining part of SF. In the outer vestibule, the turret region that consists of the extracellular loop connecting the S5 to the pore helix, significantly varies between Kv1.2 and Kv1.3 as shown in Fig. 4A. [16, 53]. The turret region together with the tip of the S6 and the loop connecting the pore helix to S6 forms the toxin binding site (highlighted in Fig. 4B.) where peptide toxins dock and block the channel by occluding the pore from the extracellular side [95]. These structural differences in the PD of

Kv1.2 and other closely related Kv1 channels are of great pharmacological importance, as these can contribute to its variable sensitivities towards animal toxins and provide opportunity to design a peptide blocker with high selectivity for single target.

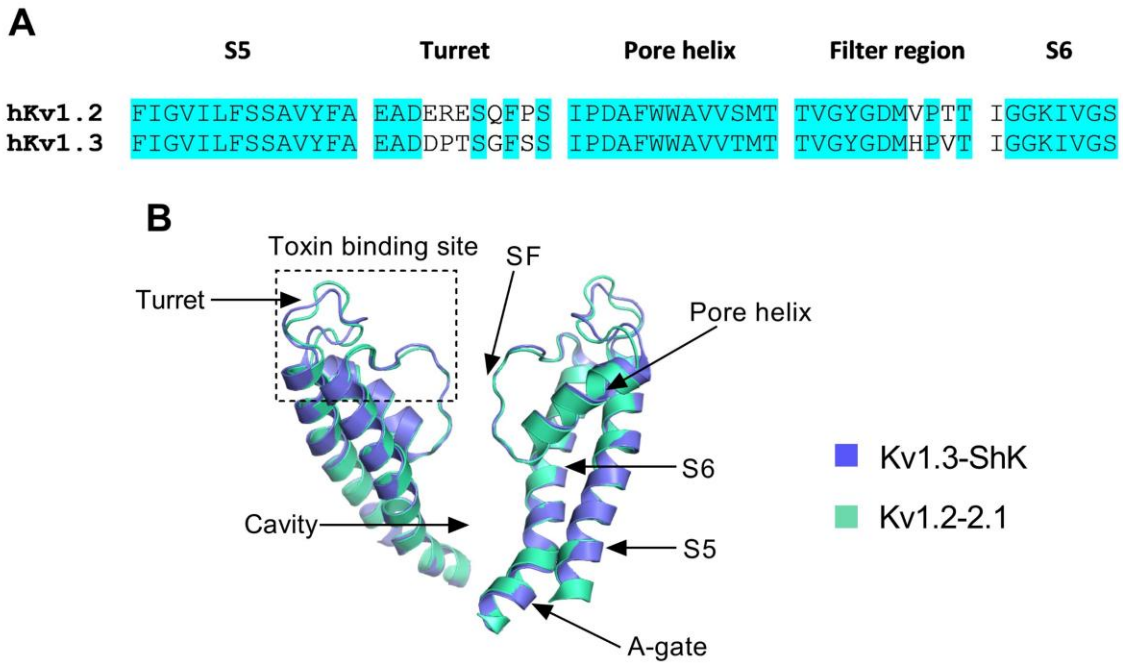

Figure 4: **Comparison of pore region conformation of Kv1.2 and Kv1.3 ion channels. (A)** Amino acid sequence alignment of Kv1.2 and Kv1.3 channels. Identical residues are highlighted in cyan color. Key regions of the pore are labeled above the alignment. **(B)** Structural alignment of the pore regions from Kv1.2-2.1 (paddle chimera) and Kv1.3-ShK channel structures. Arrows indicate specific areas of structural divergence within the pore region.

Studies showed that in the case of Kv1.2 ion channel, the filter region predominantly plays a vital role in determining the selectivity of toxin binding [96]. For example, the scorpion toxin Maurotoxin (MTX, α-KTx 6.2) binds Kv1.2 with high affinity (K_d = 0.7 nM), and mutations in the turret region had minimal effect [97]. Simulation studies showed that Kv1.2 turrets bend away from MTX, suggesting that pore region residues are primarily responsible for binding [98]. In contrast, Kv1.3 is less sensitive to MTX (K_d = 3.3 μM) but a single mutation in the filter region (His to Thr in the "TVGYGDMH" motif) greatly increased its sensitivity (K_d = 0.6 nM) [97]. Similarly, Mesomartoxin (MMTX, α-KTx 26.4) inhibits Kv1.2 with K_d = 15.6 nM and shows no affinity for Kv1.1, however mutations in Kv1.1 filter region renders the

Kv1.1 sensitivity to Mesomartoxin with similar potency as for Kv1.2 (K_d = 16.6 nM) [96, 99]. These examples verify that the filter region of Kv1.2 is critical for toxin binding and selectivity.

2.5 Kv1.2 related channelopathies

K_V1.2, encoded by *KCNA2* gene in human, plays a role in enabling efficient neuronal repolarization following an action potential. The involvement of Kv1.2 in channelopathy was first described Brew *et al.* when *KCNA2* knockout mice display neuronal hyperexcitability and an epileptic phenotype [100]. In another study, a *KCNA2* related missense mutation in mouse diminished Kv1.2 functional expression and caused cerebellar ataxia [101]. Mutations in human *KCNA2* gene could result in either loss- or gain of function (LOF and GOF) of the ion channel activity [102]. A decade ago, de novo LOF and GOF mutations in *KCNA2* were identified for the first time in patients with epileptic encephalopathy, providing clear evidence that Kv1.2 plays a significant role in neuronal channelopathies. [27].

GOF mutations in *KCNA2* lead to permanent opening of channels resulting in increased channel activity or current density, which can significantly alter neuronal excitability, whereas LOF mutations (reported relatively less severe as compared to GOF) predict hyperexcitable neuronal membranes and repetitive neuronal firing due to impaired repolarization [27, 100]. For example, I402T in *KCNA2*, a LOF mutation, affects Purkinje cell firing patterns in the cerebellum by disrupting the balance of excitatory and inhibitory inputs, leading to cerebellar ataxia [101]. Another notable LOF mutation is caused by the F233S substitution in the voltage-sensing domain of Kv1.2. This mutation impairs the trafficking of Kv1.2 channels to the cell surface, resulting in a dominant-negative effect that also reduces the surface expression of wild-type Kv1.2 and Kv1.4 subunits. Consequently, there is a substantial decrease in K^+ conductance, leading to neuronal hyperexcitability and epilepsy [103].

Another interesting type of mutation was discovered by Masnada *et al.* and termed as gain- and loss-of-function, as such mutations have both effects simultaneously. For example, L290R is on such mutation, located in the S4 segment of Kv1.2. A 1.5-fold increase in the current alongside a significant shift in the mean of the voltage-dependence of steady-state activation towards more hyperpolarized potentials was observed. Based on these characteristics L290R was predicated to be gain of function mutation. However, it was also revealed that the steady-state inactivation curves were also shifted to more hyperpolarized potentials predicting a loss-of-function effect [28].

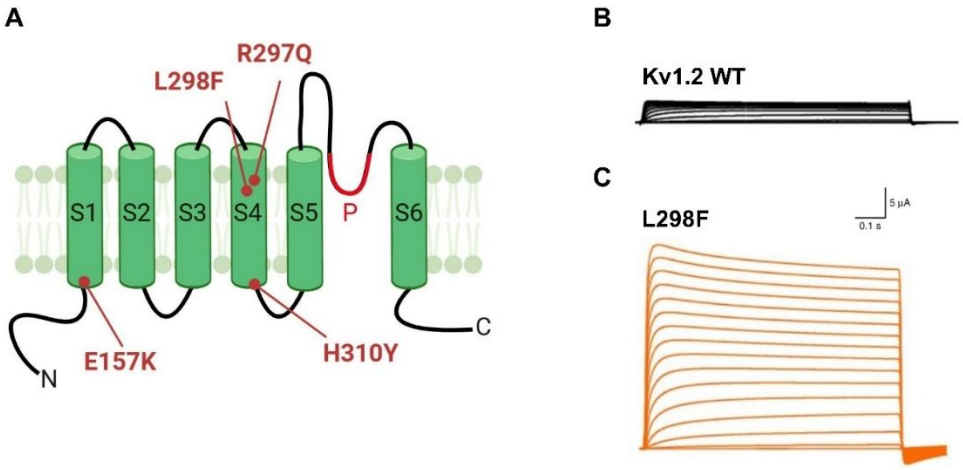

Figure 5: **GOF mutation in Kv1.2 (A)** Cartoon representation of α-subunit of Kv1.2 (S1-S6 segment) with marks indicating the location of the gain of function (GOF) mutations associated with epileptic encephalopathy (EE). **(B)** Representative current traces recorded in a cell expressing the wild-type Kv1.2 channel (Kv1.2 WT) upon increasing depolarizations between -80 mV and +70 mV. **(C)** Representative current traces from a Kv1.2-L298F cell using the same voltage protocol as in B. Current traces in B and C were adopted from Syrbe *et al*. 2015 [27].

2.5.1 Kv1.2-related GOF mutations in Epileptic encephalopathies

Epileptic encephalopathies (EE) represent a diverse group of severe childhood-onset neurological disorders, typically marked by intractable epilepsy and progressive cognitive and neurological impairments [104]. In 2015, for the first time, Syrbe *et al*. reported two Kv1.2-related GOF mutations in two different patients suffering from EE i.e., R297Q and L298F. Both these mutations exist in the S4 segment of the α- subunit (Fig. 5A.), and it has already been established that S4 segments make up the VSD of the ion channel and thus play a vital role in the activation of the channel. Both patients were presented with severe intellectual disability, moderate to severe ataxia and seizures. Upon studying biophysical characteristics, it was revealed that both R297Q and L298F mutations in Kv1.2 cause strong gain-of-function effects. R297Q increases current amplitude 9-fold and shifts the voltage dependence of steady-state activation by −40 mV, while L298F leads to a 13-fold increase (as demonstrated in Fig. 5B-C. with original current traces from wild-type and mutated Kv1.2 channel from Syrbe *et al*., 2015) with a −50 mV shift in the voltage-dependence of steady-state activation. These mutations cause the channels to remain open, resulting in resting membrane potentials approximately −40 mV more negative as compared to cells expressing the wild-type channel [27]. In 2017, another novel GOF mutation was described by Masnada *et al*. E157K, in the N-terminus of α-subunit,

causes a 5-fold increase in current amplitude and -12 mV shift in voltage-dependence of steady-state activation [28]. H310Y is another mutation in Kv1.2 involved in a dual function by increasing channel activity and the surface expression of Kv1.2 [105]. Fig. 5A demonstrates the localization of all the GOF mutation in Kv1.2.

Patients with GOF mutations in Kv1.2 tend to exhibit more severe clinical phenotypes compared to those with LOF variants. GOF mutations are associated with early onset of generalized seizures, often starting around 9 months of age. These seizures are typically followed by significant developmental delays and cognitive impairments [28]. GOF variants may suppress interneuron activity, leading to disinhibition and overall network hyperexcitability. Alongside EE, Kv1.2 GOF-mutations also cause intellectual disability/global developmental delay (ID/GDD), cerebral atrophy, autism spectrum disorder ADS, hyperactivity, aggressiveness [28, 106-108]. Table 2 summarizes the GOF-mutations in Kv1.2, their biophysical characteristics and disease phenotypes.

Table 2: **Summary of gain-of-function mutations in human *KCNA2* gene**

Mutation	Increase in current amplitude	Shift in activation voltage	Number of cases	Phenotype	References
E157K	5-fold	-12 mV	1	epileptic encephalopathy	Masnada *et al.,* 2017
R297Q	9-fold	-40 mV	15	Ataxia, myoclonic seizures and epileptic encephalopathy	Syrbe *et al.,* 2015; Masnada *et al.,* 2017
L298F	13-fold	-50 mV	1	epileptic encephalopathy	Syrbe *et al.,* 2015; Masnada *et al.,* 2017
H310Y	2.8-fold	-	1	Myoclonic epilepsy and generalized tonic-clonic seizures	Mínguez-Viñas *et al.,* 2023

2.6 Kv1.2: a drug target to cure GOF-related channelopathies

Kv1.2-related GOF-mutations lead to hyperactivity and alteration of neuronal functions, thus causing *KCNA2*-related epileptic encephalopathy, characterized by severe seizures, ataxia and ID/GDD. Upon discovery of these mutations Kv1.2 emerged as a potential target to cure GOF-related epileptic encephalopathy. It was hypothesized that the inhibition of GOF-Kv1.2 currents by a blocker would be able to restore normal electrophysiological activity of Kv1.2 in neurons. Hedrich *et al*. conducted the first study and used 4-aminopyridine (4-AP, a small

molecule) as a potential therapeutic agent to counteract the GOF effects in Kv1.2 activity [109]. 4-AP is a well-studied nonselective Kv channel blocker which inhibits the currents by binding to the pore region of channels and it is already in clinical trials for downbeat nystagmus syndrome and episodic ataxia type 2 [75, 110-113]. The effect of 4-AP was tested on three GOF-Kv1.2 mutants (E157K, R297Q and L298F, details in Table 2) [27, 28] expressed in oocytes. 1 mM 4-AP inhibited the mutant channels by decreasing current amplitudes and shifting the voltage dependence of steady-state activation toward more depolarized potentials. Moreover, R297Q mutants expressed in hippocampal neurons showed a significant decrease in the firing frequency upon application of 0.1 mM 4-AP. 4-AP was also given to eleven patients and improvement in seizure control, cognition, or ataxia in nine out of eleven cases was observed. The most significant outcomes were observed when treatment began in early childhood, highlighting the importance of early intervention [109].

Small molecule-based inhibitors of ion channels often lack selectivity. 4-AP, for example, apart from Kv1.2 also inhibits a several of other voltage gated ion channels including Kv1.1, Kv1.3, Kv1.5 and many members of Kv2.x, Kv3.x and Kv7.x families [114, 115]. On the other hand, venom-based peptide toxins have demonstrated relatively much higher selectivity and affinity for in ion channel inhibition (details are discussed in the next section) [116].

2.7 Ion channel blockers

Kv channels play crucial roles in physiological and pathological processes, making them valuable pharmacological targets [5]. They are known to have broad tissue distribution, including mitochondrial localization [7, 8]. Moreover, upregulation, downregulation and dysfunction of ion channels are linked to a number of channelopathies [117]. To understand the biophysics of ion channels, their physiological attributes and pharmacological properties for targeting the channelopathies, it is of a great interest to identify or design a selective and potent inhibitors for pharmacologically important subtypes of Kv channels [48, 95].

Currently there are two types of inhibitors that target Kv channels with varying affinity and selectivity: (i) small organic molecules and (ii) venom-derived peptide toxins. Small organic molecules usually have a molecular weight (MW) <800 Da, are usually hydrophobic and membrane permeable. They generally bind to the central cavity beneath the selectivity filter of Kv channels (Fig. 4.), however due to their small size and the structural similarity among Kv1 subtypes, small molecules tend to have low affinity and poor selectivity [118]. For

example, 4-AP blocks several Kv channels and tetraethylammonium (TEA^+) inhibits many Kv1 and KCa channel subtypes, thus exhibiting poor selectivity [114, 115, 119]. On the contrary, venom-derived peptide toxins are bigger than small molecules with MW ranging from 2-4 kDa and block the ionic current by occluding the pore of the channels. Toxins bind to the channels by making multiple interaction points with the outer vestibule of pore region which has significant structural differences among Kv1 channels. These factors contribute to the high selectivity and affinity of toxins towards channels [116]. Thus, from a pharmacological perspective, peptide toxins offer advantages over small organic molecules as they are effective at much lower concentrations and exhibit high selectivity for Kv1 channels. This selectivity helps minimize off-target interactions and reduces potential side effects [120].

2.7.1 Venom derived K^+ channel blockers

Almost 15% of the animals that exist on this planet are venomous including scorpions, spiders, snakes, sea anemones cone snails, bees etc. Animal venom is a complex cocktail of multiple components and a rich source of peptide toxins [116]. These natural toxins have potential to modulate the ion channel activity. The first K^+ channel inhibitor was discovered from the venom of scorpion *Centruroides noxius* in 1982 named as Noxiustoxin. It inhibits Kv1.2 and Kv1.3 currents with IC_{50} values of 2 nM and 1 nM, respectively [121]. Afterwards in 1985 and 1993, Charybdotoxin (ChTx) and MgTx were discovered from the venom of *Leiurus quinquestriatus var* and *Centruroides margaritatus*, respectively [122, 123]. ChTx inhibits several Kv ion channels such as Kv1.2, Kv1.3, Kv1.6 and also KCa1.1 having K_d values in the low nanomolar range [124, 125]. On the other hand, initially MgTx was considered a selective inhibitor of Kv1.3 (K_d = 50-100pM), however, later studies showed that it also inhibits Kv1.1 and Kv1.2 with comparable affinities [126].

Over the past four decades, several peptide toxins targeting potassium (K^+) channels have been identified. The Kalium database, a collection of peptides toxin that affect K^+ channels, currently includes more than 430 entries of natural toxins with 218 specifically isolated from the venom of scorpions [116, 127-129]. Potassium channel inhibitor toxins (KTxs) derived from scorpions are classified into seven different families based on their structural and functional characteristics: α-KTx, β-KTx, γ-KTx, δ-KTx, ε-KTx, κ-KTx, and λ-KTx [127, 130, 131]. These toxins exhibit diverse structural features and block various K^+ channels with affinities ranging from picomolar (pM) to micromolar (μM) concentrations. Two types of mechanisms are known by which peptide toxins modulate ion channel activity. (i) By

blocking the pore domain; such peptides are referred as pore blockers that occlude the pore domain of the ion channel thereby by hindering the flow on ions leading to current reduction [132]. (ii) By modifying the voltage-dependence of steady-state activation; such peptides are called as gating modifiers. Peptides that bind to the VSD of the ion channels lead to a prominent shift in the voltage-dependence of steady-state activation towards more positive voltages. Binding of the toxins therefore reduces the open probability of the channels at physiological voltages [133]. One such example of gating modifier is Hanatoxin, isolated from spider *Grammostola spatulata* and inhibits Kv2.1 currents by binding to the VSD of the channel [134].

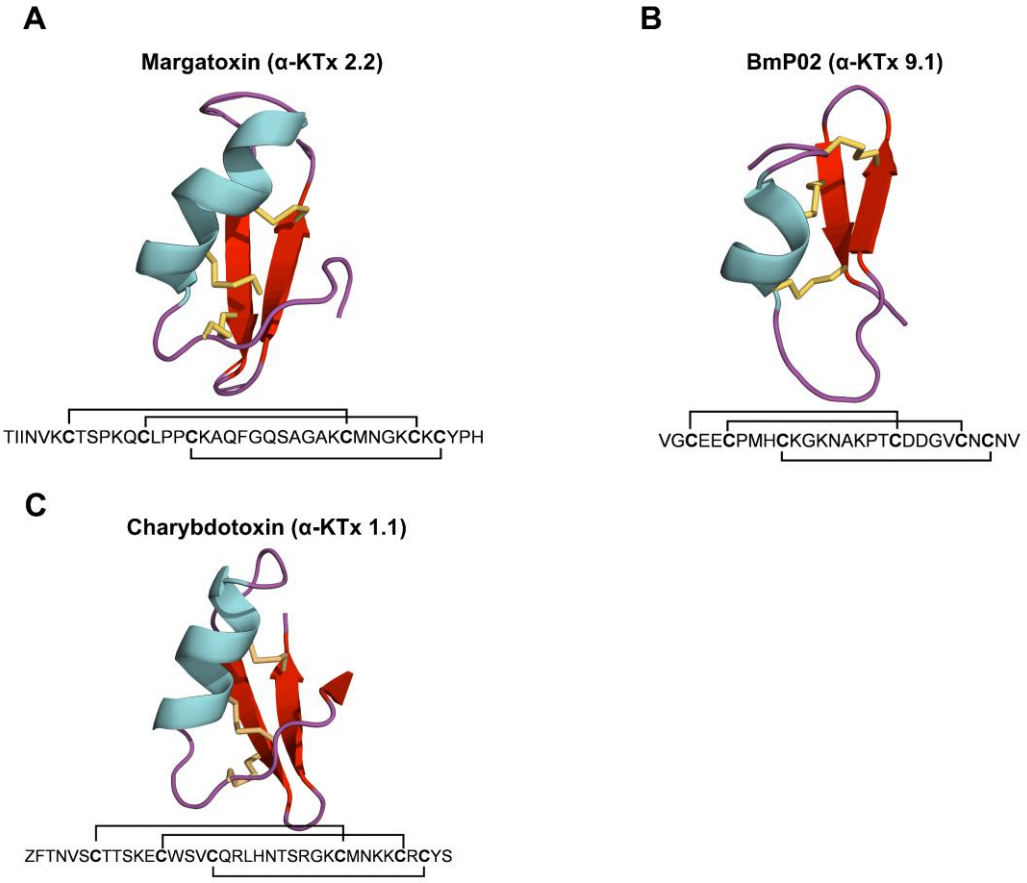

Figure 6: **The structural representation of α-KTxs toxins.** The amino acids sequences (disulfide bonds are indicated with yellow connecting lines) and 3D structures of **(A)** margatoxin (PDB: 1MTX), **(B)** BmP02 (PDB: 1DU9) **(C)** Charybdotoxin (PDB: 2CRD).

The toxins of α-KTx family, in general, inhibit Kv and KCa channels and are divided into 32 subfamilies based on the sequence similarity [130, 135]. α-KTx peptides contain 23-42 amino acid residues and share a cysteine-stabilized α/β scaffold as a common structural motif which comprises of α-helix and β-sheets stabilized by 3-4 disulfide bridges (Fig. 6). The presence of a "functional dyad" is a major feature of majority of potassium channel blocking

peptides. This dyad is composed of a critically positioned lysine (Lys27 in ChTx, Fig. 6C and 7A.) residue and an aromatic residue, typically tyrosine (Tyr), nine positions downstream [116, 136, 137]. The dyad lysine is on the beta sheet surface facing the channel pore upon binding, the 9-position difference in the primary sequence separates the Cα of the lysine by 6.6 ±1.0 Å from the center of the benzene ring of the tyrosine (Tyr36 in ChTx) in the 3D structure of ChTx [138] (see also Fig. 15. in the Results section). This functional dyad is considered essential for the interaction of peptides with K^+ channels. The Lys side chain penetrates into the selectivity filter of the channel and plugs the pore, preventing K^+ efflux [48, 124]. This interaction of Lys residue with SF of Kv1.2 channel has been shown in a crystal structure of ChTx bound Kv1.2-Kv2.1 chimera by Banerjee *et al*. [132] as represented in Fig. 7A-B. More recently, Selvakumar *et al*. have described the Lys penetration into SF of Kv1.3 in cryroEM structure of K1.3 bounded with ShK, a peptide toxin from Sea anemone *Stichodactyla helianthus*.

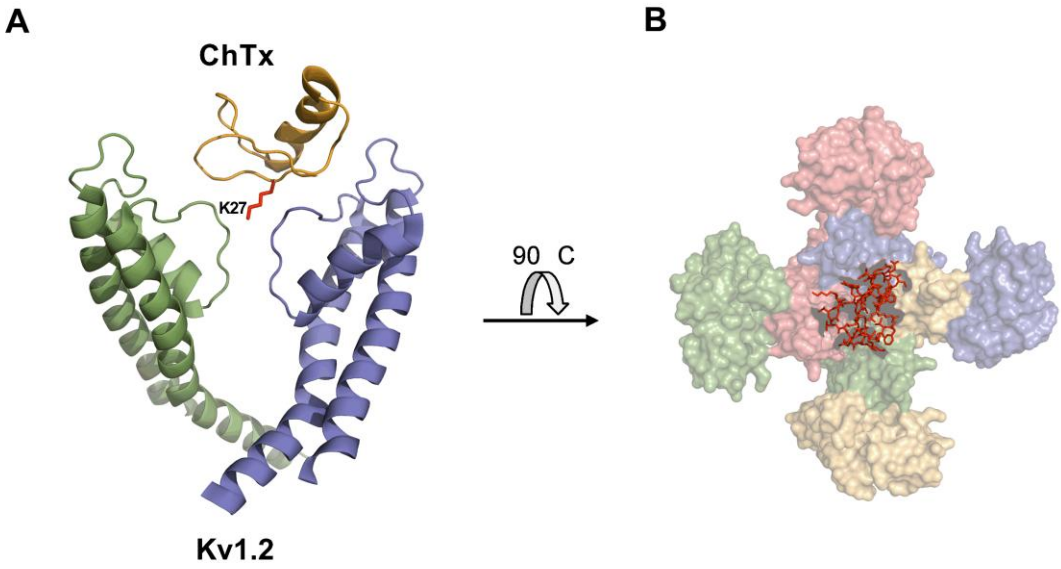

Figure 7: **Representation of crystal structure of Kv1.2 bounded with ChTx. (A)** Pore-blocking mode of ChTx on Kv1.2. The channel pore region is shown as side view (front and rear pore domains are omitted for clarity). The carton representation of the toxin is shown in light brown, and the lysine (K27) side chain sticks are shown in red that protrudes into the selectivity filter of ion channel. **(B)** Top view of channel toxin interaction, where ChTx is exhibited by red sticks and the extracellular side of channel is represented as the molecular surface. ChTx bounded Kv1.2-Kv2.1 chimera structure (PDB: 4JTA) was retrieved from from Banerjee *et al.* [132].

The central Lys residue is crucial for the high affinity of the toxin, while the aromatic Tyr residue of the dyad interacts with the outer vestibule of the channel, including the turret and the loop connecting the pore helix to S6, thus, playing a role in determining the selectivity

among Kv1.x subtypes [139, 140]. However, some peptide toxins only possess Lys residue and no automatic residue and are still inhibit Kv1 ion channels for example, HsTx1 (α-KTx 6.3), isolated from venom of *Heterometrus spinnifer*, has only Lys at position 23 [141]. On the other hand, a few peptide toxins are also known that completely lack the conventional dyad however are still functional against Kv1 channels such as Cm28 (α-KTx 32.1; isolated from *Centruroides margaritatus*) and BmP02 (a-KTx 9.1; isolated from *Buthus martensi*) [142, 143]. These facts indicate that for toxin-channel interaction, other essential residues of peptide are also important to make interactions with ion channels at multiple points.

During the last three decades many Kv channel inhibiting peptide toxins have been identified with a main focus on Kv1.3 specific inhibitors. As described in section 2.3 Kv1.3 is an attractive drug target due to its involvement in autoimmune diseases such as multiple sclerosis (MS) and psoriasis [144]. Examples of high affinity Kv1.3 inhibitors are Vm24 (K_d = 2.9 pM), native toxin isolated from the scorpion *Vaejovis mexicanus smithi* [145] and Shk-186 (K_d = 11 pM), a derivative of Shk isolated from sea anemone *Stichodactyla helianthus.* Shk-186 (Dalazatide) has already been approved for clinical trials to target autoimmune disorders [94, 146].

Kv1.2 has emerged as a potential drug target recently, after the discovery of GOF mutations in *KCNA2* that play a key role in the development of epileptic encephalopathy and relevant neuronal disorders (see 2.5.1 chapter). So far only a few peptide toxins are known that inhibit Kv1.2 with high affinity but with very low specificity. For example, MgTx (K_d = 6.4 pM), HgTx-1 (K_d = 170 pM) and Pi1 (K_d = 440 pM) block Kv1.2 with picomolar affinities, however, these toxins also inhibit Kv1.3 with similar potencies of 11 pM, 86 pM and 9.7 nM, respectively. There are very few known toxins that target Kv1.2 with high specificity and potency. Pi4 (α-KTx 6.2, isolated from scorpion *Pandinus imperator*) is the only known potent and specific inhibitor of Kv1.2. It inhibits Kv1.2 with K_d value of 8 pM and has >million-fold selectivity over Kv1.3. However, Pi4 also blocks KCa2 ion channels with K_d of 500 nM [140, 147]. High affinity and specificity peptides from venoms are attractive entities that could be exploited for the drug discovery of ion channels, therefore, identifying a specific inhibitor of Kv1.2 with minimum off-target effects would serve as a valuable therapeutic advancement in managing the GOF-related Kv1.2 channelopathies.

Scorpions are remarkably adaptable and widespread creatures and with over more than 400 million years of evolution. More than 2700 known species of scorpions are known classified into 20 families [148]. Scorpions have developed complex venoms with toxic effects on a wide array of biological targets specially ion channels [149]. Persistent identification of K^+ channel-blocking peptides underscores scorpion venom as a highly diverse and potent source of bioactive molecules which encourages scientists to explore the venom to identify novel peptides with high affinity and selectivity for a specific ion channel. Fig. 8. shows the photographs of three scorpion species whose venoms have been studied for novel peptide discovery. The two specimens *Centruroides bonito* and *Centruroides villegasi* are native to Mexico, while the third *Centruroides margaritatus* originates from Colombia.

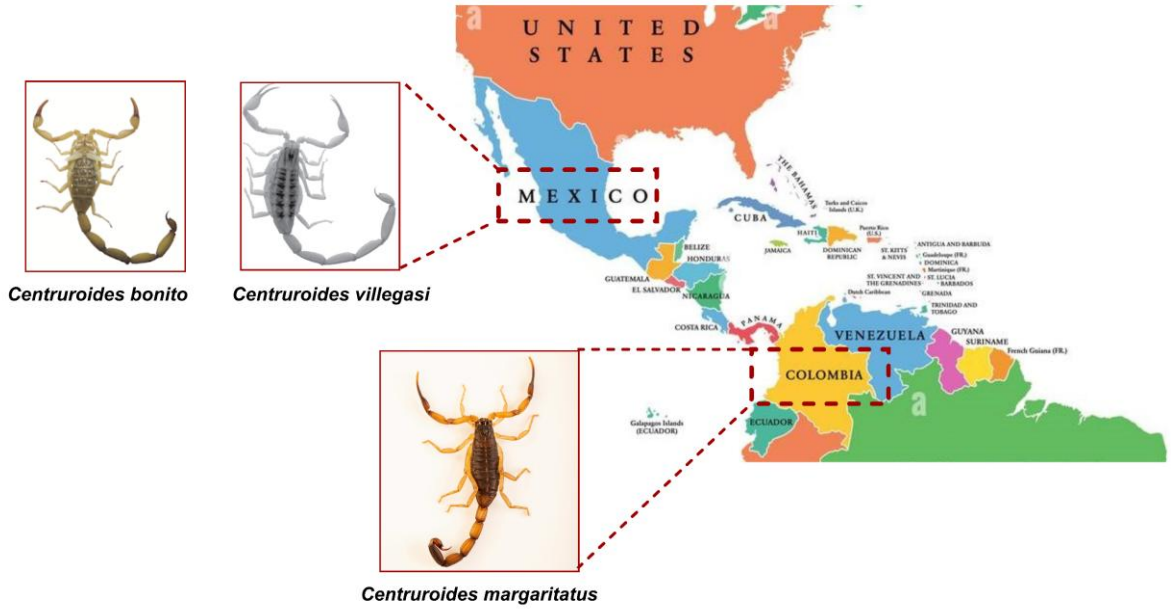

Figure 8: **Representative images and geographical diversity of three scorpion species used in this study.** *Centruroides bonito* and *Centruroides villegasi* are found in different regions of Mexico, whereas the third one *Centruroides margaritatutus* is distributed in Colombia.

3. AIMS OF OUR INVESTIGATION

3.1 Pharmacological characterization of seven novel peptide toxins isolated from *Centruroides bonito*

Scorpion venom represents a prolific source of peptide toxins that modulate voltage-gated potassium (Kv) channels. In the pursuit of potent and selective Kv1.2 ion channel blocking peptide toxins, seven novel peptides were recently isolated from the venom of *Centruroides bonito* by our collaborators and named as CboK1-7. My aim was

- to comprehensively characterize the pharmacological profile of the CboK peptides, with a particular focus on their specificity and affinity towards Kv1.1, Kv1.2 and Kv1.3 ion channels.

3.2 Pharmacological characterization of two new peptide toxins from venom of *Centruroides villegasi*

Two novel peptide toxins were identified and isolated from the venom of the scorpion *Centruroides villegasi* and named Cvill6 and Cvill7. My aims were

- to investigate the pharmacological properties of Cvill6 and Cvill7 peptides on a range of physiologically significant Kv channels.
- to study the concentration-dependent effect of Cvill peptides on Kv1.2 and Kv1.3 as well as characterize their kinetic parameters of binding to these channels.

3.3 Pharmacological characterization of synthetic peptide sCm39 against Kv1.2 and Kv1.3

Cm39 was first identified from the venom of *Centruroides margaritatus* and subsequently, produced synthetically (sCm39) for functional studies. My aims were

- to characterize the activity of the synthetic Cm39 against Kv1 channels.
- to understand the mechanism of block of Kv1.2 by sCm39 and determine the interaction kinetics.

4. MATERIALS AND METHODS

4.1 Chemicals and reagents

All chemicals and reagents utilized in this study were sourced from Sigma-Aldrich (St. Louis, MO, USA) unless specified otherwise.

4.2 Toxins

4.2.1 CboK peptide toxins

Seven novel peptide toxins were isolated from the venom of Mexican scorpion *Centruroides bonito* in Prof. Lourival Possani's laboratory (our collaborator from UNAM, Mexico). The Scorpions were captured, and venom was extracted by electrical stimulation. The three-step purification scheme was utilized to isolate the peptides from crude venom and describe in detail earlier [150, 151]. Initially, the crude venom was fractionated using size exclusion chromatography. The main fraction (FII) obtained was then subjected to ion-exchange chromatography (IEC) generating 14 subfractions. Subsequently, all IEC fractions were further purified by reverse-phase high-performance liquid chromatography (HPLC) using an analytical C_{18} column. All seven CboK peptides were obtained from subfraction 13. The amino acid sequence of the CboK peptide was determined through automated Edman degradation, performed with a Biotech PPSQ-31A/33A Protein Sequencer (Shimadzu Scientific Instruments, Inc., Columbia, MD, USA).

4.2.2 Cvill peptide toxins

Two novel peptide toxins named Cvill6 and Cvill7 were isolated in Prof. Lourival Possani's laboratory from the venom of scorpion *Centruroides villegasi* details of which are described previously [152] and in section 4.2.1.

4.2.3 sCm39

Cm39 peptide was initially identified from the venom of *Centruroides margaritatus*. To obtain a sufficient quantity of the Cm39 peptide for electrophysiology assays, it was synthesized in Prof. Possani's lab using Merrifield's solid-phase method and after refolding, peptide was purified using HPLC [153, 154].

4.3 Multiple sequence alignment

To find the phylogenetically related toxins with, CboK peptides, Cvill peptides and Cm39, BLASTP was performed. Multiple sequence alignment of mature chains was done by using MAFTT version 7.

4.4 Modeling of Cvill peptides

The tertiary structural prediction of peptides was performed using the AlphaFold3, an AI-based tool designed for predicting protein structures. Based on the amino acid sequences, peptides Alphafold3 generated multiple folding models. The model with the highest reliability scores was chosen, which had a pTM of 0.72 and a pLDDT score (the per-atom confidence measure) exceeding 90 [155].

4.5 Cell culture

4.5.1 Isolation and activation of PBMCs

Human venous blood from anonymized healthy donors was obtained from the blood bank, with sample collection approved by the Ethical Committee of the Hungarian Medical Research Council (approval number: 36255-6/2017/EKU). Peripheral blood mononuclear cells (PBMCs) were isolated using Histopaque 1077 density gradient centrifugation. The isolated cells were resuspended in Roswell Park Memorial Institute (RPMI) 1640 medium supplemented with 10% fetal calf serum (Sigma-Aldrich), 100 µg/ml penicillin, 100 µg/ml streptomycin, and 2 mM L-glutamine. Cells were seeded in 24-well culture plates at a density of 5×10^5 cells/ml and incubated at 37 °C in a humidified atmosphere with 5% CO_2 for 3 to 6 days. To activate the PBMCs and enhance Kv1.3 channel expression, phytohemagglutinin A (PHA) was added to the culture medium at concentrations of 5, 7, and 10 µg/ml. Phytohemagglutinin A (PHA) primarily activates the T-lymphocytes and stimulate the proliferation. After 3-5 days of PHA treatment, the major percentage of population comprised of activated T-lymphocytes with elevated Kv1.3 channel expression.

4.5.2 CHO cells

Chinese hamster ovary (CHO) cells were maintained under standard culture conditions in Dulbecco's Modified Eagle's Medium (DMEM; Thermo Fisher Scientific, Waltham, MA, USA; Cat. #11965084) supplemented with 10% fetal bovine serum (FBS), 2 mM L-glutamine,

100 µg/ml streptomycin, and 100 U/ml penicillin-G (Sigma-Aldrich). Cells were incubated at 37 °C in a humidified atmosphere containing 5% CO_2. Subculturing was performed three times per week using a 2–5-minute incubation with 0.05% trypsin-EDTA solution.

4.5.3 Heterologous expression of ion channels

CHO cells were used for the transient expression of ion channels as they do not have any endogenous Kv currents to cause contamination of the current records [156]. CHO cells were transfected transiently with ion channel-encoding vectors (listed in Table 3) using the Lipofectamine 2000 kit (Invitrogen, Waltham, MA, USA), following the manufacturer's protocol. The "h" indicates human origin whereas "m" in front of the gene/ion channel name indicates mouse origin. In cases where the ion channel construct lacked a fluorescent tag, cells were co-transfected with a plasmid encoding GFP to facilitate identification. Cells expressing either GFP or YFP were visualized using a Nikon TS-100 fluorescence microscope (Nikon, Tokyo, Japan), equipped with excitation and emission bandpass filters of 455–495 nm and 515–555 nm, respectively. Whole-cell electrophysiological recordings were conducted 20–30 hours post-transfection.

Table 3: **Enlisting all the ion channel-coding plasmids for heterologous expression that are used in this study**

Ion channel	Gene name	Plasmid	Source
hKv1.1	*KCNA1*	pCMV6-AC-GFP	OriGene Technologies, Rockville, MD, USA
hKv1.2	*KCNA2*	pCMV6-AC-GFP	OriGene Technologies, Rockville, MD, USA
hKv1.5	*KCNA5*	pEYFP-C1	Antonio Felipe, University of Barcelona, Barcelona, Spain
hKCa2.2	*KCNN2*	pcDNA3	Bernard Attali, Tel Aviv University, Israel
hKCa3.1	*KCNN4*	pEGFP-C1	Heike Wulff, University of California, Davis, CA, USA

Human embryonic kidney 293 cell line (HEK) that expresses hKv11.1 (hERG1, *hKCNH2* gene) in a stable manner was a kind gift from Heike Wulff (University of California, Davis, CA, USA). Th HEK293 cell line expressing mKCa1.1 (*mKcnma1* gene) in a stable manner was generously provided by Christine Beeton (Baylor College of Medicine, Houston, TX, USA).

4.6 Patch-clamp electrophysiology

Whole-cell currents were recorded using the patch-clamp technique in voltage-clamp mode, following standard protocols [157]. Recordings were performed at room temperature (20–25 °C) using either a Axopatch 200B or Multiclamp 700B amplifiers (Molecular Devices, Sunnyvale, CA, USA), connected to a personal computer via an Axon Digidata 1440 digitizer as can be visualize in Fig. 9A. Data acquisition was carried out using Clampex 10.7 software. Current traces were low-pass filtered using the amplifier's built-in 4-pole Bessel filters and sampled at 4–50 kHz, ensuring a sampling rate at least twice the filter cutoff frequency. Micropipettes were fabricated from GC150F-7.5 borosilicate glass capillaries (Harvard Apparatus, Holliston, MA, USA or Kent, UK) using a Sutter P2000 laser puller, yielding a tip resistance of 3–6 MΩ in the bath solution. Only recordings with leak currents at the holding potential (V_h) of less than 10% of the peak current at the test potential were included in the analysis. Solutions were applied to cells using a gravity-driven microperfusion system equipped with an AutoMate Perfusion Pencil Multi-Barrel Manifold Tip (AutoMate Scientific, Berkeley,CA, USA) at a flow rate of approximately 200 µl/min. Excess bath solution was continuously removed from the recording chamber using vacuum suction (graphic representation in Fig. 9B.).

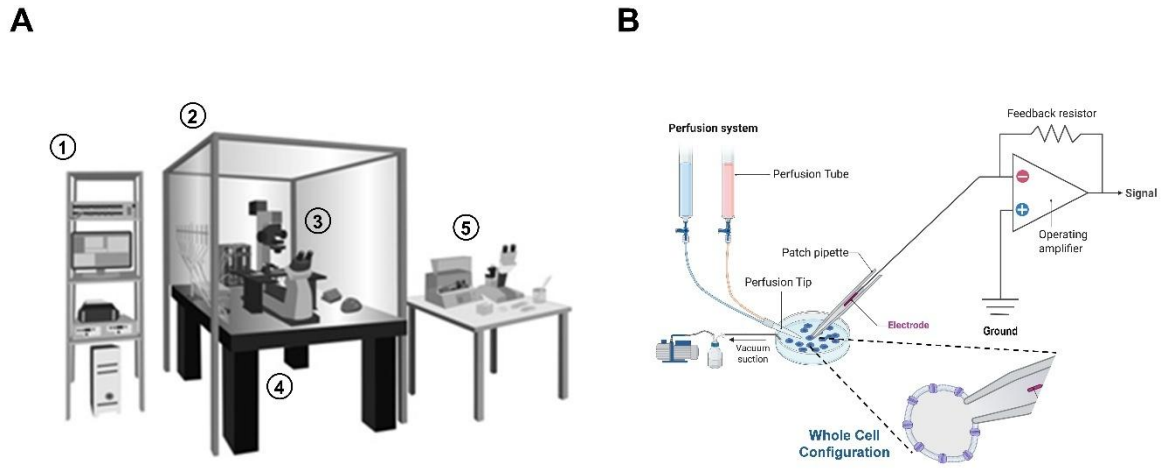

Figure 9: **Cartoon representation of patch-clamp electrophysiology setup.** (A) Components of the setup. (1) Axopatch 200B or Multiclamp 700B amplifiers and computer system, (2) Faraday's cage, (3) Microscope with micromanipulators alongside the perfusion system, (4) Air/anti vibration table, and (5) Sutter P2000 laser puller for making micropipettes. (B) Cells are patched in a whole cell configuration using micropipettes. Gravity fed perfusion system with flowrate of 200 µl/min, is used for perfusing cells with different solutions. Vacuum pump is attached for the constant removal of excess fluid.

4.6.1 Solutions

For patch-clamp measurements, extracellular and intracellular solutions were generally prepared according to the compositions listed in table 4 for the respective ion channels. In TEA^+-containing solutions, Na^+ was equimolarly replaced by tetraethylammonium chloride (TEA-Cl). The osmolarity of the extracellular solutions ranged between 302–308 mOsm/L, while intracellular solutions had an osmolarity of approximately 295 mOsm/L. All extracellular solutions were supplemented with 0.1 mg/mL bovine serum albumin (BSA) to prevent adsorption of toxins to the plastic surfaces of the perfusion system. The internal solution of KCa2.2 and KCa3.1 also contain ~1−2 µM of free Ca^{2+} based on the MaxChelator program WEBMAX-C software (C. Patton, Stanford University, https://somapp.ucdmc.ucdavis.edu/pharmacology/bers/maxchelator/webmaxc/webmaxcE.htm .

Table 4: **Recipe for extracellular/bath and intracellular/pipette solution for patch-clamp recordings for all ion channels included in this work**

Components	Extracellular solution	Intracellular Solutions		
		Kv1.x and KCa1.1	Kv11.1	KCa2.2 and KCa3.1
NaCl (mM)	145	-	-	-
KCl (mM)	5	-	140	-
$CaCl_2$ (mM)	2.5	1	-	8.5
$MgCl_2$ (mM)	1	2	2	2
HEPES (mM)	10	10	10	5
Glucose (mM)	5.5	-	-	-
KF (mM)	-	140	-	-
EGTA (mM)	-	11	10	10
K^+-aspartate (mM)	-	-	-	150
pH	7.35	7.22	7.22	7.22

4.6.2 Voltage protocols

To evoke the K^+ currents from Kv1.x channels, depolarization pulses to +50 mV from a holding potential (V_h) of −120 mV were applied every 15 s. The duration of depolarization pluses was 15 ms for Kv1.3, 50 ms for Kv1.1 and Kv1.5. However, for Kv1.2, 15-500 ms long pulses were used to achieve the saturated peak current due to the variable activation kinetics of this channel as discussed previously [71]. For Kv11.1 channels, currents were elicited by applying a voltage step to +20 mV for 1.25 s from a V_h of –80 mV followed by a step to –40 mV for 2 s, during which peak currents were measured, with pulses delivered every 30 s. mKCa1.1 currents were recorded by applying 600-ms-long voltage steps to +100 mV from a

V_h of –100 mV. KCa2.2 and KCa3.1 currents were recorded by applying a 150-ms-long voltage ramps to +50 mV from -120 mV every 10 s, the V_h was set to –85 mV.

4.7 Data analysis and statistics

The Clampfit 10.7 software package (Molecular Devices, Sunnyvale, CA, USA) was used to analyze current recordings. Before analysis, all current traces were digitally filtered using three-point boxcar smoothing and were corrected for ohmic leakage, only if required. The blocking effect of the toxin at a given concentration was calculated as remaining current fraction (RCF = I/I_0), where I represent the peak current at equilibrium block at a given toxin concentration or peak current recorded after 3 min perfusion of toxin solution in the absence of measurable block and I_0 is the peak current in the absence of the toxin. Data points in the concentration-response curve represent the mean RCF values of three to six individual cells, with error bars denoting the standard error of the mean (SEM). The Hill equation was fitted to the datapoints obtained at each concentration

$$\mathrm{RCF} = \frac{\mathrm{K_d^H}}{\mathrm{K_d^H} + [\mathrm{Toxin}]^{\mathrm{H}}} \qquad (1)$$

where K_d is the dissociation constant, H represents the Hill coefficient and [Toxin] is the concentration of the toxin.

To study the binding kinetics of Cvill toxins, peak current during the application of toxin at time point t (I_t) were normalized to the peak current (I_0) before the toxin exposure ($I_{norm} = I_t/I_0$) and plotted as a function of time. The association time constant (τ_{on}) were determined by the fitting a single exponential function to the data points during the toxin wash-in procedure (equation 2, one-phase decay to RCF) and for the dissociation time constant (τ_{off}), a single exponential function rising to maximum were fitted to data points during the wash-out procedure (equation 3, RCF followed by one-phase association) for individual cells [142, 158].

$$\mathrm{I_{norm}(t)} = \mathrm{RCF} + \left((1 - \mathrm{RCF}) \times \mathrm{e}^{-\frac{\mathrm{t}}{\tau_{on}}} \right) \qquad (2)$$

$$\mathrm{I_{norm}(t)} = \mathrm{RCF} + \left((1 - \mathrm{RCF}) \times \left(1 - \mathrm{e}^{-\frac{\mathrm{t}}{\tau_{off}}} \right) \right) \qquad (3)$$

The time constants (τ_{on} and τ_{off}) were used to calculate the association rate constant (k_{on}) and dissociation rate constant (k_{off}) based on a simple bimolecular interaction between the channel and the toxin, and using equation 4 and equation 5, respectively [124, 154, 159].

$$k_{on} = \frac{1 - (\tau_{on} \times k_{off})}{\tau_{on} \times [toxin]} \quad (4)$$

$$k_{off} = \frac{1}{\tau_{off}} \quad (5)$$

To construct the voltage-dependance of steady-state activation of $K_V1.2$, peak conductance (G) at different test potential (−60 to +100 mV in 10 mV steps) was calculated from peak current (I) at a test potential (E_m) and the K^+ reversal potential (E_K) using chord-conductance equation $G = I/(E_m - E_K)$. The G values were normalized (G_{norm}) to the maximum value and plotted as a function of test potential and data points were fitted with Boltzmann sigmoidal equation:

$$G_{norm} = \frac{1}{1 + e^{\left(\frac{V_{50} - E_m}{k}\right)}} \quad (6)$$

where V_{50} is the midpoint voltage, E_m is the test potential, and k represents slope factor of the function.

Representative graph plotting and statistical analysis were conducted using Graph pad prism software package (version 8.0.1, La Jolla, CA, USA). All the data was presented with standard errors of mean (SEM). For pairwise comparison, Student's *t*-test was used and for multiple comparisons, one-way ANOVA with post-hoc Dunnet's test was performed. Statistical significance is indicated in terms of P values.

5. RESULTS

5.1 Pharmacological characterization of seven novel peptide toxins isolated from *Centruroides bonito*

Our laboratory has a longstanding collaboration, spanning over two decades, with Prof. Lourival D. Possani and his research team at the Institute of Biotechnology, UNAM, Mexico. Over the years, this partnership has led to the identification and characterization of numerous peptide toxins isolated from scorpion venom. The processes of scorpion collection, venom extraction, and initial purification of peptides are carried out in Prof. Possani's laboratory. Subsequent pharmacological and functional characterization, including single-cell electrophysiology is primarily conducted in our facility.

The city of Acapulco, in the state of Guerrero, Mexico, has a newly described scorpion species that belongs to family *Buthidae*, named *Centruroides bonito*. This venom of *C. bontio* is toxic with a LD_{50} value of 16.7 μg/20g mouse body [150]. This species is known to cause envenomation in humans [160]; however, its venom has not yet been fully characterized. Accordingly, we have reported the proteomic analysis of the venom of *C. bonito* leading to the isolation of seven novel peptide toxins named CboK1 to CboK7. Peptide name, amino acid sequence and length (in terms the number of amino acid residues) and molecular weight of all seven peptides are enlisted in Table 5.

Table 5: **Amino acid sequences and MW of isolated peptide toxins from *C. bonito.***

Peptide Name	Amino Acid Sequence	Length	MW (Da)
CboK1	---NVACVH-RTCDSNCKR--NGYKSGKCINRKCNCYPH	33	3765.1
CboK2	----TVCVY-RTCDKDCKR--RGYRSGKCINNACKCYPY	32	3760.4
CboK3	TIINVKCTSPKQCLKPCKDLYGPHAGEKCMNGKCKCYKV	39	4323.5
CboK4	TFINVKCTSPKQCLKPCKDLYGPHAGEKCMNGKCKCYKP	39	4357.9
CboK5	IFINVKCSLPQQCLRPCKDRFGQHAGGKCINGKCKCYP-	38	4249.8
CboK6	TTINVKCSLPQQCLRPCKDRFGQHAGGKCINGKCKCYP-	38	4191.3
CboK7	TFINVKCTSPKQCLPPCKEIYGIHAGAKCMNGKCKCYKV	39	4298.5

Comparative analysis of CboK toxins showed that they can be allocated to four groups with three different lengths in the primary sequence (Fig. 10.). The first group is made up of toxins CboK1 (α-KTx 10.5) and CboK2 (α-KTx 10.6) with lengths of 32 to 33 amino acid residues (Fig. 10A.). The toxins Cobatoxin-1 (α-KTx 10.1), Cobatoxin-2 (α-KTx 10.2) from *C.*

noxius, and Toxin II.10.4 (α-KTx 10.4) from *C. tecomanus* share between 84 and 97% amino acid identity with CboK2 (α-KTx 10.6), whereas CboK1 (α-KTx 10.5) shares only 64% sequence identity with CboK2 (Fig. 10A.). The second group contains CboK5 and CboK6 (38 amino acid residue peptides), where CboK5 (α-KTx 2.10) displayed 100% sequence identity with an already described toxin Ce3 isolated from the venom of *Centruroides elegans* (α-KTx 2.10), whereas CboK5 and CboK6 (α-KTx 2.21) share 95% identity (Fig. 10B.). The third group is composed of toxins with 39 amino acids residues. CboK3 (α-KTx 2.22) and CboK4 (α-KTx 2.23) display >90% identity with toxin II.12.5 (α-KTx 2.16) from *C. tecomanus* and α-KTx 2.9 from *C. elegans* (Fig. 10C.). The fourth group has CboK7 toxin (α-KTx 2.24; C0HM78) which has >85% identity with toxin Ce4 (α-KTx 2.11) and Ce5 (α-KTx 2.12) from *C. elegans* (Fig. 10D.). Based on the high identity percentage, CboK1 and CboK2 emerged as new members of α-KTx family 10 with systematic name, α-KTx 10.5 and α-KTx 10.6, respectively. CboK3 to CboK7 toxins are classified as the new members of α-KTx family 2 with systematic names α-KTx 2.22, α-KTx 2.23, α-KTx 2.10, α-KTx 2.21, and α-KTx 2.24, respectively.

5.1.1 Pharmacological characterization of CboK Peptides

The sequence analysis shows that the seven CboK peptide toxins possess a great deal of resemblance to the α-KTxs family toxins that are known to block voltage-gated K^+ channels. Based on the percentage identity of CboK peptides with other α-KTxs and the literature available for the activity of closely related peptides, Kv1.1, Kv1.2, and Kv1.3 K^+ channels were considered as the potential target of CboK peptides. Macroscopic Kv1.1 and Kv1.2 currents were measured in transiently transfected CHO cells (see Materials and Methods for details). To record Kv1.3 currents, human peripheral T lymphocytes were activated with Phytohemagglutinin A (PHA) to boost Kv1.3 expression. Ca^{2+}-free intracellular solution was used to avoid the KCa3.1 channel opening. Thus, whole-cell currents were measured exclusively from Kv1.3 ion channels [142, 161]. Currents were evoked by applying 15-ms-long de-polarization pulses to +50 mV from a holding potential (V_h) of −120 mV except for Kv1.2, as it has highly variable activation kinetics (discussed in section 2.2.2); therefore, 15–500 ms-long pulses were applied to maximize the open probability of Kv1.2 channel [71]. All peptide toxins were dissolved in a freshly prepared bath solution supplemented with 0.1 mg/ml BSA and applied to the cells in whole cell patch configuration using a gravity-driven micro perfusion system at a flow rate of 200 µl/min. The complete exchange of solutions in the bath chamber and the proper functioning of the perfusion system were regularly verified using fully reversible inhibitors as positive controls at a concentration equivalent to their K_d values, i.e., 0.3 mM

tetraethylammonium (TEA) for Kv1.1 (Fig. 11A.), 14 nM Charybdotoxin (ChTx) for Kv1.2 (Fig. 11B.), and 10 mM TEA for Kv1.3 (Fig. 11C.). Approximately 50% reduction in K^+ current at equilibrium block in the presence of positive controls served as an indication of the expression of the proper ion channel and a complete solution exchange in recording chamber.

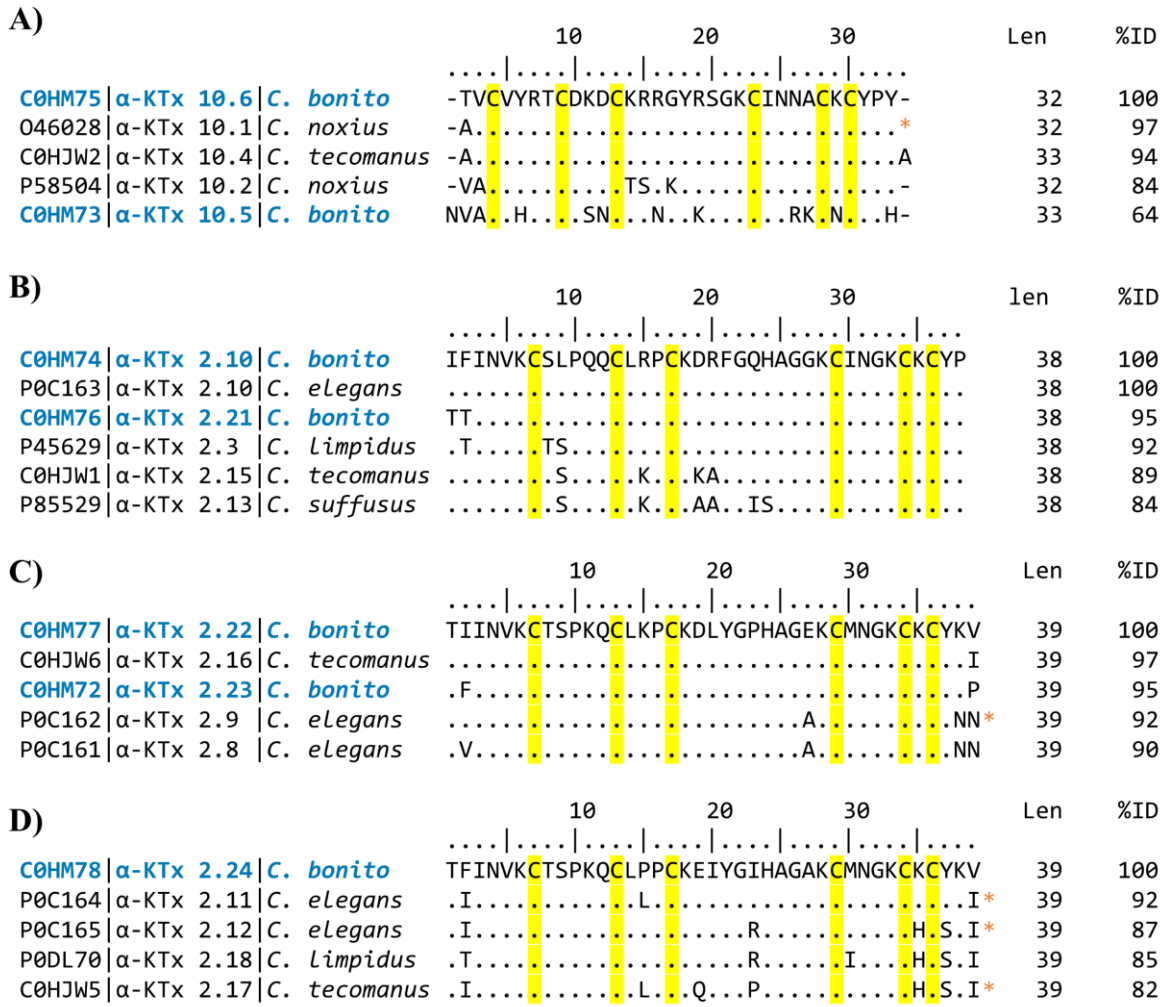

Figure 10: **Multiple alignments of *C. bonito* toxins (text in blue) and other closely related scorpion potassium toxins.** KaliumDB sequences closely related to **(A)** CboK1 (α-KTx 10.5) and CboK2 (α-KTx 10.6); **(B)** CboK5 (α-KTx 2.10) and CboK6 (α-KTx 2.21); **(C)** CboK3 (α-KTx 2.22), CboK4 (α-KTx 2.23); **(D)** CboK7 (α-KTx 2.24) are shown. The UniProt access code is shown on the left, followed by the systematic name and species name. Len indicates mature chain length; %ID indicates percent amino acid identity. Conserved cysteine residues are highlighted in yellow. Identical positions to C. bonito toxins are indicated by dots. (*) indicates that the C-terminal is amidated.

The representative whole-cell current traces for Kv1.1, Kv1.2 and Kv1.3 channels, recorded sequentially in the same cell for each channel, in the presence of control solution

(black trace), and at equilibrium block while perfusing the cell with positive control (red trace) or the CboK7 toxin at concentration of 100 nM in case of Kv1.1 and Kv1.3 and 1 nM for Kv1.2 (purple trace), are shown in Fig. 11A–C. At steady-state block, CboK7 inhibited ~42% of Kv1.1 and ~80% of Kv1.3 currents at 100 nM and >99% of Kv1.2 currents at 1 nM concentration. Fig. 11D–F. represents the summarized pharmacological screening data of CboK1 to CboK7 toxins for Kv1 channels. Generally, all the peptides were tested at 100 nM concentration (represented with hatched bars) except CboK2 to CboK7 peptides in case of Kv1.2, where 1 nM concentration (shown with purple filled bars) was used for screening due to the high affinity blockade of Kv1.2 by these peptides.

We found that CboK3 and CboK4 block less than 10% the Kv1.1 currents at 100 nM concentration; however, CboK7 showed ~42% block of Kv1.1 at this concentration (Fig. 11D.). The low blocking potency, combined with the limited availability of CboK peptides from the native source, precluded further investigation of their concentration-dependent inhibitory effects on the Kv1.1 channel. Fig. 11E. displays a 60-92% reduction in Kv1.2 currents by CboK2 to CboK6 peptides at 1 nM concentration and total insensitivity to 100 nM of CboK1 toxin. CboK7 showed outstanding potency for Kv1.2 by inhibiting ~96% of the current at 1 nM concentration. In the case of Kv1.3, CboK2–CboK7 peptides demonstrated moderate inhibitory effects with 41–81% block at 100 nM, whereas CboK1 showed less than 4% inhibition (Fig. 11F.).

5.1.2 Potent inhibition of Kv1.2 by CboK peptides at picomolar concentrations

All CboK peptides except CboK1 exhibited significant inhibiting effects on Kv1.2 currents when tested at 1 nM concentration. The initial screening experiments motivated us to conduct a more detailed study to characterize the inhibitory activities of CboK peptides on the Kv1.2 channel. Fig. 12A. shows the representative Kv1.2 current traces before and after application of 1 nM CboK5 which blocked ~75% of the peak current. The onset and recovery from the block of Kv1.2 currents at 1 nM concentration of CboK5 are shown in Fig. 12B. Normalized peak currents ($I_{norm} = I_t/I_0$, where I_t is the peak current in the presence of the toxin at time t and I_0 is the peak current in the control solution at t = 0), were plotted as a function of time. The block was completely reversed by applying a toxin-free solution to the cell. The kinetics of both association and dissociation of all the CboK peptides were very slow as represented for CboK5 peptide as an example (Fig. 12B.). It took several minutes to achieve equilibrium block and to recover fully the peak current that was measured prior to the

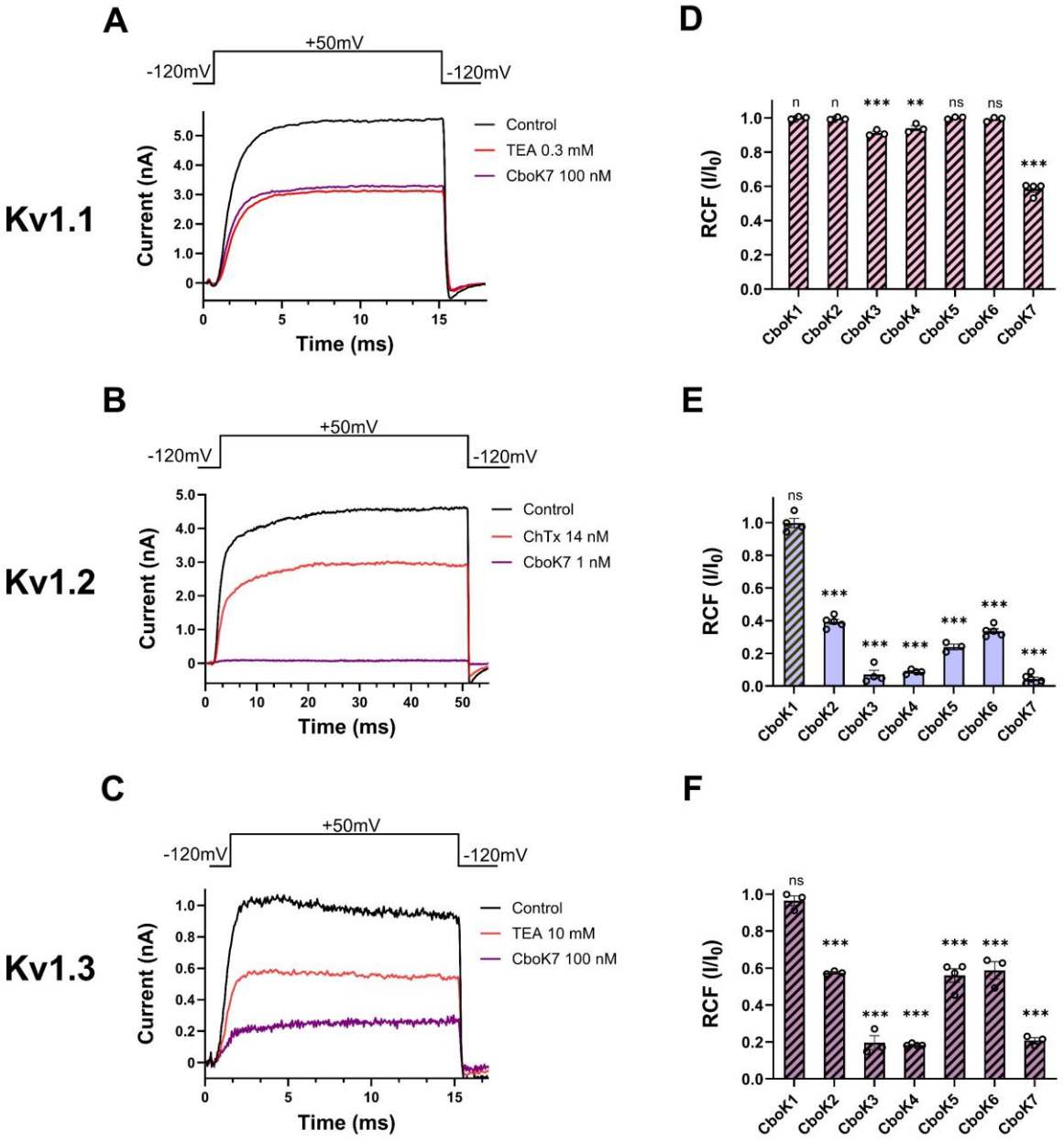

Figure 11: **Inhibition of Kv1 channels by CboK7 peptide toxin. (A–C)** Whole-cell Kv1.1 **(A)** and Kv1.2 **(B)** currents were recorded in transiently transfected CHO cells whereas Kv1.3 currents **(C)** were measured in an activated human peripheral T lymphocyte. Here, 15-ms (for Kv1.1 and Kv1.3) or 50-ms-long (Kv1.2) voltage pulses were applied to +50 mV from a holding potential of −120 mV and current traces were recorded every 15 s. Representative traces show the K^+ currents in the control solution (black), at equilibrium block when applying 0.3 mM TEA^+ (**A**), 14 nM ChTx **(B)**, or 10 mM TEA^+ **(C)** as a positive control (red) for respective ion channel or the toxin CboK7 (purple, 100 nM for Kv1.1 **(A)** and Kv1.3 **(C)**, and 1 nM for Kv1.2 **(B)**). **(D–F)** Effect of CboK1 to CboK7 toxins on Kv1.1, Kv1.2, and Kv1.3 ion channels. Bars with individual data points (empty circles) indicate the remaining current fraction (RCF = I/I_0,

where I_0 = peak current in toxin-free solution and I = peak current in the presence of toxin at given concentration at equilibrium block, see Materials and Methods for detail) values obtained from individual records at 100 nM for Kv1.1 **(D)** and Kv1.3 **(F)** (represented with hatched bars), and 1 nM for Kv1.2 (represented with filled bars) **(E)** except for CboK1 which was tested at 100 nM concentration (indicated with hatched bar). Error bars indicate ± SEM ($n \geq 3$). Statistical differences between RCF value at given concentration of respective toxin and RCF value in control condition were compared via one-way ANOVA with post-hoc Dunnet's test and marked with ns = not significant; **, $p < 0.01$; ***, $p < 0.001$

application of toxin. Consequently, slow toxin association and dissociation kinetics led us to generate the concentration–response curves for CboK peptides in a cumulative manner.

The concentration–response relationships of CboK2 to CboK6 for Kv1.2 channel inhibition are shown in Fig. 12C. Different concentrations of each peptide were applied to the cells for a sufficient period to achieve the equilibrium block, considering the slow blocking kinetics, especially at low toxin concentrations. The RCF values were calculated, and the Hill equation was fitted to the data points (see Materials and Methods for specifics) to obtain the characteristic of the concentration–response curves. The resulting dissociation constants (K_d) and the Hill coefficients were K_d = 763 pM and H = 1.5 for CboK2, K_d = 106 pM, and H = 1.2 for CboK3, K_d = 125 pM and H = 1.0 for CboK4, K_d = 376 pM and H = 1.2 for CboK5, K_d = 585 pM and H=1.3 for CboK6, and K_d = 24 pM and H = 1.3 for CboK7, respectively (Fig. 12C.). Out of all seven CboK peptides, CboK7 demonstrates outstanding with a high affinity for Kv1.2 with a K_d value of 24 pM.

5.1.3 Inhibition of Kv1.3 by CboK peptides

Kv1.3 ion channel currents were also sensitive to CboK peptides as demonstrated in the initial screening experiments earlier (Fig. 11.). Therefore, we aimed to investigate the effect of these peptides in a concertation-dependent manner on Kv1.3. The affinity of CboK1 for Kv1.3 was quite low in the screening and due to limited supply of native toxins from venom, the full concentration–response relationship was not possible to obtain. Data were not obtained for CboK5 either, as it is 100% identical to a previously known α-KTx 2.10 (Toxin Ce3), which was already characterized for Kv1.3. Fig. 13A. shows the whole-cell Kv1.3 current traces recorded chronologically in one cell in the presence of control solution (black trace) and after reaching the equilibrium block upon application of 10 mM TEA (as positive control, red trace) or in the presence of 100 nM of CboK3 (blue trace). CboK3 at 100 nM concentration inhibited

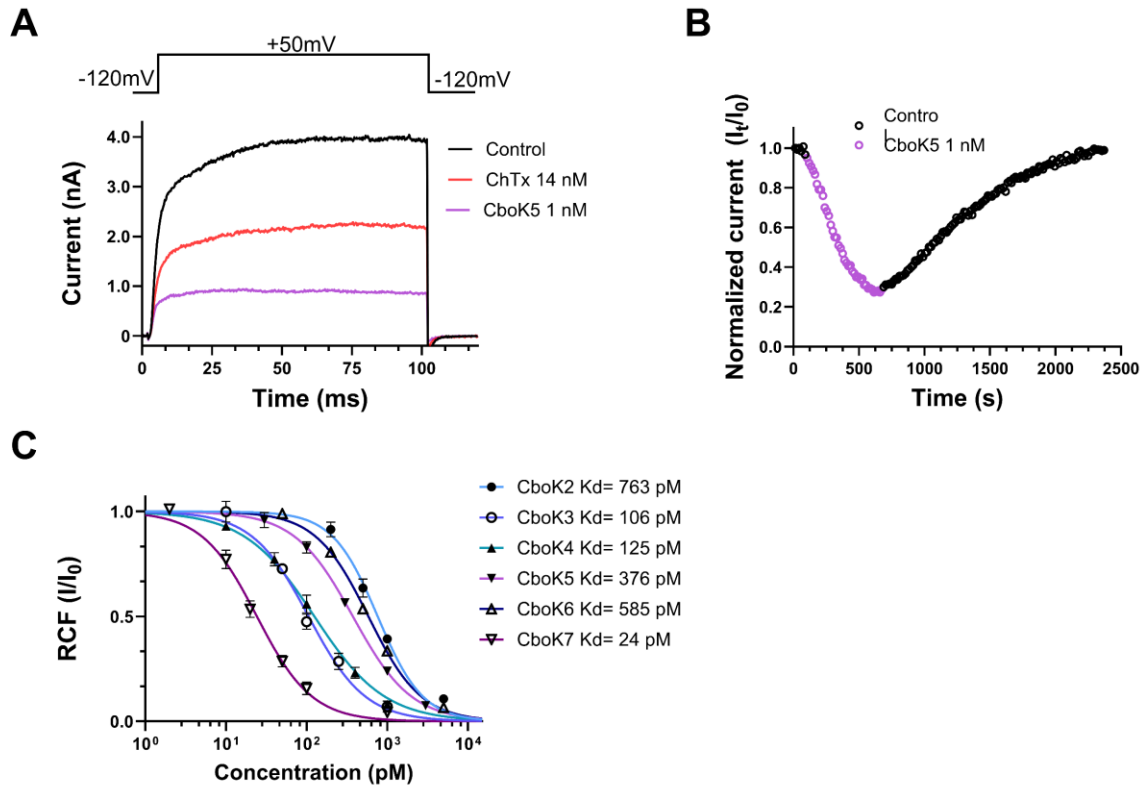

Figure 12: **Effect of CboK peptide toxins on Kv1.2 currents. (A)** Whole-cell currents were evoked in a CHO cells, transfected with the *KCNA2* gene, encoding Kv1.2, by applying 100 ms long depolarization pulses to +50 mV from a holding potential of −120 mV every 15 s. Current traces were recorded in the presence of control solution (black), at equilibrium block by 14 nM ChTx as positive control (red) or by 1 nM CboK5 (purple). **(B)** Development of and recovery from the block of Kv1.2 current. Normalized peak currents ($I_{norm} = I_t/I_0$, see text in section 5.1.2) were plotted as a function of time. Data points in purple (empty circles) represent the application of 1 nM of CboK5 and upon reaching the equilibrium block, cells were perfused with toxin-free bath solution to determine the reversibility of inhibition (empty circle in black). **(C)** Concentration-dependent block of Kv1.2 by CboK peptides. The remaining current fractions (RCF = I/I_0, where I_0 = peak current in toxin-free solution and I = peak current in the presence of toxin at given concertation at equilibrium block) values were plotted against the toxin concentration and data points were fitted with the Hill equation. The best fit resulted in K_d values of 763 pM, 106 pM, 125 pM, 376 pM, 585 pM, and 24 pM for CboK2 to CboK7, respectively. Error bars indicate mean ± SEM and n ≥ 3.

~80% of the current. The development of steady-state block and recovery of the initial current at various concentrations of CboK3 toxin is presented in Fig. 13B.

Kv1.3 channel inhibition by CboK3, as well as by the other CboK peptides, was fully reversible upon washout with toxin-free external solution. Notably, the binding kinetics to

Kv1.3 were significantly faster compared to those observed for Kv1.2. At all tested concentrations of CboK3 (5, 15, 40, 100, and 350 nM), the onset of steady-state block and complete recovery upon washout occurred within approximately one minute.

While studying the inhibition of Kv1.3 currents by CboK peptides, we observed an interesting phenomenon, i.e., the whole-cell current showed a steady increase during the 15-ms-long depolarization in the presence of the peptides, which was more obvious at high (>50 nM) peptide concentrations (Fig. 13A, C.). Therefore, the remaining current fractions, determined from the current amplitudes at the end of the depolarizations, were larger than at earlier time points, e.g., when the control traces already reached the peak (Fig. 13A., vertical dashed line). Given the very rapid dissociation of peptides, we hypothesized that the steady rise in the current may be the consequence of unbinding of the peptides, induced by the depolarized test potentials and the permeating potassium ions. This phenomenon, often referred to as the "knock-off" effect, is likely driven by the outward flux of permeating potassium ions during sustained depolarization [122, 124, 162]. To validate the presence of knock-off effect, we compared the inhibitory activity of the CboK2 peptide at 1 μM (sufficient native toxin material was available for this peptide only) at two different test potentials i.e., +50 mV and 0 mV applied for 15 ms (Fig. 13C, E.). There are two important differences in the currents between Fig. 13C. and E measured in the presence of CboK2. First, the steady increase in the current in the presence of CboK2 is absent in Fig. 13E., and second, the RCF measured at the end of the pulse in 1 μM CboK2 was ~0.34 at +50 mV (Fig. 13C.), whereas the RCF value was ~0.23 at 0 mV (Fig. 13E.). The statistical analysis showed that the RCF is smaller at 0 mV test potential as compared to the one determined at +50 mV test potential (Fig. 13G.). Another indication of the dissociation of the peptide from Kv1.3 at depolarized test potentials is shown in Fig. 13D. when 1000 ms depolarizing test pulses were applied to +50 mV. The Kv1.3 current shows a characteristic inactivation kinetics in the absence of the peptides (black) whereas the kinetics is drastically altered in the presence of 1 μM CboK2 (blue): (1) there is an additional, very slow component of the activation kinetics of the current, (2) the absence of the sharp peak of the current, (3) the slow and incomplete inactivation kinetics, and (4) the crossover of the current traces recorded in control solution or in the presence of CboK2. These characteristic changes in the shape of the Kv1.3 current are consistent with time-dependent unbinding of the CboK2 during the depolarization. Repeating the experiment shown in Fig. 13D. at 0 mV test potential (Fig. 13F.) demonstrates the unbinding of CboK2 is decreased (i.e., more block), and the very slow component of current activation is virtually missing. On the other hand, the

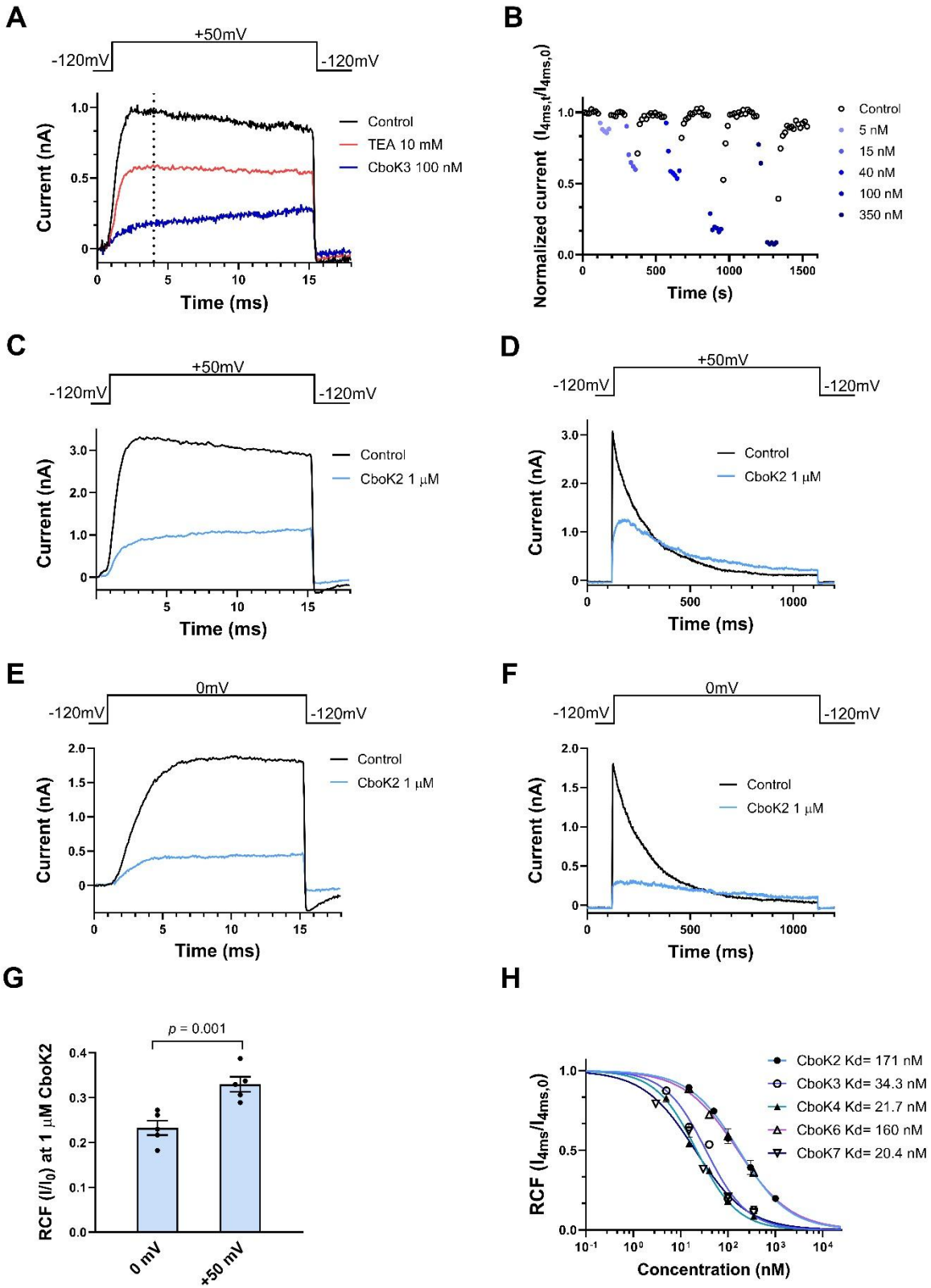

Figure 13: **Inhibition of Kv1.3 currents by CboK peptides. (A)** Whole-cell currents through Kv1.3 in a human T lymphocyte were evoked by applying 15-ms-long depolarization pulses to +50 mV from a holding potential of −120 mV every 15 s. Current traces were recorded in the control solution (black) and at equilibrium block by 10 mM TEA (red) or 100 nM of CboK3

(blue). The vertical dashed line indicates the isochronal time point (4 ms) at which Kv1.3 peak currents were taken. **(B)** Time course of development and removal of Kv1.3 current blockage by different concentrations of CboK3 peptide. Normalized currents were determined at the 4 ms time point ($I_{norm} = I_{4ms,t}/I_{4ms,0,}$ see text, isochronal RCF) and plotted against time. Data points in shades of blue (filled circles) represent the application of CboK3 (5−350 nM) to the cell. After reaching the inhibition equilibrium at each concentration of toxin, cells were perfused with the control solution (lacking the toxin) to display the reversibility of the block (data points in black, empty circles). **(C–F)** The voltage-dependent inhibition of the Kv1.3 current by 1 μM of CboK2. The T cell was depolarized by applying voltage steps of +50 mV **(C and D)** or 0 mV **(E and F)** from −120 mV holding potential for 15 ms or 1 s long durations as indicated above the panel, every 15 s (for 15-ms-long depolarizations) or every 60 s (for 1-s-long depolarization). The current traces were recorded in the presence of external solution (black traces) or at equilibrium block in the presence of 1 μM CboK2 (light blue traces). **(G)** Statistical analysis of RCF (I/I_0) values obtained during 15-ms-long depolarization at 0 mV (panel E) and +50 mV (panel C). The filled black circles indicate individual data points. Error bars represent the mean ± SEM (n = 5). The p value from paired t-test is given above the bar plots. **(H)** Concentration-dependent inhibition of Kv1.3 by CboK peptides. Isochronal RCF ($I_{4ms}/I_{4ms,0}$) values were plotted as a function of toxin concentration and data points were fitted with the Hill equation (see Materials and Methods). Error bars indicate mean ± SEM and n ≥ 3. The best fits resulted in K_d values as indicated.

changes in the inactivation kinetics are still observable (slow and incomplete inactivation and crossover).

The data above indicate that at a test potential of +50 mV, significant unbinding of CboK toxins occurs. As a result, 0 mV test potential should be used to determine the RCF values accurately from the peak currents, since unbinding is minimal at that voltage. However, due to the insufficient quantity of native peptides, we were unable to repeat the experiments at 0 mV test potential, where peak currents are reliably determined in the absence of significant unbinding. Therefore, for concentration–response curves, current amplitudes were determined at the isochronal time point of 4 ms as indicated with vertical dashed line in Fig. 13A., where the control traces would display the peak current. Isochronal RCF data points obtained this way (isochronal RCF = $I_{4ms}/I_{4ms,0}$ where $I4_{ms,0}$ and I_{4ms} are the currents at 4 ms time point in the absence and presence of CboK peptides, respectively) at different toxin concentrations and were fitted with the Hill equation to obtain concentration–response curves of CboK peptides as shown in Fig. 13H. The resulting K_d values and the Hill coefficients were K_d = 171 nM (H = 0.8) for CboK2, K_d = 34.3 nM (H = 0.96) for CboK3, K_d = 21.7 nM (H = 0.94) for CboK4, K_d = 160 nM (H = 0.77) for CboK6 and, K_d = 20.4 nM (H = 0.8) for CboK7, respectively.

5.2 Pharmacological characterization of two new peptide toxins from venom of *Centruroides villegasi*

A new species of scorpion from the genus *Centruroides*, named *C. villegasi* was described in the town of Chilapa, in state of Guerrero, Mexico [163]. The venom of *C. villegasi* is toxic with a LD_{50} value of 12.2 µg/20g of mouse body [164]. The venom extraction of scorpion *C. villegasi*, purification and primary amino acid sequence determination was carried out in UNAM, Mexico, in Prof. Possani's Laboratory (as already described in section 5.1). The venom of *C. villegasi* was purified using a three-step purification scheme as published elsewhere [152]. In summary, the crude venom was purified using Sephadex G-50 column which resulted in three fractions (I-III). Out of the three, fraction II was toxic to mice and thus purified further using ion exchange chromatography (IEC). F-II yielded 12 subfractions which were further purified using HPLC. Two K^+ channels inhibiting peptides were found in subfraction F-II-10 and F-II-11, which were sequenced using Edman degradation and MW were determined using mass spectrometry. Table 6 enlists the details including peptide name, amino acid sequence, length (in terms of amino acid residues) and molecular weight of the two new peptides.

Table 6: **Amino acid sequences and MW of isolated peptide toxins isolated from *C. villegasi.***

Peptide	Amino Acid Sequence	Length	MW (Da)
Cvill6	IFINVKCDLPQQCLRPCKDRFGQHAGGKCINGKCKCYP-	38	4277.7
Cvill7	TFINVKCTSPKQCLKPCKDLYGPHAGGKCMNGKCKCYNN	39	4287.3

We initiated our study with a search for peptides, similar in sequence to Cvill peptides using BLASTP, followed by the alignment with MAFFT (version 7). The analysis revealed that both Cvill6 and Cvill7 share significant sequence similarities with members of the α-KTx 2 subfamily of scorpion K^+-channel blockers (Fig. 14A-B.). Cvill6 exhibited 97% identity to toxin Ce3 (α-KTx 2.10), 92% to CboK6 (α-KTx 2.21), and 92% to CIITx1 (α-KTx 2.3) as shown in Fig. 14A. In contrast, Cvill7 demonstrates 95% identity with toxin Ce1 (α-KTx 2.8), toxin Ce2 (α-KTx 2.9), and Ct28 (α-KTx 2.20) as shown in Fig. 14B. Considering this high identity index, Cvill6 and Cvill7 were classified as α-KTx 2.25 and α-KTx 2.26, respectively and the newest members of the α-KTx 2 subfamily.

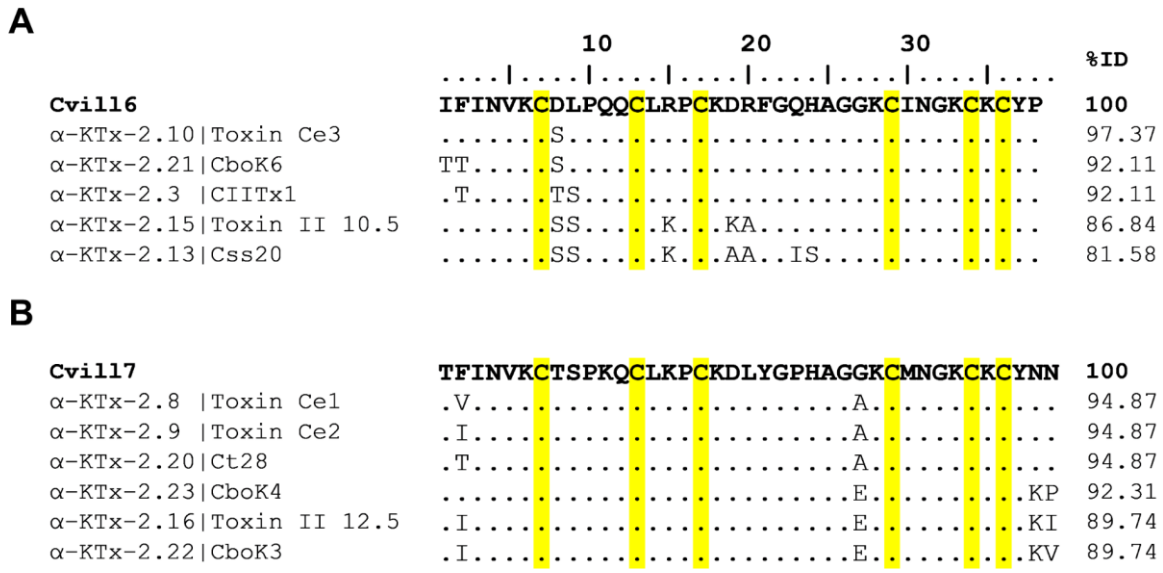

Figure 14: **Multiple sequence alignments of Cvill6 and Cvill7 peptide and other scorpion potassium toxins**. Peptide toxins closely related (>80% identical) to Cvill6 **(A)** and Cvill7 **(B)** are shown. The systematic name followed by the common names are shown in the left column. %ID indicates percent amino acid identity. Conserved cysteine residues are highlighted in yellow.

The three-dimensional (3D) structures of Cvill6 and Cvill7 peptides (Fig. 15A-B.) were predicted using AlphaFold3, an artificial intelligence (AI) structure-prediction tool based on machine learning [155]. The predicted structures of Cvill6 and Cvill7 are quite similar to the NMR solution structures of MgTx (α-KTx 2.2) and HgTx1 (α-KTx 2.5) which share >70% identity with Cvill peptides. The sequence and structural alignment of Cvill peptides and MgTx are shown in Fig. 15C. and 15D., respectively. Both Cvill6 and Cvill7 predicted structures reveal one α-helix connected to an anti-parallel β-sheet stabilized by 3 disulfide bonds (CS α/β), a similar motif found in the other known structures of α-KTx family of toxins. The α-KTx 2 family has six conserved cysteine residues with Cys1-Cys4, Cys2-Cys5 and Cys3-Cys6 bonds, identical disulfide connectivity for Cvill6 and Cvill7 were predicted by AlphaFold models (Fig. 15C.).

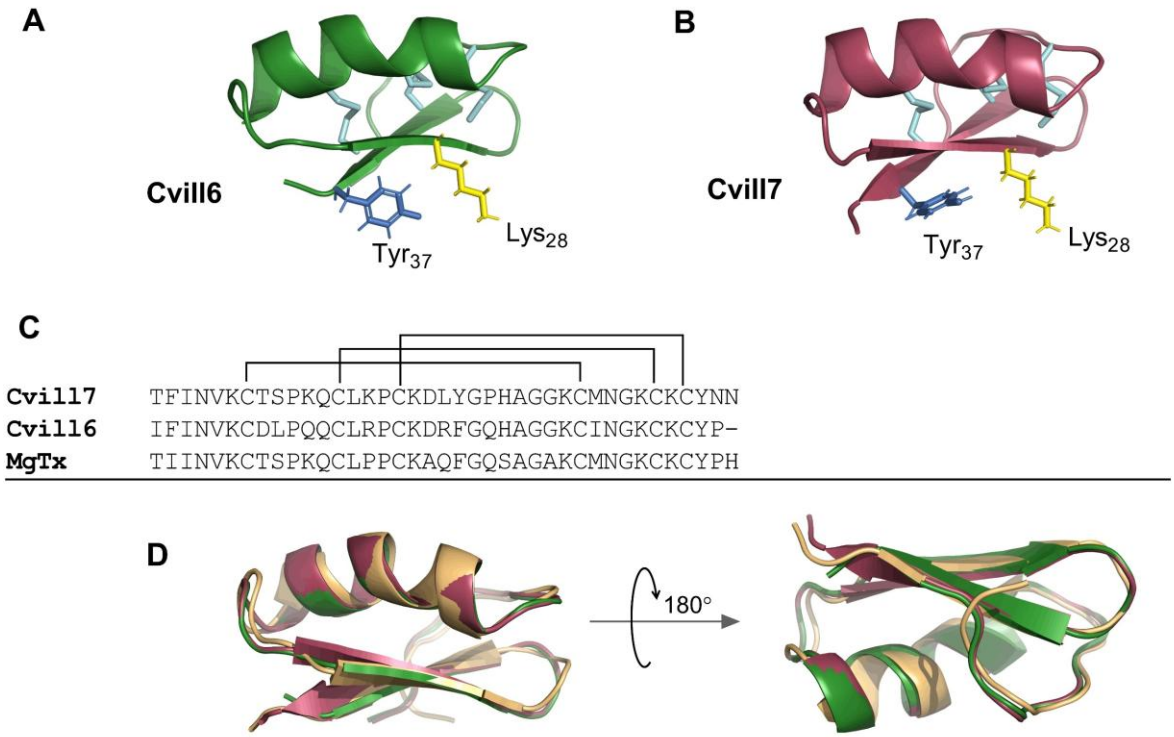

Figure 15: **Predicted 3D models of Cvill6 (A) and Cvill7 (B) obtained using AlphaFold3**. Ribbon rep-resentation (Cvill6 in forest green and Cvill7 in raspberry color) of backbone structure with dyad related residues indicated in colored (Tyr in blue and Lys in yellow) sticks and di-sulfide bonds shown in cyan sticks. **(C)** Primary sequence comparison of Cvill peptides and MgTx. Cysteines are shown in bold and similarity-based predicted disulfide connec-tivity are indicated above the sequence. **(D)** Structural alignment between predicted mod-els of Cvill6 (shown in forest green), Cvill7 (shown raspberry color) and MgTx (PDB: 1MTX, shown in light orange color).

5.2.1 Effect of Cvill peptides on voltage-gated potassium channels

The primary amino acid sequences of Cvill6 and Cvill7 exhibit a high percentage identity to members of the α-KTx 2 subfamily, which are generally known as inhibitors of Kv ion channels. Therefore, to pursue the quest of identifying a potent and selective Kv1.2 inhibitor we aimed to investigate the effects of Cvill6 and Cvill7 on Kv ion channels. Among the tested ion channels there were four members from the *Shaker*-related human Kv1 family, hKv1.1, hKv1.2, hKv1.3, and hKv1.5 (Fig. 16A-E.) and one member of human ether-a-go-go-related (hERG) cardiac K^+ channel hKv11.1 (hERG1, Fig. 16F.). For current recordings, Kv1.1, Kv1.2, and Kv1.5 were transiently expressed in CHO cells whereas for Kv11.1 a stable HEK293 cell line was used. To record Kv1.3 currents human peripheral T lymphocytes were used, details of

which are mentioned above (section 5.1.1). Appropriate voltage protocols were applied to record the K^+ currents from voltage-clamped cells in whole-cell configurations (described in section 4.6.2). The complete exchange of solutions in the bath chamber and the proper functioning of the perfusion system were regularly verified using fully reversible inhibitors as positive controls, such as TEA^+ for Kv1.1, Kv1.3, and Kv1.5; Charybdotoxin (ChTx) for Kv1.2; and E4031 1μM for Kv11.1. The inhibition of peak current upon perfusing the cell with these controls as shown in Fig. 16A-F. (traces in blue) served as an indication of the expression of the proper ion channel and the complete solution exchange in recording chamber.

Fig. 16A–F. shows the representative whole-cell K^+ current traces for various Kv channels, recorded sequentially in the same cell for the respective ion channel, in the absence of toxin (control, black trace) and in the presence of Cvill6 (green trace) or Cvill7 (red trace) toxin at a concentration of 1 nM (only for Kv1.2) or 100 nM. Traces in the presence of the toxins were recorded upon reaching the equilibrium block or after ~3 min of perfusion with toxin solution when no apparent block was observed. Representative records show that Cvill6 blocked ~28% of Kv1.2 current (1 nM concentration, Fig. 16B.) but only ~13% of the Kv1.3 current is inhibited (100 nM concentration, Fig. 16D.). However, no change was observed in currents amplitudes for hKv1.1 (Fig. 16A.), hKv1.5 (Fig. 16E.), and hKv11.1 (Fig. 16F.) at 100 nM of Cvill6. On the other hand, Cvill7 blocked >97% of the Kv1.2 current at 1 nM concentration (Fig. 16C.), indicating an extraordinary potency. In addition, Cvill7 also inhibited the Kv1.1 (Fig. 16A.) and Kv1.3 (Fig. 16D.) currents by reducing ~32% and ~86% of the peak amplitudes at 100 nM concentration, respectively. Nevertheless, Cvill7 did not show any effect on Kv1.5 (Fig. 16E.) and Kv11.1 (Fig. 16F.) currents. Fig. 16G shows the summary of the inhibition of the Kv channels by Cvill toxins, indicating that Cvill6 affects only Kv1.2 and Kv1.3 while Cvill7 affects Kv1.1, Kv1.2 and Kv1.3. The estimated K_d values of Cvill6 from a single concentration, based on bimolecular interaction of channel and toxin (1:1) [124], yielded ~0.84 μM for Kv1.3. Similar estimates for Cvill7 yielded ~192 nM for Kv1.1. The quantity of native toxins was insufficient to conduct the full concentration-response analysis when the affinity of the toxin for a channel was low, estimated to be above 50 nM.

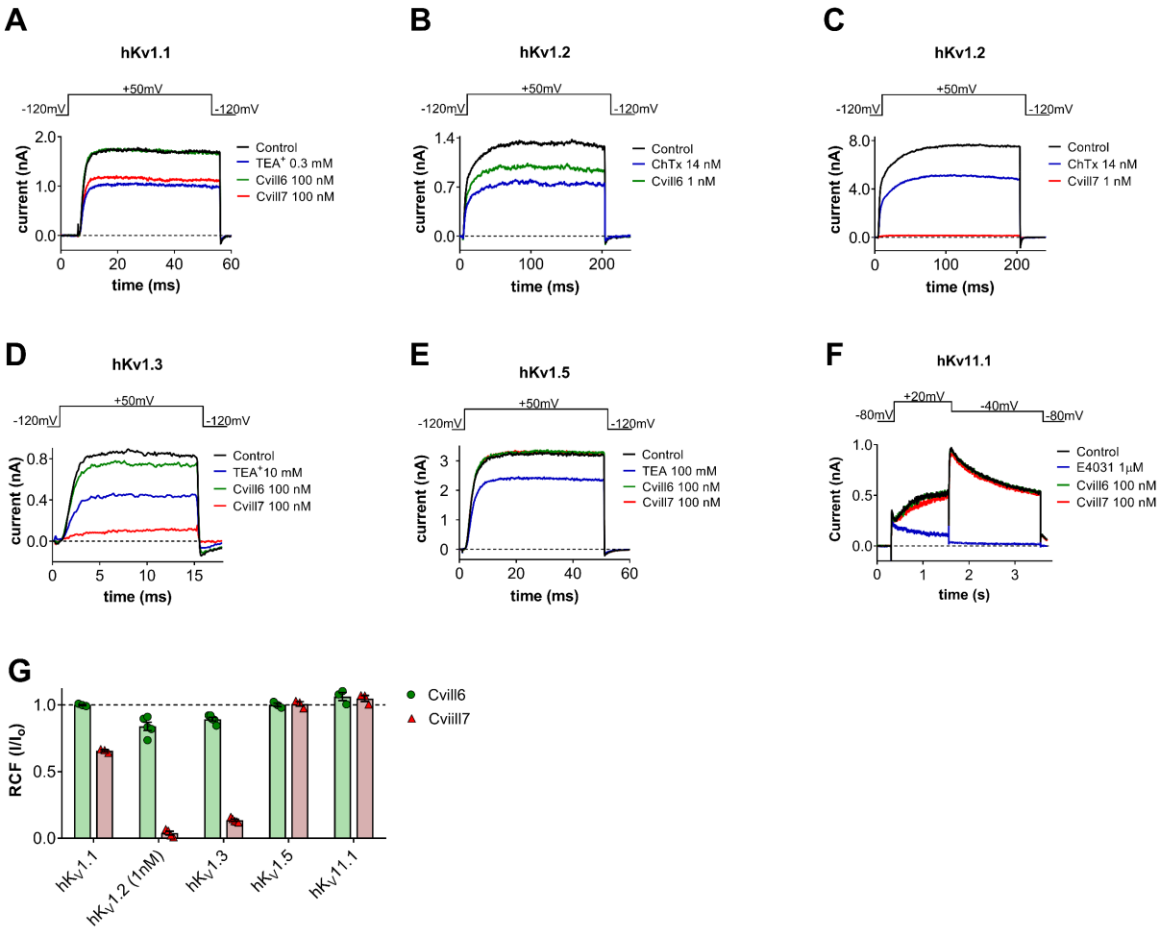

Figure 16: **Effect of Cvill6 and Cvill7 on Kv ion channels. (A–F)** Representative current traces shown for each channel were recorded in the absence (control, black) and in the presence of 100 nM (except panel C for Kv1.2, where 1 nM of either toxin was used) of Cvill6 (green) and Cvill7 (red) at steady-state block **(A-D)** or after 6-12 depolarization pulses (3 min **E-F**). Complete solution exchange in the recording chamber was confirmed using TEA^+: Tetraethylammonium chloride, ChTx: Charybdotoxin and E4031, known inhibitors of appropriate channels as indicated (blue). Voltage protocols are displayed above the current traces in each panel. For extracellular and intracellular solution composition see Materials and Methods section. **(G)** The remaining current fraction (RCF, I/I_0) values were calculated as the ratio of the peak currents in the presence (I) or absence (I_0) of 100 nM (or 1 nM for Kv1.2) of Cvill6 and Cvill7 at equilibrium block or after 3 min of toxin application. Bars (green: Cvill6, light red: Cvill7) with individual data points (green sold circles for Cvill6 or red solid triangles for Cvill7) represent the RCF values determined from individual cells. Error bars indicate the mean ± SEM (n = 3−6).

5.2.2 Cvill7 selectively inhibits Kv1.2 over Kv1.3 with low-picomolar affinity

Since Cvill7 peptide demonstrated remarkably high affinity towards Kv1.2 in our initial screening against Kv channels, we further extended our experiments to determine the concentration-dependent inhibition of Kv1.2 and Kv1.3 currents by Cvill7 and its binding

kinetics. The development and recovery of the block of Kv1.2 at 100 pM concentration of Cvill7 are shown in Fig. 17A. Normalized peak currents ($I_{norm} = I_t/I_0$, see material and methods for details) for individual cells (n = 4) were averaged and plotted against the time. The loss of Kv1.2 current apparently saturated to 96 ± 1.4% of the initial (t = 0) peak current in 7-8 min upon application of 100 pM of Cvill7. Fitting the individual block kinetics (cell-by-cell) using a single-exponential decay function (see section 4.7 for details) gave the time constant (τ_{on}) of 104 ± 15 s (n = 4) for the development of block. A representative fitting of single-exponential function to data points during wash-in procedure is shown in Fig. 18A. The dissociation kinetics of Cvill7 were also extremely slow. Equilibrium block was followed by application of toxin-free solution for ~15 min, during which just one-fifth of the blocked current recovered with extremely slow kinetics, suggesting that Cvill7 is a virtually irreversible inhibitor of Kv1.2. The dissociation constant (τ_{off}) of Cvill7 for Kv1.2 channel was 5978 ± 538 s (n = 4), obtained by fitting a single-exponential rising function to the normalized peak currents during the wash-out procedure (see section 4.7 for details) as demonstrated in Fig.18A. On the other hand, unlike Kv1.2 the block of Kv1.3 by Cvill7 was fully reversible with rapid association and dissociation kinetics (Fig. 17C.). The onset of equilibrium block to 67 ± 3% occurred with a τ_{on} of 20 ± 1.8 s (n = 3) upon 15 nM of toxin exposure and it fully recovered to initial normalized peak current with a τ_{off} of 34 ± 6 s (n = 3) upon perfusing the cell with toxin-free solution as shown in Fig. 17C. and Fig. 18B.

Assuming a simple bimolecular interaction between the toxin and the channel, the rate constants for association (k_{on}) and dissociation (k_{off}) were obtained from the time constants for the onset and recovery from the block using equations (4) and (5), respectively (see section 4.7 and [124] [142]). The rate constants obtained using these data are in Table 7.

To determine the concentration-dependence of current inhibition of Kv1.2 and Kv1.3 ion channels, different concentrations of Cvill7 peptide were applied to the cells for a sufficient amount of time, taking into account the slow blocking kinetics specifically at low picomolar concentrations. At low-picomolar concentrations the concentration-response curve was determined in a cumulative manner. The remaining current fractions (RCF) were determined using the ratio I/I_0 (for details see Materials and Methods section) and plotted as a function of toxin concentration. The concentration-response curves were obtained by fitting the data points with the Hill equation (refer to Materials and Methods for details). The best fit resulted in the K_d value of 16 ± 1.56 pM with a Hill coefficient (H) of 1.03 for Kv1.2 (Fig. 17B.) and K_d value

of 7.2 ± 0.64 nM with an H coefficient of 0.73 for Kv1.3 (Fig. 17D.). Thus, Cvill7 displays ~450-fold selectivity for Kv1.2 over Kv1.3.

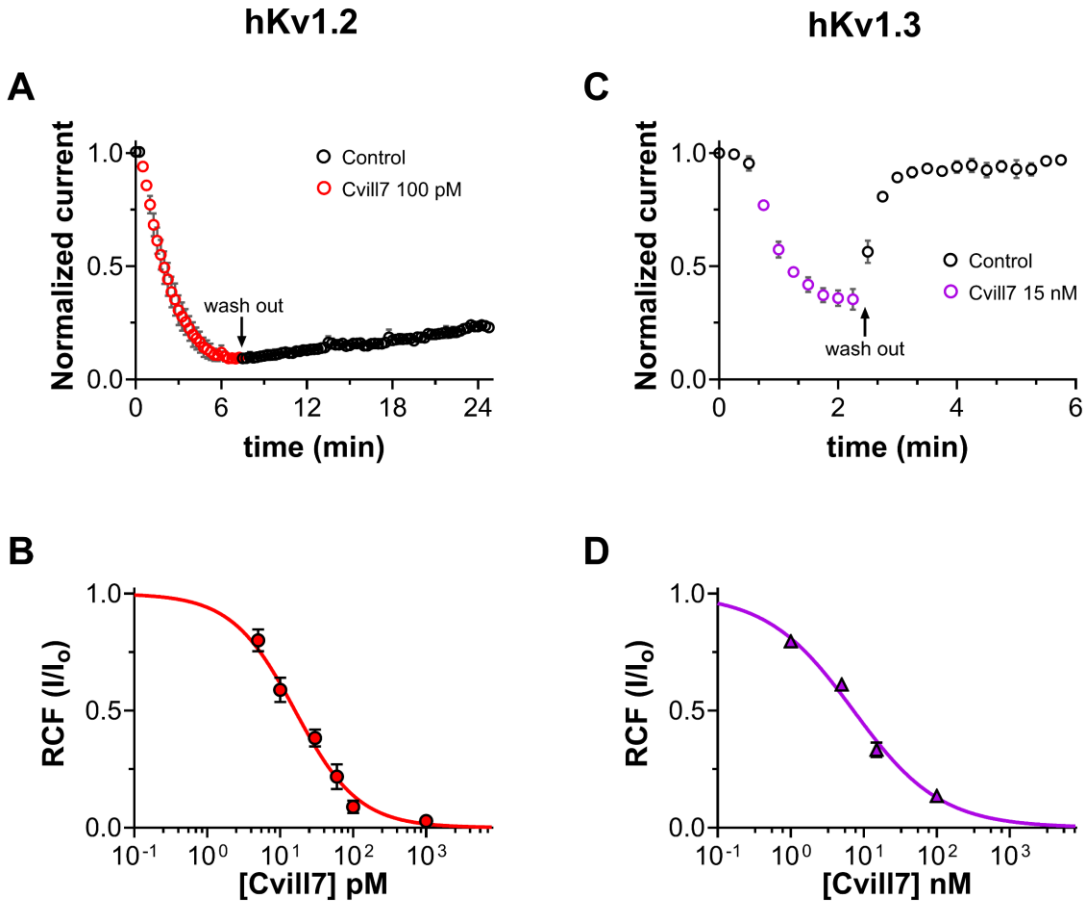

Figure 17: **Inhibition of Kv1.2 and Kv1.3 currents by Cvill7. (A & C)** The time course of development and recovery of Kv1.2 **(A)** and Kv1.3 **(C)** current inhibition. Normalized peak (I/I_0) currents from different cells were averaged at each time point and plotted as a function of time (mean ± SEM, n ≥ 3). Data points in red (A, Kv1.2) and in purple (C, Kv1.3) represent the application of 100 pM or 15 nM of Cvill7 to Kv1.2 or Kv1.3 currents, respectively. Upon reaching equilibrium, cells were perfused with bath solution lacking the toxin (arrow, wash-out) to demonstrate the reversibility of block (empty black circles). **(B & D)** Concentration-dependent block of Kv1.2 (B) and Kv1.3 (D) currents by Cvill7. A Hill equation (see Materials and Methods for details) was fitted to the remaining current fraction (RCF, I/I_0) values (red solid circles in B, purple solid triangles in D) calculated at various toxin concentrations (solid lines). The best fits yielded K_d = 16 pM, H = 1.03 for Kv1.2 (B) and K_d = 7.2 nM, H = 0.73 for Kv1.3 (D). Error bars represent the standard error of the mean (SEM), and n = 3–7.

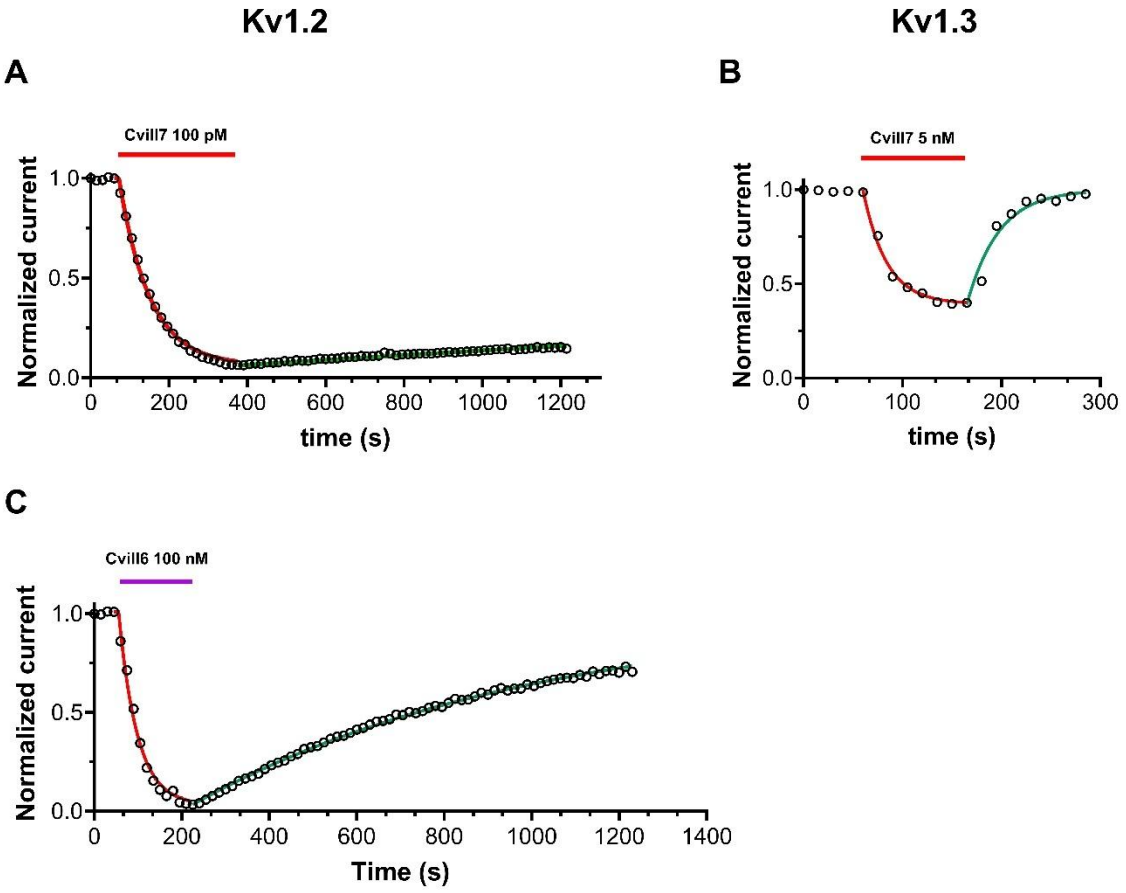

Figure 18: **Representative fits to determine the time constants of development and recovery of Kv1.2 (A & C)** and Kv1.3 **(C)** current inhibition by Cvill7 (indicated with red horizontal bars, A-B) and Cvill6 (purple horizontal bar, C). The normalized peak currents during the toxin application (wash-in procedure) were fitted using a single exponential decay function (the fitted lines are shown in red), yielding wash-in time constants (τ_{on}), Kv1.2: 75.3 s (A) and 38.7 s (C) for Cvill7 and Cvill6, respectively, and Kv1.3: 22.6 s (B) for Cvill7. The data points after application of toxin-free solution (wash-out procedure) were fitted single-exponential rise function (the fitted lines are shown in green) to give gave wash-out time constants (τ_{off}) for Kv1.2: 7380 s (A) and 776.4 s (C) for Cvill7 and Cvill6, respectively, and Kv1.3: 34.5 s (B) for Cvill7.

Table 7: **Kinetic parameters of Cvill toxins and Kv1 ion channels**

Toxins	Channel	k_{on} ($nM^{-1}s^{-1}$)	k_{off} (s^{-1})	*n*
Cvill7	Kv1.2	0.1 ± 0.015	$1.7 \times 10^{-4} \pm 1.5 \times 10^{-5}$	4
	Kv1.3	$1.3 \times 10^{-3} \pm 1.6 \times 10^{-4}$	$0.032 \pm 6.8 \times 10^{-3}$	3
Cvill6	Kv1.2	$2.9 \times 10^{-4} \pm 2.5 \times 10^{-5}$	$9.1 \times 10^{-4} \pm 1.6 \times 10^{-4}$	5

The k_{on} and k_{off} parameters were calculated from time constants (τ_{on} and τ_{off}) of development and relief from the block in the presence of 100 pM Cvill7 (for Kv1.2) or 15 nM Cvill7 (for Kv1.3) or 100 nM Cvill6 (for Kv1.2, details of which will be discussed in next section).

5.2.3 Cvill6 inhibits Kv1.2 with nanomolar affinity

Cvill6 peptide has 74% identity with Cvill7. However, during the screening experiments for Kv channels, it moderately inhibited hKv1.2 currents (~16% at a 1 nM concentration) and displayed slight inhibition of Kv1.3 (~11% at 100 nM) as shown in Fig. 16G. To further understand the binding features of Cvill6 with Kv1.2, we conducted a similar set of experiments as for Cvill7. The onset and relief from the block of Kv1.2 by Cvill6 are shown in Fig. 19A. and time constants were determined as described in section 4.7. Upon application of 100 nM of Cvill6, it rapidly attained the steady-state block to 97 ± 1.2% with the τ_{on} of 35 ± 2.7 s (n = 5, as demonstrated in Fig. 18C.). Unlike Cvill7, the block of Kv1.2 by Cvill6 was reversible but with the very slow dissociation kinetics, recovery up to 65% of the initial current occurred with the τ_{off} of 1287 ± 259 s (n = 5, Fig. 18C.) following the application of the toxin-free solution. The rate constants characterizing the binding kinetics of Cvill6 to Kv1.2 channels were also calculated based on their bimolecular interaction from the time constants and resulting rate constants are given in Table 7.The concentration-dependence of the block was obtained as detailed in Fig.17B. Fitting of the Hill equation to mean RCF values at different concentrations of Cvill6 resulted in a K_d of 3.9 ± 0.27 nM and Hill coefficient of 1.4 (Fig. 19B.).

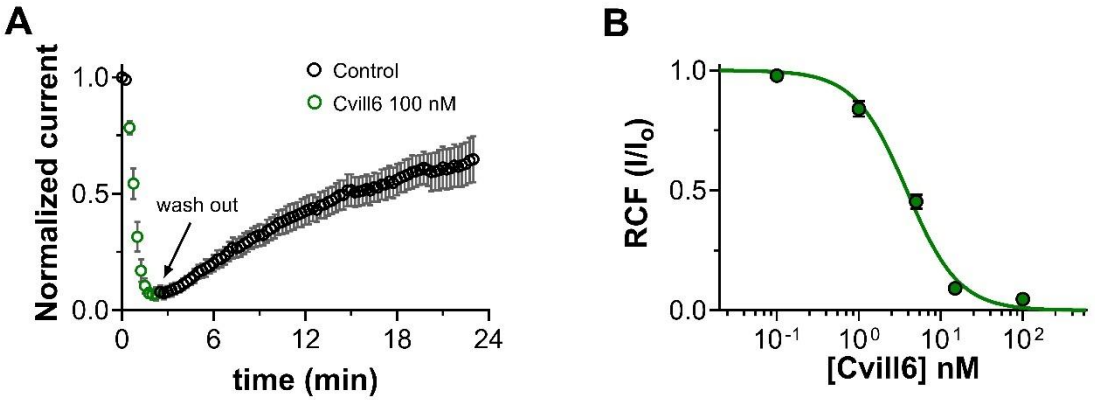

Figure 19: **Inhibition of Kv1.2 currents by Cvill6**. **(A)** Time course of onset and relief of Kv1.2 inhibition by Cvill6. Data points (averaged normalized currents, see legend and text to Fig. 15 for details) in green indicate the Cvill6 (100 nM) application to bath solution and in black represents the perfusion of cell with toxin-free solution (wash-out) following the equilibrium block. **(B)** Dose-dependent block of Kv1.2 by Cvill6. Fitting of RCF values (green solid circles) with a Hill equation resulted in a K_d = 3.9 nM and H = 1.4. Error bars denote SEM and n = 3−6.

5.2.4 Activity of Cvill6 and Cvill7 toxins on Ca^{2+}-activated potassium channels

The scorpion toxins from α-KTx 2 family also modulate the function of Ca^{2+}-activated potassium channels, in addition to Kv1 channels [75, 165]. Therefore, we investigated the activity of Cvill6 and Cvill7 toxins on three different types of Ca^{2+}-activated K^+ channels: 1) hKCa2.2 (SKCa2), the small-conductance Ca^{2+}-activated channel; 2) hKCa3.1 (IKCa1, SKCa4), the intermediate-conductance Ca^{2+}-activated channels, and 3) mKCa1.1 (BK or Slo1); the large-conductance voltage- and Ca^{2+}-activated channel of mice. Appropriate depolarization protocols were applied to record the K^+ current through respective KCa channels as shown in the inset of each panel in Fig. 20A-C. The representative current traces, shown in Fig. 20A-C. were sequentially recorded from the same cell expressing the respective KCa channel before the toxin application (black) or in the presence of toxin for 2−3 min or at equilibrium block at 100 nM concentration of Cvill6 (green) or Cvill7 (red). Traces in blue represent the equilibrium block of the respective channels in the presence of positive control (TEA^+ for KCa1.1, apamin for KCa2.2, and sCm39 toxin for KCa3.1 [154], confirming both the expression of the desired ion channel and the proper operation of the perfusion system). Neither Cvill6 nor Cvill7 showed any effect on KCa1.1 or KCa2.2 (Fig. 20A-B & D.). Cvill6 reduced ~40% of KCa3.1 current (Fig. 20C.), the RCF value was 0.73 ± 0.05 (n = 5) at 100 nM (Fig. 20D.). On the other hand, Cvill7 inhibited ~25% of the current at the same concentration (Fig. 20C.), with RCF value 0.84 ± 0.03 (n = 5) (Fig. 20D.). The time course of inhibition of KCa3.1 currents at 100 nM of Cvill6 or Cvill7 is shown in Fig. 20E. & 20F., respectively. The normalized peak currents for individual cells (n = 5) were averaged at each time point and plotted as a function of time. The steady-state block was reached in 5-6 consecutive traces (~1 min) after per-fusing the cell with 100 nM of Cvill6 or Cvill7 toxins. The recovery from the block with Cvill6 to initial peak current occurred in 4-5 consecutive traces (~0.8 min) and in case of Cvill7 it took only 2-3 consecutive traces (~0.5 min) after perfusing the cell with toxin-lacking solution. This demonstrates that both Cvill6 and Cvill7 inhibit KCa3.1 channel reversibly with quick association and dissociation kinetics. The estimated K_d values for KCa3.1 from a single concentration yielded ~268 nM and ~527 nM of Cvill6 and Cvill7, respectively. Thus, Cvill6 has a 2-fold higher affinity for KCa3.1 than Cvill7. The quantity of native toxins was insufficient to conduct the full concentration-response curves at this high concentration range (see above).

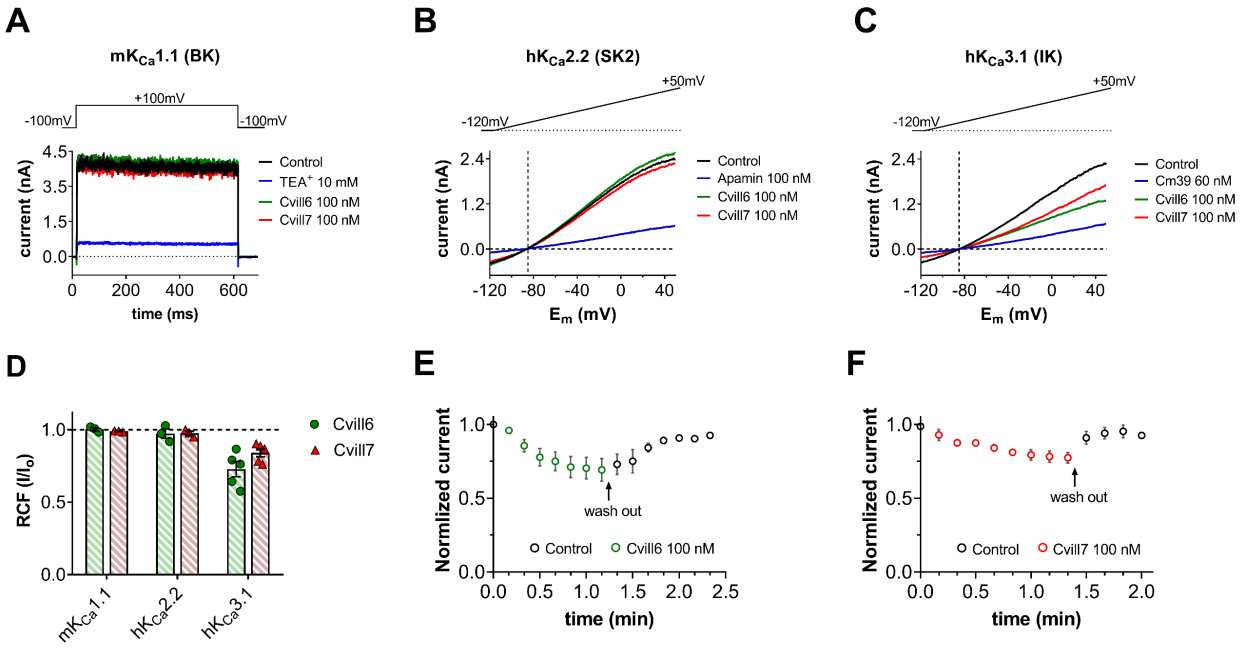

Figure 20: **Effect of Cvill toxins on Ca^{2+}-activated K^+ channels. (A-C)** Representative current traces for mKCa1.1, hKCa2.2 and hKCa3. in the control solution (traces in black) and at equilibrium block or after 12-20 depolarization pulses (~3 min) upon perfusing 100 nM of Cvill6 (green) or Cvill7 (red). Traces in blue indicate the equilibrium block in the presence of positive control TEA^+, apamin and Cm39 for respective channels (for details see Materials and Methods). Voltage protocols are shown in the inset above the representative current traces. **(D)** Summary of RCF (I/I_0), representing current inhibition in the presence of 100 nM of either toxin at steady-state block or after ~3 min of toxin application. For KCa2.2 and KCa3.1, peak currents were measured at +48 mV (time point 148 ms) of the voltage ramp. Bars (green: Cvill6, light red: Cvill7) with data points (green sold circles for Cvill6 or red solid triangles for Cvill7) represent the RCF (I/I_0) values determined from individual cells. (E & F) Time course of inhibition of KCa3.1 by Cvill6 **(E)** and Cvill7 **(F)**. The averaged values of normalized peak currents indicate the application of 100 nM of Cvill6 (green empty circles, E) of Cvill7 (red empty circles, F) to the bath solution and black empty circles represent the perfusion of cell with toxin-free solution (wash-out) following the equilibrium block. Error bars indicate the mean ± SEM (n = 3−5).

5.3 Pharmacological characterization of synthetic peptide sCm39 against Kv1.x channels

Centruroides margaritatus, a scorpion species from the Buthidae family, possessing relatively low venom toxicity, with an LD_{50} of 59.9 mg/kg [166]. The venom of *C. margaritatus* has not been extensively studied, one peptide, MgTx (αKTx 2.2), was isolated and characterized in 1993 [123]. Recently, our collaborators conducted a comprehensive proteomic analysis of *C. margaritatus* venom. Alongside the identification of the Kv11.1 channel inhibitor toxin

CmERG1 (γ-KTx 10.1) [167], they also discovered a few uncharacterized peptide toxins and among them is a peptide with a molecular weight of 3980.2 Da and named as Cm39. The peptide was synthesized later in our collaborator's lab (Prof. Lourival Possani) in UNAM, Mexico for the detailed study and electrophysiological characterization in our lab.

The search for close relatives of Cm39, based on primary amino acid sequence, was done using BLASTP which revealed that it shares similarity with α-KTx 4 family members. Cm39 is 64.9% identical to Tityustoxin (α-KTx 4.1), Toxin TdK1 (α-KTx 4.3), Toxin Tc30 (α-KTx 4.4) and Tst26 (α-KTx 4.6) [161, 168-170]. Based on this Cm39 was classified as αKTx 4.8, a new member of α-KTx 4 family [129]. Considering the spectrum of the activity of toxins belonging to the α-KTx4 family, Kv channels were considered as potential targets of Cm39. The initial screening of Cm39 was performed against a battery of ion channels including six members of Kv channels family (Kv1.1-Kv1.6); three members of Ca^{2+}-activated potassium channels (KCa1.1, KCa2.2 and KCa3.1) and two members of human voltage-gated sodium (hNav) channels (Nav1.4 and Na1.5) [154].

5.3.1 Effect of sCm39 on Kv1.x ion channels

My contribution in this project was to study the effect of sCm39 against Kv1.1, Kv1.2 and Kv1.3 ions channels. To record Kv1.1 and Kv1.2 currents, transiently transfected CHO cells were used (details of which are in Materials and Methods). However, to record Kv1.3 currents, activated T-lymphocytes were utilized. Ion channel currents were evoked by applying appropriate protocols (see 4.6.2). Representative current traces were recorded in the presence of the control solution (black), in presence of positive control (blue trace), i.e., 0.3 mM and 10 mM TEA^+ for Kv1.1 and Kv1.3, respectively, and in presence of 1 μM sCm39 (red trace) for Kv1.2, as indicated in Fig. 21A-C. Both Kv1.1 and Kv1.3 displayed no sensitivity, whereas at equilibrium block 1μM of sCm39 inhibited 95% of Kv1.2 currents (Fig. 21B.).

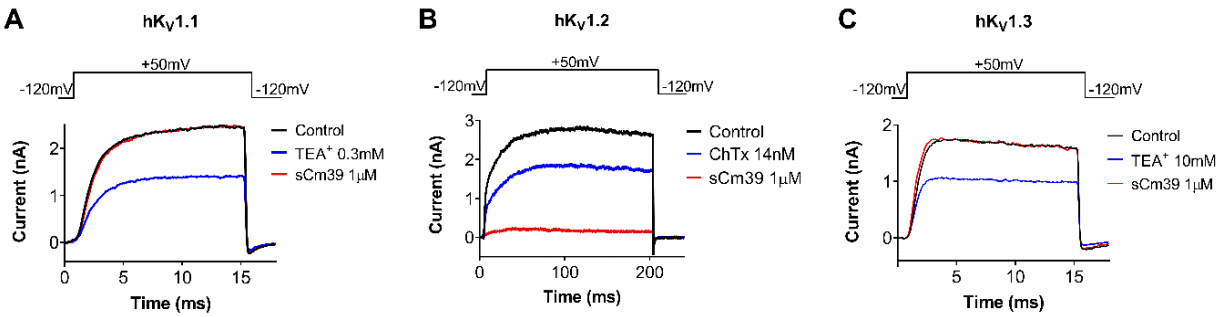

Figure 21: **Effect of sCm39 on Kv1.x ion channels. (A–C)** Representative current traces shown for each Kv1.x channel were recorded in the absence (control, black) and in the presence of 1µM sCm39 (red trace) at the development of steady-state block (B) or after 6-12 depolarization pulses (3-4 min, A and C). Complete solution exchange in the recording chamber was confirmed using positive inhibitors of ion channels (blue trace); TEA^+ (0.3 mM and 10 mM for Kv1.1 and Kv1.3, respectively) and 14 nM ChTx for Kv1.2. Voltage protocols are displayed above the current traces in each panel. For extracellular and intracellular solution composition see Materials and Methods (section 4.6.1).

5.3.2 Mechanism of Kv1.2 block by sCm39

In the case of sCm39 sufficient amount of peptide was available to comprehensively characterize the activity of Cm39 on Kv1.2 channels. We conducted a detailed study including concentration–response relationships for current inhibition, binding kinetics, and its impact on the voltage dependence of steady-state activation. Kv1.2 currents were recorded in CHO cells by applying appropriate protocols for sufficient time to reach maximum currents at the applied test potential (section 4.6.2 for details). Fig. 22A. shows Kv1.2 current traces recorded sequentially in the same cell in the absence (control solution, black trace) and in the presence of different concentration (5-500 nM) of sCm39 (traces in shades of red). sCm39 inhibited Kv1.2 in a concentration-dependent manner, i.e., 5-500 nM concentrations inhibited approximately 5-87% of current at equilibrium block. The remaining current fractions (RCF = I/I_0) were calculated for different concentrations of sCm39 and plotted as a function of concentration in Fig. 22B. The Hill equation (refer to Materials and Methods for specifics) was fit to the data points to characterize the concentration–response relationship which resulted in a K_d value of 65 nM with a Hill coefficient of 0.96.

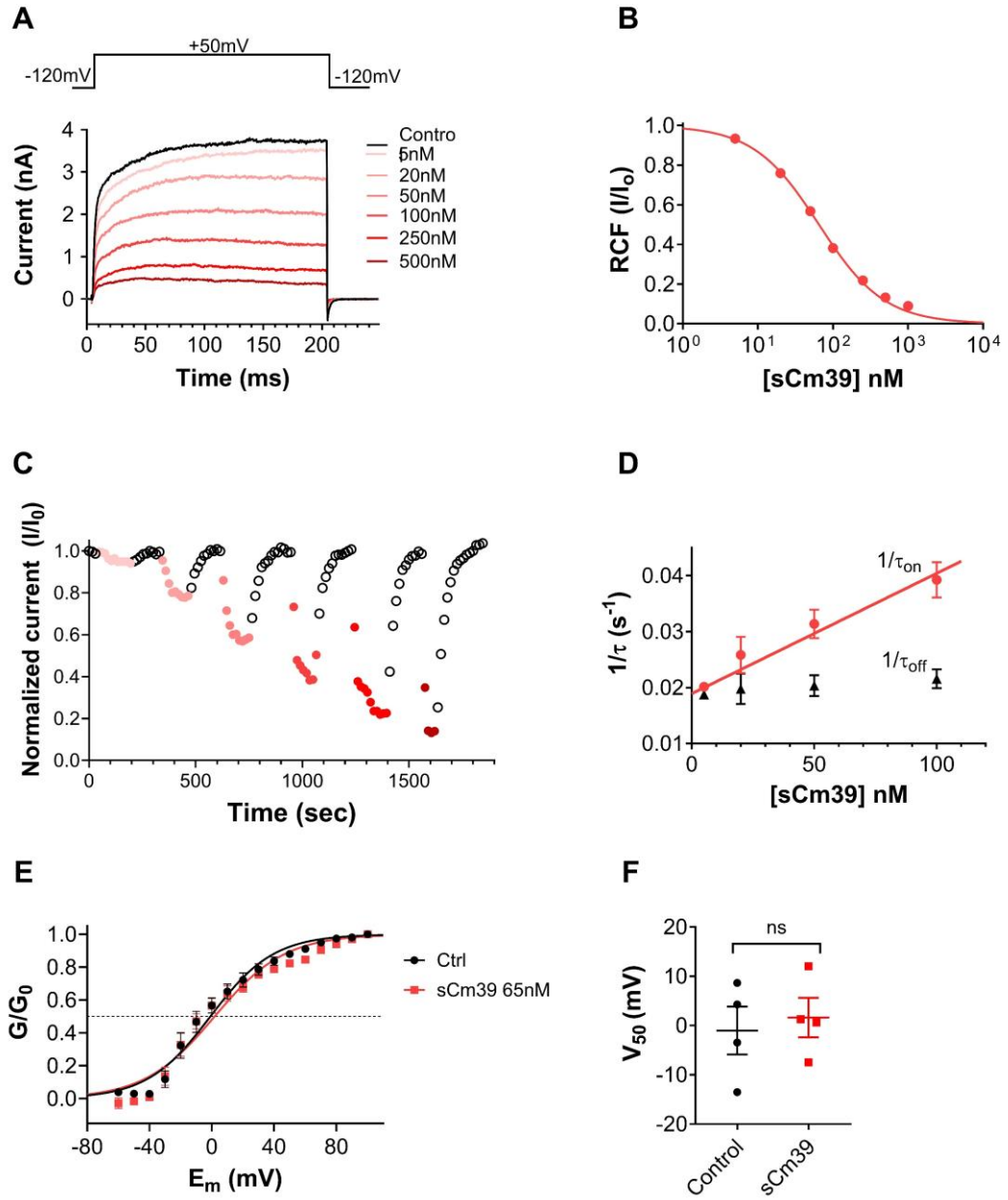

Figure 22: **Mechanism of Kv1.2 block by sCm39. (A)** The whole-cell Kv1.2 currents were recorded in transiently transfected CHO cells. Currents were evoked by applying a voltage protocol (as shown above the traces). Representative current traces showing the current before the application of toxin (black trace) and at equilibrium block upon application of different concentration of sCm39. **(B)** Concentration-dependence block of Kv1.2 by sCm39. A Hill equation (see Materials and Methods) was fitted to the RCF (I/I_0) values calculated at different concentrations of sCm39 (solid lines). The best fit resulted in a K_d value of 65 nM and Hill coefficient of 0.96. **(C)** Time course of onset and recovery of the Kv1.2 current inhibition. Normalized peak currents were plotted as a function of time. Data points in red shades (filled circles) represent the decrease in current. Upon application of sCm39 (5-500 nM). After attaining the block equilibrium cells were perfused with a bath solution to show reversibility of the block (data points in black, empty circles). **(D)** Effect of sCm39 concentration on blocking

kinetics. The $1/\tau_{on}$ values, (filled circles in red) and dissociation rate constant ($1/\tau_{off}$, triangles in black) were plotted as a function of peptide concentration. **(E)** Conductance-voltage (G-V) relationship was constructed by recording the peak Kv1.2 currents in CHO cells at test potentials ranging from −60 mV to +100 mV in 10 mV steps from Vh of −120 mV. Normalized conductance (G/G_0) was calculated for each test potential using the chord-conductance equation (see Materials and Methods), averaged, and plotted as function of membrane potential (E_m). Data points were fitted with the Boltzmann sigmoidal equation (solid lines). The G-V relationship was determined in the absence (filled circles in black) or in the presence (filled squares in red) of 65 nM sCm39. The dashed reference line indicates the normalized conductance value of 0.5. **(F)** $V_{1/2}$ values from G-V relationship of individual cells were determined and plotted. Symbols show individual data points acquired in the absence (filled circles in black) or in the presence (filled squares in red) of 65 nM sCm39. Mann–Whitney test gave p = 0.89. ns = not significant. (C–F) Error bars represent SEM and *n* = 3.

Fig. 22C. demonstrates the development and recovery from the block at various concentrations of sCm39 (5-500 nM) where normalized peak currents are plotted against time. The block was fully reversible, and the association and dissociation kinetics were very rapid. Fig. 22D. shows the analysis of the kinetic parameters of Kv1.2 current inhibition by sCm39. Single-exponential decay functions were fitted to the normalized peak currents in the presence of various sCm39 concentration (Fig. 22C., data points in red shades) to determine the time constant for the onset of block (τ_{on}). The dissociation time constant for the relief from block (τ_{off}) was obtained by fitting a single exponential rising function to the normalized peak currents in the wash-out procedure (Fig. 22C., data points in black empty circles). The fitting of single-exponential equations to the wash-in and wash-out procedures were performed similarly as demonstrated in section 4.7 and Fig. 18. for Cvill peptides.

The kinetic parameters of toxin binding, k_{on} and k_{off} of sCm39 for Kv1.2, were calculated by plotting the $1/\tau_{on}$ and $1/\tau_{off}$ values (determined at different concentrations of sCm39) as a function of toxin concentration. $1/\tau_{on}$ rises linearly with the Cm39 concentration, however the dissociation rate ($1/\tau_{off}$) remains constant with a k_{off} value of 0.019 ± 0.0013 s^{-1} (Fig. 22D.), as also described for the many other toxins which blocks the pore of the Kv1 channel [124, 142]. The second-order rate constant of association (k_{on}) was determined by fitting the $1/\tau_{on}$ data points using linear regression with k_{off} as the y-intercept. The slope of the regression line corresponds to the k_{on} of $2.15 \times 10^{-4} \pm 2.19 \times 10^{-5}$ nM^{-1} s^{-1} ($r^2 = 0.97$; Fig. 22D.). The dissociation constants ($K_d = k_{off}/k_{on}$) calculated from the block kinetic parameters resulted in 87.8 nM, which is comparable to the K_d value determined from equilibrium block (Fig. 22B.).

To study the blocking mechanism, conductance–voltage (G–V) relationship for Kv1.2 in the absence and presence of the of sCm39 was determined. Whole-cell currents of Kv1.2 expressing CHO cells were recorded by applying the 300 ms long depolarization pulses from −70 to +80 mV in 10 mV steps from holding potential of −120 mV. Due to the highly variable activation properties of Kv1.2 (as discussed above) [71] we constrained the analysis to the records which displayed similar gating mode. The normalized conductance values were calculated for each voltage step and plotted as a function of membrane potential (E_m) as shown in Fig. 22E. The Boltzmann sigmoidal function (eq.6, see section 4.7 for details) fitted to the average data points which resulted in the superimposed lines (Fig. 22E.) suggesting that the presence of sCm39 (65 nM) did not affect the voltage dependence of steady-state activation of Kv1.2. The midpoint voltage ($V_{1/2}$) of the G–V relationship in the control solution (−1.0 ± 4.8, n = 4) was statistically similar to the $V_{1/2}$ value at equilibrium block with 65 nM sCm39 (1.6 ± 4.0, n = 4) as shown in Fig. 22F. These results indicate that sCm39 is not a gating modifier rather it is a pore blocker.

6. DISCUSSION

6.1 Pharmacological characterization of seven novel peptide toxins isolated from *Centruroides bonito*

In this chapter of my dissertation, we investigated the pharmacological properties of seven new peptides isolated from the venom of a newly identified species of scorpion, named *Centruroides bonito* [171]. This scorpion is dangerous to humans and its venom composition was not known [160]. Upon performing proteomic analysis of the venom seven new peptides were identified and named as CboK1-CboK7. Comparative analysis of amino acid sequences of CboK peptides showed that they belong to the α-KTx family of K^+-channels-inhibiting peptides. Phylogenetic tree analysis (Fig. 23.) also revealed that CboK1 and CboK2 toxins are new members of α-KTx family 10, whereas CboK3-CboK7 toxins are classified as the new members of α-KTx family 2. All seven peptides contain the traditional six cystine residues (that make up three disulfide bonds). Moreover, they also have the functional Lys-Tyr dyad which is considered essential for high affinity binding of the peptide toxins with Kv channels.

CboK1 (α-KTx 10.5) showed 68% and 66% sequence identity with Cobatoxin (CoTx1, α-KTx 10.1) isolated from *Centruroides noxius* and Toxin II-10.4 (α-KTx 10.4) isolated from *Centruroides tecomanus*. Both CoTx and Toxin II-10.4 inhibit Kv1 channels with K_d values ranging between nM to μM (see Table 8A) [165, 172, 173]. Electrophysiological assay showed that Kv1.1–Kv1.3 channels remain insensitive to CboK1 peptide at 100 nM concentration. The lack of current inhibition by CboK1 may be related to the missing positively charged amino acid residues that are otherwise present in KTx 10.1 and α-KTx 10.4, as electrostatic interactions are very important in the toxin-channel interaction [174]. CboK2 (α-KTx 10.6) peptide inhibited Kv1.2 with moderate affinity (K_d = 760 pM) and showed 225-fold selectivity over Kv1.3 ion channel (K_d = 171 nM), however did not block Kv1.1 at 100 nM concentration. The amino acid sequence of CboK2 is 97% identical to CoTx1 (α-KTx 10.1), having a difference of just one amino acid: Thr1 instead of Ala1. CoTx1 inhibits Kv1.2 with K_d = 27 nM but has very low affinity for Kv1.1 and Kv1.3 (see Table 8B) [173]. At this moment we do not understand how Thr-Ala substitution in CboK2 vs Cotx1 influence so drastically the pharmacological properties of the channel. The N-terminus of the ion channel blocking peptides are usually quite tolerant to modifications and conjugation with additional peptides for example His-tag [158, 175], however, the dynamic properties of the peptides can be drastically influenced by single amino acid substitution (N17A in AnTx) close to the N-terminus [176]

and/or toxins may lose their potency with conjugation at N-terminus for example, conjugation of Cy5 to N-terminus of HsTX1[R14A] [177] and conjugation of Blood-brain barrier (BBB) shuttle peptides to N-terminus of Vm24 toxin (unpublished data Shakeel *et al*.).

CboK5 is 100% identical with a previously reported toxin Ce3 (α-KTx 2.10, isolated from *Centruroides elegans*). CboK5 peptide blocked Kv1.2 with K_d value of 376 pM and Kv1.3 with K_d = ~126 nM whereas Ce3 was shown to inhibit Kv1.3 (estimated K_d = 366 nM). The activity of Ce3 on Kv1.1 and Kv1.2 is not determined (Table 8D) [162]. CboK6 peptide has a sequence similarity of 95% with CboK5 (Ce3, α-KTx 2.10), 92% with Toxin II-10.9 (α-KTx 2.3). CboK6 (α-KTx 2.21) inhibited Kv1.2 and Kv1.3 currents with K_d values of 585 pM and 160 nM, respectively, and does not block Kv1.1 however, Toxin II-10.9 is not active on any of the three ion channels (Kv1.1–Kv1.3) at 10 nM concentration (Table 8E) [165]. This is again a striking result based on the sequence comparison: a single amino acid substitution in Toxin II-10.9 (Thr8 vs. Ser in similar toxins) renders Toxin II-10.9 (α-KTx 2.3) ineffective as inhibitor of Kv1.1. Kv1.2 and Kv1.3

CboK3 (α-KTx 2.22) and CboK4 (α-KTx 2.23) toxins are 39 amino acids residues long and share more than 95% sequence similarity. CboK3 differs from CboK4 by two amino acids only (Ile to Phe and Val to Pro at position 2 and 39 respectively), however this difference does not cause any drastic change in the inhibitory effects for Kv1.1-Kv1.3. CboK3 and Cbok4 blocks Kv1.2 with almost similar picomolar affinity (106 and 125 pM, respectively), Kv1.3 with moderate affinity (34.3 and 21.7 nM, respectively) and Kv1.1 with low affinity (1 μM and 1.5 μM, respectively). CboK3 and CboK4 have 97% and 95% sequence identity with Toxin II-12.5 (α-KTx 2.16, isolated from *Centruroides tecomanus*). CboK3 differs by (Ile to Val at position 39) whereas CboK4 differs by (Ile to Phe and Pro at position 2 and 39, correspondingly) Toxin II-12.5 blocks Kv1.2 and Kv1.3 with comparable affinities having K_d values of 700 pM and 26.2 nM, respectively (see Table 8C) [165]. Overall, the pharmacological properties of CboK3 and CboK4 are consistent with their similarity in the primary structure to other toxins that have already been characterized (Table 8C).

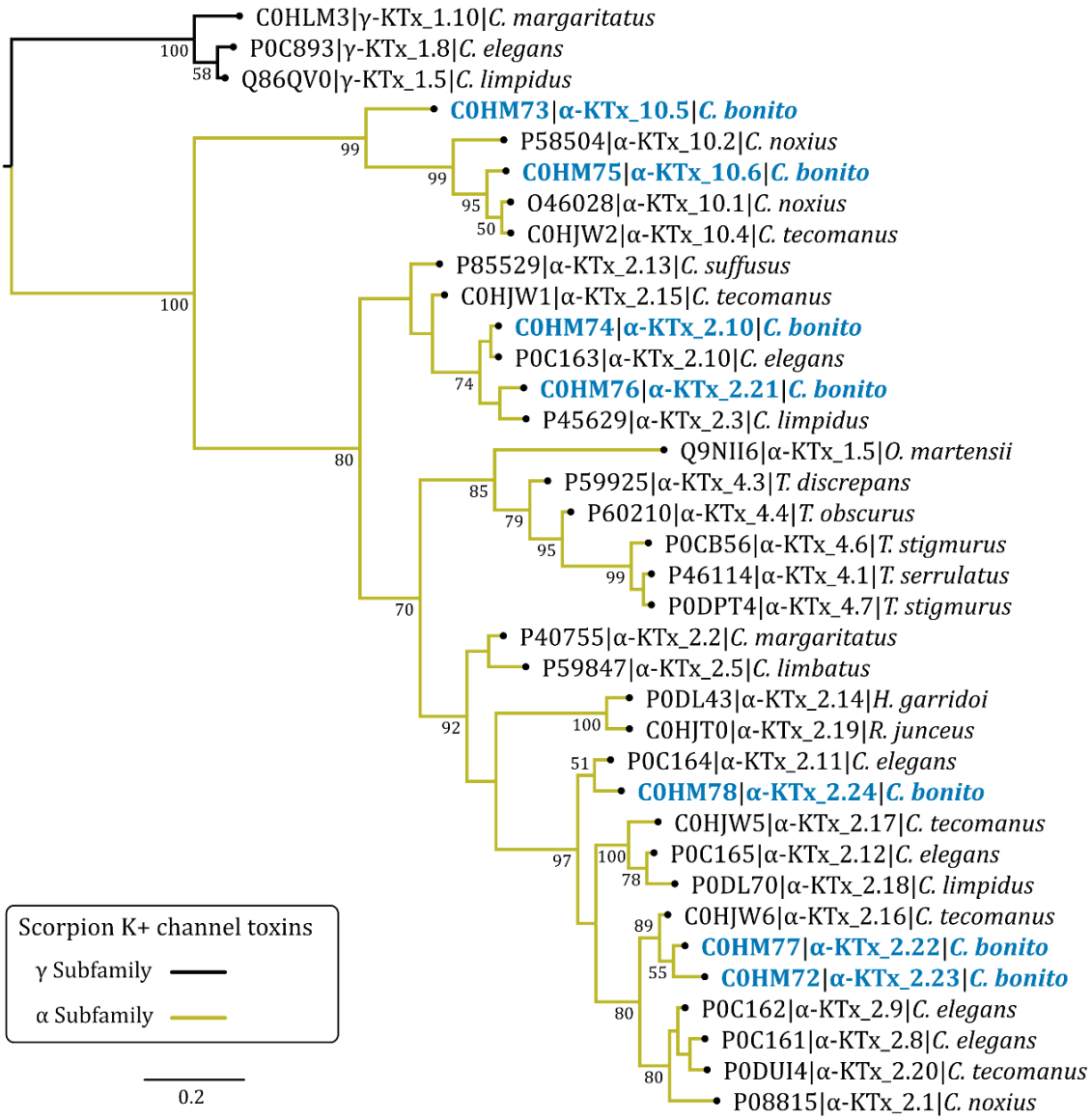

Figure 23: **Bayesian phylogenetic tree of C. bonito toxins and other potassium toxins (KTx) from scorpion.** Numbers below the nodes indicate percentage posterior probability values greater than 50. Sequence names are composed of the UniProt accession number, followed by the systematic name of the toxin and the species name. Three γ-KTx (UniProt accession no. P0C893, Q86QV0, and C0HLM3) were used as outgroups.

Table 8: **Comparison of K_d values of CboK peptides with their closest relatives.**

Toxin Name	Accession Number	Systematic Name	Sequence	% Identity	K_d Values		
					Kv1.1	Kv1.2	Kv1.3
A							
CboK1	**C0HM73**	**α-KTx 10.5**	**NVACVHRTCDSNCKRNGYKSGKCINRKCNCYPH-**	**100%**	*	*	*
Cotx1	O46028	α-KTx 10.1	-AV..Y....KD...R..R......NA.K...Y-	68%	24.4 μM	27 nM	5.3 μM
II-10.4	C0HJW2	α-KTx 10.4	-AV..Y....KD...R..R......NA.K...YA	66%	*	3.6 nM	72 nM
B							
CboK2	**C0HM75**	**α-KTx 10.6**	**TVCVYRTCDKDCKRRGYRSGKCINNACKCYPY-**	**100%**	*	**760 pM**	**171 nM**
Cotx1	O46028	α-KTx 10.1	A.....-	97%	24.4 μM	27 nM	5.3 μM
II-10.4	C0HJW2	α-KTx 10.4	A.....A	94%	*	3.6 nM	72 nM
CoTx2	P58504	α-KTx 10.2	VA.....TS.K.....-	84%	1 μM	*	*
C							
CboK3	**C0HM77**	**α-KTx 2.22**	**TIINVKCTSPKQCLKPCKDLYGPHAGEKCMNGKCKCYKV**	**100%**	**1 μM**	**106 pM**	**34.3 nM**
CboK4	**C0HM72**	**α-KTx 2.23**	**.F.....P**	**95%**	**1.5 μM**	**125 pM**	**21.7 nM**
CboK7	**C0HM78**	**α-KTx 2.24**	.F.....P...EI..I...A.....	**85%**	**141 nM**	**24 pM**	**20.4 nM**
II-12.5	C0HJW6	α-KTx 2.16	I	97%	*	700 pM	26.2 nM
Ce4	P0C164	α-KTx 2.11	.....L...EI..I...A.....I	85%	ND	ND	0.98 nM
II-12.8	C0HJW5	α-KTx 2.17	.....L...QI.....A.....H.S.I	82%	4.8 nM	2.9 nM	*
D							
CboK5	**C0HM74**	**α-KTx 2.10**	**IFINVKCSLPQQCLRPCKDRFGQHAGGKCINGKCKCYP**	**100%**	*	**376 pM**	**126 nM**
Ce3	P0C163	α-KTx 2.10	.....	100%	ND	ND	366 nM
E							
CboK6	**C0HM76**	**α-KTx 2.21**	**TTINVKCSLPQQCLRPCKDRFGQHAGGKCINGKCKCYP**	**100%**	*	**585 pM**	**160 nM**
Ce3	P0C163	α-KTx 2.10	IF.....	95%	ND	ND	366 nM
II-10.9	P45629	α-KTx 2.3	I.....TS.....	92%	*	*	*
II-10.5	C0HJW1	α-KTx 2.15	IF.....S.....K...KA.....	84%	*	300 pM	8.3 nM

Sections in the table contain the peptide common names, UniProt accession numbers, systematic names, and the aligned amino acid sequence of peptides with high sequence similarity to CboK1 (A), CboK2 (B), CboK3, CboK4 and CboK7 (C), CboK5 (D), and CboK6 (E), and their K_d values measured on Kv1.1 to Kv1.3 ion channels (highlighted in bold). In the "sequence" column, identical positions to CboK toxins are indicated by dots whereas (-) represents the gaps. In the "K_d values" column, data in bold are from this study, other data are from literature (see citations in the corresponding sections of the discussion). Missing values indicate that either the peptide does not inhibit that specific channel (*) or its activity is not determined (ND).

On the other hand, CboK7 (α-KTx 2.24) demonstrates a remarkable affinity for Kv1.2 (K_d = 24 pM) and displays moderate affinity for Kv1.1 and Kv1.3 with 141 nM and 20.4 nM K_d values. CboK7 also shares a high percentage identity with CboK3 and CboK4, as indicated in Table 8C. CboK7 differs from CboK3 and CboK4 by five amino acids but at different positions. CboK7 has Phe2, Pro15, Glu19, Ile at positions 20 and 23 and Ala27. In comparison with the previously described peptides, CboK7 is 92% identical to toxins Ce4 (α-KTx 2.11) isolated from scorpion *Centruroides elegans.* The activity of Ce4 was only tested against Kv1.3 and was shown to inhibit with 0.98 nM K_d value (see Table 8C) [162]. The high degree of similarity in the primary structures of Ce4 and CboK7 argues for experimental determination of the affinity of Ce4 for Kv1.2. This would shed light on the role of Lys15 vs. Pro15 and Val39 vs Ile39 in the determination of Kv1.2 affinity.

Overall, among the CboK toxins reported in this study, CboK7 showed remarkable affinity for Kv1.2 (K_d = 24 pM) with considerable selectivity of ~6000-fold over Kv1.1 and 850-fold over Kv1.3.

6.2 Pharmacological characterization of two new peptide toxins from venom of *Centruroides villegasi*

In this part of my dissertation, we described the electrophysiological characterization of two new peptide toxins isolated from the venom of Mexican scorpion *Centruroides villegasi*, commonly found in town Chilapa in state of Gurrero, Mexico [163]. Cvill6 and Cvill7 consist of 38 and 39 amino acids with six cysteines, respectively. Lys-Tyr dyad (at position 28 and 37 respectively) is also present in both peptides which is generally considered essential for high affinity block of Kv1 ion channels [178].The primary amino acid sequence analysis revealed that Cvill6 and Cvill7 have a large extent of identity, with already known 24 members of the α-KTx 2 family of scorpion toxins. Cvill6 has more than 90% of identity with scorpion toxins Ce3 (α-KTx 2.10), CboK6 (α-KTx 2.21), and CIITx1 (α-KTx 2.3) [151, 162, 179]. On the other hand, Cvill7 has more than 90% identity with toxins Ce1 (α-KTx 2.8), Ce2 (α-KTx 2.9), Ct28 (α-KTx 2.20) and CboK4 (α-KTx 2.23) [151, 162, 180]. Based on the high identity percentages (Fig. 14.) Cvill6 and Cvill7 were considered as the new members of α-KTx 2 subfamily with systematic names (α-KTx 2.25 and α-KTx 2.26, respectively).

It has already been proven that members of the α-KTx 2 subfamily possess moderate to high affinity of Kv1 ion channels (specifically towards Kv1.2 and Kv1.3). In line with this, electrophysiological characterization of Cvill6 revealed that it inhibits Kv1.2 (K_d = 3.9 nM)

with moderate affinity and displays relatively less affinity for Kv1.3 (K_d = ~0.84 μM), exhibiting ~215-fold selectivity for Kv1.2 over Kv1.3. Cvill6 has >97% identity index with Toxin Ce3 (αKTx-2.10), differs only by single amino acid residue (Asp to Ser at position 8). Ce3 inhibits Kv1.2 and Kv1.3 with 376 pM and 126 nM K_d values, respectively, and shows ~335-fold selectivity for Kv1.2 [151, 162]. This 10-fold decrease in affinity of Cvill6 occurred due to a change in single amino acid. The 10-fold difference in the affinities should experimentally be confirmed using the same assay conditions (ionic composition, etc.) before further conclusions can be drawn regarding the importance of a single amino acid substitution. Cvill6 also inhibited 40% of KCa3.1 currents at 100 nM concentration and single point estimation yielded a K_d value of 268 nM. However, other Kv1 channels (Kv1.1, Kv1.5 and Kv11.1) and Ca^{2+}-activated channels (mKCa1.1, KCa2.2) remained insensitive to higher concentration of Cvill6 (100 nM).

On the other hand, Cvill7 inhibited Kv1.2 with low picomolar affinity (K_d = 16 pM) and Kv1.3 with low nanomolar affinity (K_d = 7.2 nM), having a 450-fold selectivity for Kv1.2 over Kv1.3. The closely related toxins of Cvill7, namely Ce1, Ce2, and Ct28 (>94% identical), have not been evaluated for Kv1.2 inhibition according to available literature. However, for Kv1.3, Ce1 and Ce2 have 0.7 nM and 0.25 nM K_d values. As explained in the preceding chapter, CboK4 inhibits Kv1.2 (K_d = 125 pM) and Kv1.3 (K_d = 22 nM) with ~176-fold selectivity for Kv1.2 over Kv1.3. CboK4 differs by 3 residues (~92% similarity) from Cvill7 which resulted in only 8-fold decrease in the affinity of CboK4 for Kv1.2 [151]. The affinity of toxins for Kv1.2 and Kv1.3 is largely influenced by the presence of the "functional dyad" consisting of a conserved Lys residue and an aromatic or polar residue ~6–7 Å apart. This latter residue of the dyad is Tyr for high affinity blockers of Kv1.2 and Thr or Asn for high affinity blockers of Kv1.3 [116, 132, 178]. Comparison of amino acid sequences revealed that Cvill6 shares 74% identity with Cvill7, and both have Lys28-Tyr37 dyad however, Cvill6 has 244 times less potency for Kv1.2 than Cvill7 with the K_d values in low nanomolar and picomolar ranges, respectively. Based on these we conclude that the other differences in amnio acids between Cvill6 and Cvill7 may correspond to the determinants of high affinity for Kv1.2 which can be further explored through molecular dynamics studies of toxin and channel interaction.

For quantitative understandings of binding kinetics of Cvill peptides to Kv1.2 and Kv1.3 ion channels, we determined the association and dissociation rate constants (k_{on} and k_{off}, as enlisted in Table 7). The dissociation constant (K_d) values, calculated by taking the k_{off}/k_{on} ratios, of Cvill 7 are 1.7 pM and 25 nM for Kv1.2 and Kv1.3, respectively, and in case of Cvill6,

it is 3.3 nM for Kv1.2. These calculated K_d values are comparable to the K_d values obtained from the concentration-response relationships (as given in Fig. 17-19.), similar findings were previously reported for many other Kv1 channel blockers [124, 126, 142, 154]. The differences may arise from the difficulty in accurately determining block equilibrium, particularly at low toxin concentrations, as well as from incomplete wash-out of the toxin and the extended duration of the experiments, which can be affected by current run-down. Due to these limitations, we measured the association (k_{on}) and dissociation (k_{off}) rate constants at only one peptide concentration per channel: 100 pM for Cvill7 with Kv1.2, 15 nM for Cvill7 with Kv1.3, and 100 nM for Cvill6 with Kv1.2. Notably, fitting the concentration-response curves with the Hill equation yielded Hill coefficients close to 1 (ranging from 0.7 to 1.4), and the wash-in and wash-out kinetics were well-fit by single exponential functions (see Fig. 18.). These findings suggest that, similar to many known pore blockers, Cvill7 and Cvill6 interact with their target channels with 1:1 stoichiometry in a bimolecular interaction [124, 142]. The presence of Lys residue, shown important to plug the pore of K^+ channels [132, 178, 181], of the functional dyad in both Cvill6 and Cvill7 further supports the pore blocking property these peptides.

6.2.1 CboK7 and Cvill7 offer a new insight into Kv1.2 blockade

Several venom derived peptide toxins are identified till date that inhibit Kv1.2 channel currents with high affinity for example MgTx (α-KTx 2.2), HgTx-1 (α-KTx 2.5) and Pi1 (α-KTx 6.1) having K_d values of 6 pM, 170 pM, 440 pM nevertheless, these toxins also block Kv1.3 currents with similar potencies (11 pM, 86 pM and 9.7 nM, respectively) [123, 126, 158, 182-184]. In the group of high affinity and moderately selective blockers of Kv1.2 only a few toxins are known for examples, Maurotoxin (α-KTx 6.2) inhibits Kv1.2 (K_d = 0.8 nM) with ~56-fold selectivity over Kv1.1 and 225-fold over Kv1.3 [185, 186]. CoTx1 (α-KTx 10.1) has moderate affinity for Kv1.2 (27 nM) but exhibits ~900-fold selectivity over Kv1.1 and ~200-fold over Kv1.3. It also inhibits KCa2.x and KCa3.1 channels [173].

Finding selective inhibition among Kv1 ion channel subtypes specifically Kv1.1, Kv1.2 and Kv1.3 is a major challenge in Kv1 channel pharmacology. Kv1.2 and Kv1.3 have highly similar pore regions where mostly scorpion toxins bind (Fig. 4.), that explains the poor selectivity profile of the toxins among the two ion channels [49, 50, 54, 187]. Despite these, subtle differences exist among Kv1 channel types in the extracellular vestibule (generally called as “turret” and “selectivity filter”) which can contribute to the differential affinities for scorpion toxins [48, 181, 188]. There is only one known scorpion toxin so far which displays remarkably

high affinity for Kv1.2 and high selectivity over Kv1.3. Pi4 (α-KTx 6.4), isolated from scorpion *Pandinus imperator* has 8 pM K_d for Kv1.2 and does not inhibit Kv1.3 at 10 μM concentration, having >million times selectivity for Kv1.2. However, Pi4 inhibits KCa2 channels with a K_d of 500 nM [140, 147].

This study aimed to identify a novel high-affinity peptide blocker of Kv1.2. Fortunately, two distinct candidates (CboK7 and Cvill7) were found from the venom of two different scorpions and both exhibit potent Kv1.2 inhibition (Fig. 24.). Cvill7 exhibits a negligibly higher affinity for Kv1.2 (K_d = 16 pM) as compared to CboK7 (K_d = 24 pM), however this small difference in the affinity is not very significant as both fall in the picomolar range indicating the potent inhibition of Kv1.2. CboK7 showed potentially high selectively over Kv1.3 (K_d = 20.4 nM, 850-fold) as compared to Cvill7 (K_d = 7 nM, 450-fold) shown in Fig. 24C. On the other hand, both CboK7 and Cvill7 demonstrate high selectivity over Kv1.1, 6000-fold and 12000-fold respectively (Fig. 24C.). Due to the inadequate amount of native CboK7 it was not possible to conduct selectivity profiling assays to determine its activity against another physiologically significant Kv1 and KCa ion channels. However, the selectivity profiling of Cvill7 revealed that it also has 33000-fold selectivity for Kv1.2 over KCa3.1 (K_d = 527 nM).

Studies have shown that the affinity of toxins for Kv1.2 and Kv1.3 is largely influenced by the presence of the "functional dyad" consisting of a conserved Lys residue and an aromatic or polar residue ~6–7 Å apart. This latter residue of the dyad is Tyr for high affinity blockers of Kv1.2 and Thr or Asn for high affinity blockers of Kv1.3 [116, 132, 178]. Both CboK7 and Cvill7 possess the functional dyad Lys28 and Tyr37. The primary amino acid sequence comparison showed 82% sequence identity in both peptides, having amino acids differences at seven distinct positions as shown in Fig. 24A. A tertiary structure alignment is also shown in Fig. 24B. based on AlphaFold3 predicted 3-D models of CboK7 and Cvill7 peptides. Considering the potency and selectivity of both CboK7 and Cvill7 we may conclude that the differences in the primary sequences do not cause significant alteration in the predicted structures.

In the era of CryoEM a trivial solution for finding the interaction partners between the peptides and the target channel would be the analysis of the toxin-bound channel complexes. These are already available e.g. for Kv1.3 and bound ShK [181]. Unfortunately, the “turret region” of the channels, where the toxins make multiple interactions with the channels were poorly resolved due to the very flexible nature of this region. Thus, to get more insight into the

binding of these high affinity peptides, systematic mutagenesis studies and/or novel techniques (e.g. NMR analysis of toxin-channel interaction) are required [189].

A

```
CboK7    TFINVKCTSPKQCLPPCKEIYGIHAGAKCMNGKCKCYKV
Cvill7   TFINVKCTSPKQCLKPCKDLYGPHAGGKCMNGKCKCYNN
```

B

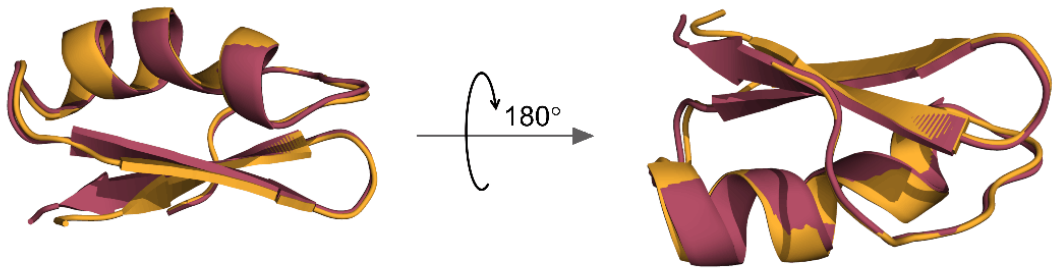

C

Peptide	Kv1.1	Kv1.2	Kv1.3	KCa3.1
CboK7	141 nM*	24 pM	20.4 nM	ND
Cvill7	192 nM*	16 pM	7 nM	527 nM*

Figure 24**: Structural and functional comparison of CboK7 and Cvill7 peptides. (A)** Amino acid sequence comparison of CboK7 and Cvill7. Conserved residues are highlighted with cyan color. %ID indicated the percentage of identity. **(B)** Structural alignment of AlphaFold3 predicted models of CboK7 (shown in light brown color) and Cvill7 (shown raspberry color). **(C)** Summary of inhibitory properties of Cbok7 and Cvill7 for K^+ channels in terms of K_d values. Asterisk indicates the K_d values estimation based RCF value at single concentration of the given peptide.

6.3 Pharmacological characterization of synthetic peptide Cm39 against Kv1.2 and Kv1.3

In this part of my thesis, we describe the characterization of pharmacological activities of a peptide toxin, Cm39, from the venom of *Centruroides margaritatus*. Synthetically synthesized Cm39 is composed of 37 amino acid residues, having six cysteines and a Lys-Tyr dyad [178]. When the amino acid sequence was compared, sCm39 showed high identity index with peptides of subfamily 4 of α-KTx family (~60%) and phylogenetic tree analysis (Fig. 25.)

displayed the clustering of Cm39 with all other α-KTx 4 toxins, indicating that sCm39 belongs to this subfamily Most peptides in subfamily 4 exhibit high sequence similarity, with identity ranging from 78% to 97%, and share common pharmacological targets such as Kv1.x and KCa channels.

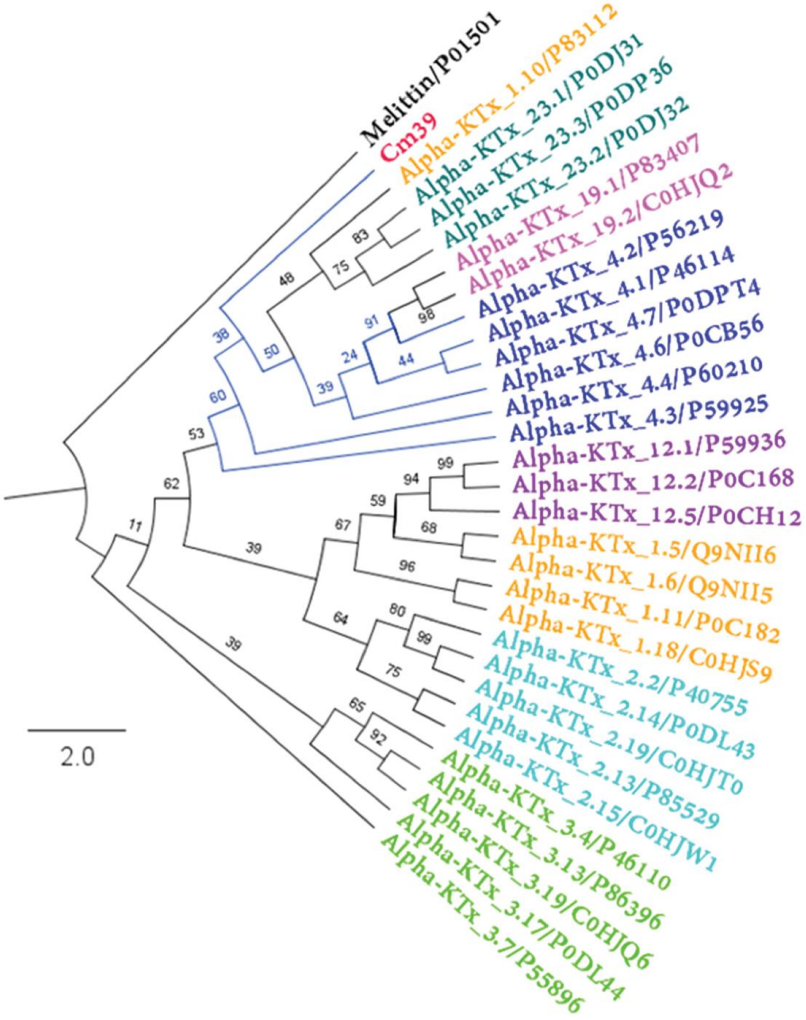

Figure 25: **Phylogenetic tree analysis of sCm39.** Maximum likelihood tree topology obtained from the analysis of sCm39 and other related α-KTxs (Log-likelihood = −1284.532). Each color represents a different α-KTx subfamily. Each toxin is indicated with its corresponding UniProt accession number. The numbers in the nodes indicate the bootstrap support values. Melittin protein sequence was used as an outgroup.

In electrophysiological evaluation against Kv1.x (Kv1.1 - Kv1.3), sCm39 demonstrated moderate inhibitory activity against Kv1.2 (K_d = 65 nM) and has no effect on Kv1.1 and Kv1.3 at the concentration of 1 μM. TsTXα (α-KTx 4.1), TdK1 (α-KTx 4.3), Tc30 (α-KTx 4.4) and Tst26 (α-KTx 4.6) shared 64.9% sequence identity with Cm39 [161, 169, 170, 190]. However, as per literature only TsTXα and Tst26 were tested against Kv1.2, the reported K_d values were of 0.2 nM and 1.9 nM respectively [161, 190]. The interesting factor of sCm39 is that it did not

show any inhibitory effects on Kv1.3. Further upon determining the binding kinetics and mechanism of block, it was found that the voltage dependence of steady-state-activation of Kv1.2 channel was completely insensitive to the presence of sCm39. Thereby clarifying that it does not interfere with the VSD, we proposed that Cm39 binds to the pore region of the ion channel and Lys27 is responsible for occluding the pore. In addition, the binding kinetics analysis showed a simple bimolecular interaction between sCm39 and Kv1.2 channel as described previously for typical pore blocker toxins such as ChTx and MgTx [124, 158]. The apparent first-order association rate increased proportionally with sCm39 concentration, indicating faster binding at higher toxin levels. In contrast, the first-order dissociation rate remained unchanged across different toxin concentrations. The K_d for Kv1.2 calculated by the k_{off}/k_{on} ratio (87.8 nM) is comparable to the K_d value determined by fitting the Hill equation to the concentration dependence of current inhibition (65 nM).

The detailed study conducted by Naseem *et al*. demonstrate that apart from Kv1.2, sCm39 also exhibited a blocking effect on intermediate-conductance Ca^{2+}-activated (KCa3.1) ion channels (K_d = 58 nM) and the small-conductance Ca^{2+}-activated channel (KCa2.2), albeit with lower affinity (K_d = 502 nM) [154]. As we discussed already in section 2.7 a number of scorpion-derived peptide toxins are known to block K^+ channels with high affinity. However, poor selectivity among Kv subtypes compromises the therapeutic use of peptide toxins in the management of channelopathies. For example, Urotoxin (α-KTx-6.21) and MgTx (α-KTx-2.2) inhibit numerous Kv1.x channel subtypes and Ca^{2+}-activated channels with high affinity ranging from picomolar to nanomolar [123, 191]. Protein engineering could be utilized to enhance the selectivity of potential drugs. For example, by substituting two residues (N17A/F32T) in Anuroctoxin (α-KTx 6.12) it gained 16,000-fold selectivity for Kv1.3 over Kv1.2 [176]. sCm39 inhibits Kv1.2 and KCa3.1 ion channels with similar potencies and this pattern of ion channel inhibition prevents the practical application of the non-selective inhibitors.

As Kv1.2 is a typical ion channel in the central nervous system, a peptide such as sCm39, that has dual targets, is not an ideal candidate to manage Kv1.2-related channelopathies. In this regard CboK7 and Cvill7 are promising candidates treat channelopathies associated with gain-of-function mutations of Kv1.2 such as severe epileptic encephalopathy (EE) [27, 109, 192]. The selective inhibition of mutated Kv1.2 channels on neuron in central nervous system (CNS) using Cvill7 as potential drugs will have minimum risk of off-target effects on other K^+ channels (Kv1.1, Kv1.3, Kv1.4 and K1.6) which are also widely expressed in CNS [84, 193].

However, the therapeutic application of these peptide toxins is challenged by the restrictive nature of the blood–brain barrier (BBB), which limits their delivery to brain tissues [194]. This limitation can be effectively addressed by conjugating Cvill7 or CboK7 with BBB shuttle peptides, which have been shown to significantly enhance CNS penetration and improve peptide bioavailability [195-197].

6.4 Potential of peptide-based drugs in the management of the diseases of the CNS

Peptides-based drugs have emerged as a unique class of therapeutics due to their distinctive biochemical properties and strong therapeutic potential. However, poor membrane permeability and low in vivo stability hinder their broader application in drug development. Their inability to efficiently cross cell membranes limit their access to intracellular targets, while their linear structure and susceptibility to enzymatic degradation result in short half-lives and rapid clearance from the body [198-201]. In the past decade significant progresses to overcome the poor CNS availability of peptide-based drugs have been made by the development of various invasive and non-invasive approaches. For the targeted delivery of peptides an intracerebroventricular (ICV) delivery system can be utilized. For example, in case of Dravet syndrome (an epileptic disease caused due to haploinsufficiency of Nav1.1 ion channels), Hm1a peptide derived from spider venom, has been infused via ICV to Dravet Syndrome mice and significant reduction in whole brain hyperexcitability has been observed. This proof-of-concept study confirms the practical application of the ICV for drug administration to CNS [202]. Ziconotide is the synthetic version of ω-conotoxin MVIIA peptide isolated from the venom of fish-hunting marine snail Conus magus [203]. Ziconotide is an FDA approved drug for the treatment of severe chronic pain by blocking N-type calcium channels [204]. Ziconotide has limited capacity to cross the blood–brain barrier; therefore, to maximize its analgesic effect it must be administered intrathecally. For continuous delivery of the drug in the intrathecal space programmable surgically implanted variable rate infusion device such as the Medtronic SynchroMed has been utilized [205].

Apart from the invasive strategies discussed earlier, noninvasive methods for delivering peptide-based drugs are gaining increasing attention due to their clinical practicality and reduced risk [206]. One widely explored approach involves the encapsulation of peptide drugs into nanoparticles or liposomes, enabling targeted delivery, protection from enzymatic degradation, and controlled release at the desired site. Another promising technique is the

transient disruption of the blood-brain barrier (BBB) using focused ultrasound (FUS) or osmotic agents like mannitol, which can temporarily increase BBB permeability to facilitate drug passage into the brain. A particularly effective and extensively studied noninvasive strategy is the use of cell-penetrating peptides (CPPs) or BBB shuttle peptides for example angiopep-2, TAT (HIV protein), melanotransferrin fragment (MTFP) etc [207-209]. These small peptides, typically composed of 10–30 amino acids, can cross the BBB either through direct translocation or via receptor-mediated transcytosis. By conjugating therapeutic peptides to CPPs or shuttle peptides, researchers have significantly enhanced CNS delivery while avoiding the need for invasive administration techniques. Conjugation of Ziconotide with TAT enables effective peripheral and intranasal delivery while preserving its analgesic efficacy, offering a less invasive alternative with fewer side effects [210]. Similarly, N-terminal linkage of Vm24, a high-affinity Kv1.3 blocker, to BBB shuttle peptides retains its target affinity and is under investigation for microglial Kv1.3 targeting (unpublished data, Shakeel et al.). These strategies show strong potential to enhance CNS delivery and expand the therapeutic utility of peptide-based drugs in neurological disorders.

7. SUMMARY

The Kv1.2 ion channels play a vital role in the regulation of membrane potential and excitability of neurons and are widely distributed in CNS. In 2016, Kv1.2 related GOF mutations and their role in the progression of epileptic encephalopathy (EE) were described. It has been experimentally verified that the inhibition of the Kv1.2 current can be a potential approach to cure EE. The aim of this research was to identify and characterize a potent and selective inhibitor of Kv1.2 ion channel from the venom of scorpions. With the help of our collaborators, we isolated seven new peptides (CboK1-CboK7, 32-39 amino acid residues) from venom of *C. bonito*, two peptides from the venom of *C. villegasi* (Cvill6 and Cvill7, 38 and 39 amino acid residues) and a synthetic peptide, sCm39, which was identified from the venom of a known scorpion *C. margaritatus.*

Electrophysiological characterization of seven peptides showed that among all except CboK1 all six peptides inhibit Kv1.2 with high affinity (K_d values between 24-763 pM) and have reasonable selectivity over Kv1.3 (K_d values between 20.4-171 nM). Of these seven, CboK7 emerged as a high affinity and selective blocker of Kv1.2 having 850-fold and 6000-fold selectivity over Kv1.3 and Kv1.1.

Pharmacological analysis of Cvill peptides shows that Cvill6 has moderate affinity for Kv1.2 (K_d = 3.9 nM) whereas Cvill7 possesses high Kv1.2 affinity (K_d = 16 pM). Cvill6 has 215-fold and 59-fold selectivity over Kv1.3 and KCa3.1, respectively. In contrast Cvill7 has high selectivity for Kv1.2 over Kv1.3 and KCa3.1 (450-fold and 33000-fold, respectively). Binding kinetics analysis suggests that Cvill6 and Cvill7 follow the binding pattern of classical pore blockers.

sCm39 inhibited Kv1.2 currents with K_d value of 65 nM and does not show any effect on Kv1.1 and Kv1.3 at 1 at 1 μM. The investigation for the mechanism of block and binding kinetics revealed that Cm39 binds to the pore of the Kv1.2 ion channel thus it is not a gating-modifier.

In summary, this dissertation presents the electrophysiological characterization of ten peptide toxins, among which two CboK7 and Cvill7 emerged as potent, high-affinity blockers of the Kv1.2 ion channel. These findings lay the groundwork for identifying key amino acid residues critical for high-affinity Kv1.2 blockade. Moreover, they provide a valuable foundation for the potential therapeutic application of Kv1.2-targeting peptides in the treatment of epileptic encephalopathy (EE) and other related neurological disorders.

8. REFERENCES

1. Chaffey, N., Alberts, B., Johnson, A., Lewis, J., Raff, M., Roberts, K. and Walter, P. *Molecular biology of the cell. 4th edn*. 2003, Oxford University Press.
2. Feske, S., H. Wulff, and E.Y. Skolnik, *Ion channels in innate and adaptive immunity.* Annual review of immunology, 2015. **33**(1): p. 291-353.
3. Becchetti, A. and A. Arcangeli, *Integrins and ion channels: molecular complexes and signaling*. Vol. 674. 2010: Springer Science & Business Media.
4. Petkov, G.V., *Ion channels*, in *Pharmacology*. 2009, Elsevier. p. 387-427.
5. Alexander, S.P., et al., *The concise guide to pharmacology 2019/20: Catalytic receptors.* British journal of pharmacology, 2019. **176**: p. S247-S296.
6. Zheng, J. and M.C. Trudeau, *Handbook of ion channels*. 2015: Crc Press.
7. González, C., et al., *K+ channels: function-structural overview.* Comprehensive physiology, 2012. **2**(3): p. 2087-2149.
8. Capera, J., et al., *The potassium channel odyssey: mechanisms of traffic and membrane arrangement.* International journal of molecular sciences, 2019. **20**(3): p. 734.
9. Hibino, H., et al., *Inwardly rectifying potassium channels: their structure, function, and physiological roles.* Physiological reviews, 2010. **90**(1): p. 291-366.
10. Ilan, N. and S.A. Goldstein, *Kcnkø: single, cloned potassium leak channels are multi-ion pores.* Biophysical Journal, 2001. **80**(1): p. 241-253.
11. Kollewe, A., et al., *A structural model for K2P potassium channels based on 23 pairs of interacting sites and continuum electrostatics.* Journal of General Physiology, 2009. **134**(1): p. 53-68.
12. Wulff, H., N.A. Castle, and L.A. Pardo, *Voltage-gated potassium channels as therapeutic targets.* Nature reviews Drug discovery, 2009. **8**(12): p. 982-1001.
13. Kohler, M., et al., *8: Adelman IP.(1996) Small—conductance, calcium—activated potassium channels from mammalian brain.* Science. **273**.
14. Wei, A.D., et al., *International Union of Pharmacology. LII. Nomenclature and molecular relationships of calcium-activated potassium channels.* Pharmacological reviews, 2005. **57**(4): p. 463-472.
15. Salkoff, L., et al., *High-conductance potassium channels of the SLO family.* Nature Reviews Neuroscience, 2006. **7**(12): p. 921-931.
16. Doyle, D.A., et al., *The structure of the potassium channel: molecular basis of K+ conduction and selectivity.* science, 1998. **280**(5360): p. 69-77.
17. Heinemann, S.H., et al., *Functional characterization of Kv channel beta-subunits from rat brain.* The Journal of physiology, 1996. **493**(3): p. 625-633.
18. Gutman, G.A., et al., *International Union of Pharmacology. LIII. Nomenclature and molecular relationships of voltage-gated potassium channels.* Pharmacological reviews, 2005. **57**(4): p. 473-508.
19. Feria Pliego, J.A. and C.M. Pedroarena, *Kv1 potassium channels control action potential firing of putative GABAergic deep cerebellar nuclear neurons.* Scientific reports, 2020. **10**(1): p. 6954.
20. Goldberg, E.M., et al., *K+ channels at the axon initial segment dampen near-threshold excitability of neocortical fast-spiking GABAergic interneurons.* Neuron, 2008. **58**(3): p. 387-400.
21. Kirizs, T., et al., *Distinct axo-somato-dendritic distributions of three potassium channels in CA 1 hippocampal pyramidal cells.* European Journal of Neuroscience, 2014. **39**(11): p. 1771-1783.
22. Willis, M., et al., *Shaker-related voltage-gated potassium channels Kv1 in human hippocampus.* Brain Structure and Function, 2018. **223**: p. 2663-2671.

23. Ovsepian, S.V., et al., *Distinctive role of KV1. 1 subunit in the biology and functions of low threshold K+ channels with implications for neurological disease.* Pharmacology & therapeutics, 2016. **159**: p. 93-101.
24. Glaudemans, B., et al., *A missense mutation in the Kv1. 1 voltage-gated potassium channel–encoding gene KCNA1 is linked to human autosomal dominant hypomagnesemia.* The Journal of clinical investigation, 2009. **119**(4): p. 936-942.
25. Browne, D.L., et al., *Episodic ataxia/myokymia syndrome is associated with point mutations in the human potassium channel gene, KCNA1.* Nature genetics, 1994. **8**(2): p. 136-140.
26. Robbins, C.A. and B.L. Tempel, *Kv1. 1 and Kv1. 2: similar channels, different seizure models.* Epilepsia, 2012. **53**: p. 134-141.
27. Syrbe, S., et al., *De novo loss-or gain-of-function mutations in KCNA2 cause epileptic encephalopathy.* Nature genetics, 2015. **47**(4): p. 393-399.
28. Masnada, S., et al., *Clinical spectrum and genotype–phenotype associations of KCNA2-related encephalopathies.* Brain, 2017. **140**(9): p. 2337-2354.
29. Panyi, G., C. Beeton, and A. Felipe, *Ion channels and anti-cancer immunity.* Philosophical Transactions of the Royal Society B: Biological Sciences, 2014. **369**(1638): p. 20130106.
30. Lewis, R.S. and M.D. Cahalan, *Subset-specific expression of potassium channels in developing murine T lymphocytes.* Science, 1988. **239**(4841): p. 771-775.
31. Beeton, C., et al., *Kv1. 3 channels are a therapeutic target for T cell-mediated autoimmune diseases.* Proceedings of the National Academy of Sciences, 2006. **103**(46): p. 17414-17419.
32. Kundu-Raychaudhuri, S., et al., *Kv1. 3 in psoriatic disease: PAP-1, a small molecule inhibitor of Kv1. 3 is effective in the SCID mouse psoriasis–xenograft model.* Journal of autoimmunity, 2014. **55**: p. 63-72.
33. Rangaraju, S., et al., *Potassium channel Kv1. 3 is highly expressed by microglia in human Alzheimer's disease.* Journal of Alzheimer's disease, 2015. **44**(3): p. 797-808.
34. Sarkar, S., et al., *Kv1. 3 modulates neuroinflammation and neurodegeneration in Parkinson's disease.* The Journal of clinical investigation, 2020. **130**(8): p. 4195-4212.
35. Ding, W.-G., et al., *Improved functional expression of human cardiac kv1. 5 channels and trafficking-defective mutants by low temperature treatment.* PloS one, 2014. **9**(3): p. e92923.
36. Olson, T.M., et al., *Kv1. 5 channelopathy due to KCNA5 loss-of-function mutation causes human atrial fibrillation.* Human molecular genetics, 2006. **15**(14): p. 2185-2191.
37. Thomas, D., C. Karle, and J. Kiehn, *The cardiac hERG/IKr potassium channel as pharmacological target: structure, function, regulation, and clinical applications.* Current pharmaceutical design, 2006. **12**(18): p. 2271-2283.
38. Sanguinetti, M.C., et al., *A mechanistic link between an inherited and an acquird cardiac arrthytmia: HERG encodes the IKr potassium channel.* Cell, 1995. **81**(2): p. 299-307.
39. Sanguinetti, M.C. and M. Tristani-Firouzi, *hERG potassium channels and cardiac arrhythmia.* Nature, 2006. **440**(7083): p. 463-469.
40. Oliveira, M.S., et al., *Altered expression and function of small-conductance (SK) Ca2+-activated K+ channels in pilocarpine-treated epileptic rats.* Brain research, 2010. **1348**: p. 187-199.
41. Orfali, R. and N. Albanyan, *Ca2+-sensitive potassium channels.* Molecules, 2023. **28**(2): p. 885.

42. Xia, X.-M., et al., *Mechanism of calcium gating in small-conductance calcium-activated potassium channels.* Nature, 1998. **395**(6701): p. 503-507.
43. Ishii, T.M., et al., *A human intermediate conductance calcium-activated potassium channel.* Proceedings of the National Academy of Sciences, 1997. **94**(21): p. 11651-11656.
44. Kshatri, A.S., A. Gonzalez-Hernandez, and T. Giraldez, *Physiological roles and therapeutic potential of Ca2+ activated potassium channels in the nervous system.* Frontiers in molecular neuroscience, 2018. **11**: p. 258.
45. Grimm, P.R., et al., *Identification and localization of BK-β subunits in the distal nephron of the mouse kidney.* American Journal of Physiology-Renal Physiology, 2007. **293**(1): p. F350-F359.
46. Long, S.B., E.B. Campbell, and R. MacKinnon, *Crystal structure of a mammalian voltage-dependent Shaker family K+ channel.* Science, 2005. **309**(5736): p. 897-903.
47. Long, S.B., et al., *Atomic structure of a voltage-dependent K+ channel in a lipid membrane-like environment.* Nature, 2007. **450**(7168): p. 376-382.
48. Wu, Y., et al., *CryoEM structures of Kv1. 2 potassium channels, conducting and non-conducting.* eLife, 2025. **12**: p. RP89459.
49. DeCoursey, T.E., et al., *Voltage-gated K+ channels in human T lymphocytes: a role in mitogenesis?* Nature, 1984. **307**(5950): p. 465-468.
50. Long, S.B., E.B. Campbell, and R. MacKinnon, *Voltage sensor of Kv1. 2: structural basis of electromechanical coupling.* Science, 2005. **309**(5736): p. 903-908.
51. Zhou, Y., et al., *Chemistry of ion coordination and hydration revealed by a K+ channel–Fab complex at 2.0 Å resolution.* Nature, 2001. **414**(6859): p. 43-48.
52. Kuang, Q., P. Purhonen, and H. Hebert, *Structure of potassium channels.* Cellular and molecular life sciences, 2015. **72**: p. 3677-3693.
53. Heginbotham, L., et al., *Mutations in the K+ channel signature sequence.* Biophysical journal, 1994. **66**(4): p. 1061-1067.
54. Nimigean, C.M. and T.W. Allen, *Origins of ion selectivity in potassium channels from the perspective of channel block.* Journal of General Physiology, 2011. **137**(5): p. 405-413.
55. Morais-Cabral, J.H., Y. Zhou, and R. MacKinnon, *Energetic optimization of ion conduction rate by the K+ selectivity filter.* Nature, 2001. **414**(6859): p. 37-42.
56. Bezanilla, F., *The voltage sensor in voltage-dependent ion channels.* Physiological reviews, 2000. **80**(2): p. 555-592.
57. Larsson, H.P., et al., *Transmembrane movement of the shaker K+ channel S4.* Neuron, 1996. **16**(2): p. 387-397.
58. Baker, O., et al., *Three transmembrane conformations and sequence-dependent displacement of the S4 domain in shaker K+ channel gating.* Neuron, 1998. **20**(6): p. 1283-1294.
59. Ledwell, J.L. and R.W. Aldrich, *Mutations in the S4 region isolate the final voltage-dependent cooperative step in potassium channel activation.* Journal of General Physiology, 1999. **113**(3): p. 389-414.
60. Demo, S.D. and G. Yellen, *The inactivation gate of the Shaker K+ channel behaves like an open-channel blocker.* Neuron, 1991. **7**(5): p. 743-753.
61. Bett, G.C., et al., *A model of the interaction between N-type and C-type inactivation in Kv1. 4 channels.* Biophysical journal, 2011. **100**(1): p. 11-21.
62. Tan, X., et al., *Structure of the Shaker Kv channel and mechanism of slow C-type inactivation.* Biophysical Journal, 2022. **121**(3): p. 294a-295a.
63. Panyi, G., Z. Sheng, and C. Deutsch, *C-type inactivation of a voltage-gated K+ channel occurs by a cooperative mechanism.* Biophysical journal, 1995. **69**(3): p. 896-903.

64. MacKinnon, R., *Determination of the subunit stoichiometry of a voltage-activated potassium channel.* Nature, 1991. **350**(6315): p. 232-235.
65. Hoshi, T. and C.M. Armstrong, *C-type inactivation of voltage-gated K+ channels: pore constriction or dilation?* Journal of General Physiology, 2013. **141**(2): p. 151-160.
66. Reddi, R., et al., *Structural basis for C-type inactivation in a Shaker family voltage-gated K+ channel.* Science advances, 2022. **8**(16): p. eabm8804.
67. Suárez-Delgado, E., et al., *KV1. 2 channels inactivate through a mechanism similar to C-type inactivation.* Journal of General Physiology, 2020. **152**(6): p. e201912499.
68. Matthies, D., et al., *Single-particle cryo-EM structure of a voltage-activated potassium channel in lipid nanodiscs.* eLife, 2018. **7**: p. e37558.
69. Song, Z., et al., *The Effect of THz Electromagnetic Field on the Conductance of Potassium and Sodium Channels.* bioRxiv, 2024: p. 2024.08. 27.609902.
70. Tiffany, A.M., et al., *PSD-95 and SAP97 exhibit distinct mechanisms for regulating K+ channel surface expression and clustering.* The Journal of cell biology, 2000. **148**(1): p. 147-157.
71. Rezazadeh, S., et al., *An activation gating switch in Kv1. 2 is localized to a threonine residue in the S2-S3 linker.* Biophysical Journal, 2007. **93**(12): p. 4173-4186.
72. Minor, D.L., et al., *The polar T1 interface is linked to conformational changes that open the voltage-gated potassium channel.* Cell, 2000. **102**(5): p. 657-670.
73. Koopmann, R., et al., *Role of the S2 and S3 segment in determining the activation kinetics in Kv2. 1 channels.* The Journal of membrane biology, 2001. **182**: p. 49-59.
74. Scholle, A., et al., *Rate-limiting reactions determining different activation kinetics of kv1. 2and kv2. 1 channels.* The Journal of membrane biology, 2004. **198**: p. 103-112.
75. Grissmer, S., et al., *Pharmacological characterization of five cloned voltage-gated K+ channels, types Kv1. 1, 1.2, 1.3, 1.5, and 3.1, stably expressed in mammalian cell lines.* Molecular pharmacology, 1994. **45**(6): p. 1227-1234.
76. Pinatel, D. and C. Faivre-Sarrailh, *Assembly and function of the juxtaparanodal Kv1 complex in health and disease.* Life, 2020. **11**(1): p. 8.
77. Chung, Y.H., et al., *Immunohistochemical study on the distribution of the voltage-gated potassium channels in the gerbil cerebellum.* Neuroscience letters, 2005. **374**(1): p. 58-62.
78. Sheng, M., et al., *Contrasting subcellular localization of the Kv1. 2 K+ channel subunit in different neurons of rat brain.* Journal of Neuroscience, 1994. **14**(4): p. 2408-2417.
79. Shen, W., et al., *Kv1. 2-containing K+ channels regulate subthreshold excitability of striatal medium spiny neurons.* Journal of neurophysiology, 2004. **91**(3): p. 1337-1349.
80. Grider, M.H., R. Jessu, and R. Kabir, *Physiology, action potential.* 2019.
81. Niday, Z. and A.V. Tzingounis, *Potassium channel gain of function in epilepsy: an unresolved paradox.* The Neuroscientist, 2018. **24**(4): p. 368-380.
82. Dodson, P.D., et al., *Presynaptic rat Kv1. 2 channels suppress synaptic terminal hyperexcitability following action potential invasion*. 2003, Wiley Online Library.
83. Higgs, M.H. and W.J. Spain, *Kv1 channels control spike threshold dynamics and spike timing in cortical pyramidal neurones.* The Journal of physiology, 2011. **589**(21): p. 5125-5142.
84. Lai, H.C. and L.Y. Jan, *The distribution and targeting of neuronal voltage-gated ion channels.* Nature Reviews Neuroscience, 2006. **7**(7): p. 548-562.
85. Liu, C.-H., et al., *Rearrangement of potassium ions and Kv1. 1/Kv1. 2 potassium channels in regenerating axons following end-to-end neurorrhaphy: ionic images from TOF-SIMS.* Histochemistry and Cell Biology, 2017. **148**: p. 407-416.

86. Trimmer, J.S., *Subcellular localization of K+ channels in mammalian brain neurons: remarkable precision in the midst of extraordinary complexity.* Neuron, 2015. **85**(2): p. 238-256.
87. Gu, C., Y.N. Jan, and L.Y. Jan, *A conserved domain in axonal targeting of Kv1 (Shaker) voltage-gated potassium channels.* Science, 2003. **301**(5633): p. 646-649.
88. Shi, G., et al., *βSubunits promote K+ channel surface expression through effects early in biosynthesis.* Neuron, 1996. **16**(4): p. 843-852.
89. Lamothe, S.M. and H.T. Kurata, *Slc7a5 alters Kvβ-mediated regulation of Kv1. 2.* Journal of General Physiology, 2020. **152**(7): p. e201912524.
90. Cachero, T.G., A.D. Morielli, and E.G. Peralta, *The small GTP-binding protein RhoA regulates a delayed rectifier potassium channel.* Cell, 1998. **93**(6): p. 1077-1085.
91. Chandy, K., et al., *Voltage-gated potassium channels are required for human T lymphocyte activation.* Journal of Experimental Medicine, 1984. **160**(2): p. 369-385.
92. Chiang, E.Y., et al., *Potassium channels Kv1. 3 and KCa3. 1 cooperatively and compensatorily regulate antigen-specific memory T cell functions.* Nature communications, 2017. **8**(1): p. 14644.
93. Tajti, G., et al., *The voltage-gated potassium channel KV1. 3 as a therapeutic target for venom-derived peptides.* Biochemical pharmacology, 2020. **181**: p. 114146.
94. Tarcha, E.J., et al., *Durable pharmacological responses from the peptide ShK-186, a specific Kv1. 3 channel inhibitor that suppresses T cell mediators of autoimmune disease.* The Journal of pharmacology and experimental therapeutics, 2012. **342**(3): p. 642-653.
95. Aiyar, J., et al., *Topology of the pore-region of a K+ channel revealed by the NMR-derived structures of scorpion toxins.* Neuron, 1995. **15**(5): p. 1169-1181.
96. Zhao, Y., et al., *Diverse structural features of potassium channels characterized by scorpion toxins as molecular probes.* Molecules, 2019. **24**(11): p. 2045.
97. Visan, V., et al., *Mapping of maurotoxin binding sites on hKv1. 2, hKv1. 3, and hIKCa1 channels.* Molecular pharmacology, 2004. **66**(5): p. 1103-1112.
98. Yi, H., et al., *Molecular basis of inhibitory peptide maurotoxin recognizing Kv1. 2 channel explored by ZDOCK and molecular dynamic simulations.* Proteins: structure, function, and bioinformatics, 2008. **70**(3): p. 844-854.
99. Wang, X., et al., *Mesomartoxin, a new Kv1. 2-selective scorpion toxin interacting with the channel selectivity filter.* Biochemical pharmacology, 2015. **93**(2): p. 232-239.
100. Brew, H.M., et al., *Seizures and reduced life span in mice lacking the potassium channel subunit Kv1. 2, but hypoexcitability and enlarged Kv1 currents in auditory neurons.* Journal of neurophysiology, 2007. **98**(3): p. 1501-1525.
101. Xie, G., et al., *A new Kv1. 2 channelopathy underlying cerebellar ataxia.* Journal of Biological Chemistry, 2010. **285**(42): p. 32160-32173.
102. Pena, S. and R. Coimbra, *Ataxia and myoclonic epilepsy due to a heterozygous new mutation in KCNA2: proposal for a new channelopathy.* Clinical genetics, 2015. **87**(2): p. e1-e3.
103. Nilsson, M., et al., *An epilepsy-associated KV1. 2 charge-transfer-center mutation impairs KV1. 2 and KV1. 4 trafficking.* Proceedings of the National Academy of Sciences, 2022. **119**(17): p. e2113675119.
104. Pantazis, A., et al., *Tracking the motion of the KV1. 2 voltage sensor reveals the molecular perturbations caused by a de novo mutation in a case of epilepsy.* The Journal of physiology, 2020. **598**(22): p. 5245-5269.
105. Mínguez-Viñas, T., et al., *Two epilepsy-associated variants in KCNA2 (KV1. 2) at position H310 oppositely affect channel functional expression.* The Journal of Physiology, 2023. **601**(23): p. 5367-5389.

106. Schwarz, N., et al., *Generation of an induced pluripotent stem cell (iPSC) line from a patient with developmental and epileptic encephalopathy carrying a KCNA2 (p. Leu328Val) mutation.* Stem Cell Research, 2018. **33**: p. 6-9.
107. Gong, P., et al., *Genotype and phenotype of children with KCNA2 gene related developmental and epileptic encephalopathy.* Zhonghua er ke za zhi= Chinese Journal of Pediatrics, 2020. **58**(1): p. 35-40.
108. Uysal, B., et al., *Generation of an induced pluripotent stem cell (iPSC) line (HIHDNEi003-A) from a patient with developmental and epileptic encephalopathy carrying a KCNA2 (p. Thr374Ala) mutation.* Stem Cell Research, 2019. **40**: p. 101543.
109. Hedrich, U.B., et al., *4-Aminopyridine is a promising treatment option for patients with gain-of-function KCNA2-encephalopathy.* Science translational medicine, 2021. **13**(609): p. eaaz4957.
110. Armstrong, C.M. and A. Loboda, *A model for 4-aminopyridine action on K channels: similarities to tetraethylammonium ion action.* Biophysical journal, 2001. **81**(2): p. 895-904.
111. Strupp, M., et al., *A randomized trial of 4-aminopyridine in EA2 and related familial episodic ataxias.* Neurology, 2011. **77**(3): p. 269-275.
112. Giordano, I., et al., *Experience in a short-term trial with 4-aminopyridine in cerebellar ataxia.* Journal of neurology, 2013. **260**: p. 2175-2176.
113. Kalla, R. and M. Strupp, *Aminopyridines and acetyl-DL-leucine: new therapies in cerebellar disorders.* Current neuropharmacology, 2019. **17**(1): p. 7-13.
114. Khammy, M.M., et al., *4-Aminopyridine: a pan voltage-gated potassium channel inhibitor that enhances Kv7. 4 currents and inhibits noradrenaline-mediated contraction of rat mesenteric small arteries.* British journal of pharmacology, 2018. **175**(3): p. 501-516.
115. Kerr, P.M., et al., *Heteromultimeric Kv1. 2-Kv1. 5 channels underlie 4-aminopyridine-sensitive delayed rectifier K+ current of rabbit vascular myocytes.* Circulation research, 2001. **89**(11): p. 1038-1044.
116. Kuzmenkov, A., E. Grishin, and A. Vassilevski, *Diversity of potassium channel ligands: focus on scorpion toxins.* Biochemistry (Moscow), 2015. **80**: p. 1764-1799.
117. Kim, J.-B., *Channelopathies.* Korean journal of pediatrics, 2014. **57**(1): p. 1.
118. Chandy, K.G., et al., *K+ channels as targets for specific immunomodulation.* Trends in pharmacological sciences, 2004. **25**(5): p. 280-289.
119. Russell, S.N., et al., *Block by 4-aminopyridine of a Kv1. 2 delayed rectifier K+ current expressed in Xenopus oocytes.* The Journal of Physiology, 1994. **481**(3): p. 571-584.
120. Ignatova, A.A., et al., *New High-Affinity Peptide Ligands for Kv1. 2 Channel: Selective Blockers and Fluorescent Probes.* Cells, 2024. **13**(24): p. 2096.
121. Carbone, E., et al., *Selective blockage of voltage-dependent K+ channels by a novel scorpion toxin.* Nature, 1982. **296**(5852): p. 90-91.
122. Miller, C., et al., *Charybdotoxin, a protein inhibitor of single Ca2+-activated K+ channels from mammalian skeletal muscle.* Nature, 1985. **313**(6000): p. 316-318.
123. Garcia-Calvo, M., et al., *Purification, characterization, and biosynthesis of margatoxin, a component of Centruroides margaritatus venom that selectively inhibits voltage-dependent potassium channels.* Journal of Biological Chemistry, 1993. **268**(25): p. 18866-18874.
124. Goldstein, S. and C. Miller, *Mechanism of charybdotoxin block of a voltage-gated K+ channel.* Biophysical journal, 1993. **65**(4): p. 1613-1619.
125. Qiu, S., et al., *Molecular Information of charybdotoxin blockade in the large conductance calcium-activated potassium channel.* Journal of chemical information and modeling, 2009. **49**(7): p. 1831-1838.

126. Bartok, A., et al., *Margatoxin is a non-selective inhibitor of human Kv1. 3 K+ channels.* Toxicon, 2014. **87**: p. 6-16.
127. Tabakmakher, V.M., et al., *Kalium 2.0, a comprehensive database of polypeptide ligands of potassium channels.* Scientific data, 2019. **6**(1): p. 73.
128. Chen, Z.-Y., et al., *Structural and functional diversity of acidic scorpion potassium channel toxins.* PloS one, 2012. **7**(4): p. e35154.
129. Krylov, N.A., et al., *Kalium 3.0 is a comprehensive depository of natural, artificial, and labeled polypeptides acting on potassium channels.* Protein Science, 2023. **32**(11): p. e4776.
130. Tytgat, J., et al., *A unified nomenclature for short-chain peptides isolated from scorpion venoms: α-KTx molecular subfamilies.* Trends in pharmacological sciences, 1999. **20**(11): p. 444-447.
131. de la Vega, R.C.R.g. and L.D. Possani, *Current views on scorpion toxins specific for K+-channels.* Toxicon, 2004. **43**(8): p. 865-875.
132. Banerjee, A., et al., *Structure of a pore-blocking toxin in complex with a eukaryotic voltage-dependent K+ channel.* Elife, 2013. **2**: p. e00594.
133. Swartz, K.J., *Tarantula toxins interacting with voltage sensors in potassium channels.* Toxicon, 2007. **49**(2): p. 213-230.
134. Swartz, K.J. and R. MacKinnon, *Hanatoxin modifies the gating of a voltage-dependent K+ channel through multiple binding sites.* Neuron, 1997. **18**(4): p. 665-673.
135. Goudet, C., C.-W. Chi, and J. Tytgat, *An overview of toxins and genes from the venom of the Asian scorpion Buthus martensi Karsch.* Toxicon, 2002. **40**(9): p. 1239-1258.
136. Panyi, G., et al., *K+ channel blockers: novel tools to inhibit T cell activation leading to specific immunosuppression.* Current pharmaceutical design, 2006. **12**(18): p. 2199-2220.
137. Dauplais, M., et al., *On the convergent evolution of animal toxins: conservation of a diad of functional residues in potassium channel-blocking toxins with unrelated structures.* Journal of Biological Chemistry, 1997. **272**(7): p. 4302-4309.
138. Song, J., et al., *NMR solution structure of a two-disulfide derivative of charybdotoxin: structural evidence for conservation of scorpion toxin α/β motif and its hydrophobic side chain packing.* Biochemistry, 1997. **36**(13): p. 3760-3766.
139. Jouirou, B., et al., *Toxin determinants required for interaction with voltage-gated K+ channels.* Toxicon, 2004. **43**(8): p. 909-914.
140. M'Barek, S., et al., *Synthesis and characterization of Pi4, a scorpion toxin from Pandinus imperator that acts on K+ channels.* European journal of biochemistry, 2003. **270**(17): p. 3583-3592.
141. LEBRUN, B., et al., *A four-disulphide-bridged toxin, with high affinity towards voltage-gated K+ channels, isolated from Heterometrus spinnifer (Scorpionidae) venom.* Biochemical journal, 1997. **328**(1): p. 321-327.
142. Naseem, M.U., et al., *Cm28, a scorpion toxin having a unique primary structure, inhibits KV1. 2 and KV1. 3 with high affinity.* Journal of General Physiology, 2022. **154**(8).
143. Zhu, L., et al., *Two dyad-free Shaker-type K+ channel blockers from scorpion venom.* Toxicon, 2012. **59**(3): p. 402-407.
144. Chandy, K.G. and R.S. Norton, *Peptide blockers of Kv1. 3 channels in T cells as therapeutics for autoimmune disease.* Current opinion in chemical biology, 2017. **38**: p. 97-107.
145. Varga, Z., et al., *Vm24, a natural immunosuppressive peptide, potently and selectively blocks Kv1. 3 potassium channels of human T cells.* Molecular pharmacology, 2012. **82**(3): p. 372-382.

146. Tarcha, E.J., et al., *Safety and pharmacodynamics of dalazatide, a Kv1. 3 channel inhibitor, in the treatment of plaque psoriasis: A randomized phase 1b trial.* PloS one, 2017. **12**(7): p. e0180762.
147. Guijarro, J.I., et al., *Solution structure of Pi4, a short four-disulfide-bridged scorpion toxin specific of potassium channels.* Protein science, 2003. **12**(9): p. 1844-1854.
148. Xia, Z., et al., *Scorpion venom peptides: Molecular diversity, structural characteristics, and therapeutic use from channelopathies to viral infections and cancers.* Pharmacological Research, 2023. **197**: p. 106978.
149. Sunagar, K., et al., *Evolution stings: the origin and diversification of scorpion toxin peptide scaffolds.* Toxins, 2013. **5**(12): p. 2456-2487.
150. Restano-Cassulini, R., et al., *Characterization of Sodium Channel Peptides Obtained from the Venom of the Scorpion Centruroides bonito.* Toxins, 2024. **16**(3): p. 125.
151. Shakeel, K., et al., *Of Seven New K+ Channel Inhibitor Peptides of Centruroides Bonito, α-KTx 2.24 Has a Picomolar Affinity for Kv1. 2.* Toxins, 2023. **15**(8): p. 506.
152. Riaño-Umbarila, L., et al., *Toxic Peptides from the Mexican Scorpion Centruroides villegasi: Chemical Structure and Evaluation of Recognition by Human Single-Chain Antibodies.* Toxins, 2024. **16**(7): p. 301.
153. Merrifield, R.B., *Solid phase peptide synthesis. I. The synthesis of a tetrapeptide.* Journal of the American Chemical Society, 1963. **85**(14): p. 2149-2154.
154. Naseem, M.U., et al., *Characterization and chemical synthesis of Cm39 (α-KTx 4.8): a scorpion toxin that inhibits voltage-gated K+ channel KV1. 2 and small-and intermediate-conductance Ca2+-Activated K+ channels KCa2. 2 and KCa3. 1.* Toxins, 2023. **15**(1): p. 41.
155. Abramson, J., et al., *Accurate structure prediction of biomolecular interactions with AlphaFold 3.* Nature, 2024. **630**(8016): p. 493-500.
156. Voros, O., et al., *The C-terminal HRET sequence of Kv1. 3 regulates gating rather than targeting of Kv1. 3 to the plasma membrane.* Scientific Reports, 2018. **8**(1): p. 5937.
157. Hamill, O.P., et al., *Improved patch-clamp techniques for high-resolution current recording from cells and cell-free membrane patches.* Pflügers Archiv, 1981. **391**: p. 85-100.
158. Naseem, M.U., et al., *Optimization of Pichia pastoris expression system for high-level production of margatoxin.* Frontiers in pharmacology, 2021. **12**: p. 733610.
159. Zhao, R., et al., *Selective block of human Kv1. 1 channels and an epilepsy-associated gain-of-function mutation by AETX-K peptide.* The FASEB Journal, 2024. **38**(1): p. e23381.
160. González-Santillán, E. and L.D. Possani, *North American scorpion species of public health importance with a reappraisal of historical epidemiology.* Acta tropica, 2018. **187**: p. 264-274.
161. Papp, F., et al., *Tst26, a novel peptide blocker of Kv1. 2 and Kv1. 3 channels from the venom of Tityus stigmurus.* Toxicon, 2009. **54**(4): p. 379-389.
162. Olamendi-Portugal, T., et al., *Novel α-KTx peptides from the venom of the scorpion Centruroides elegans selectively blockade Kv1. 3 over IKCa1 K+ channels of T cells.* Toxicon, 2005. **46**(4): p. 418-429.
163. Baldazo-Monsivaiz, J.G., J. Ponce-Saavedra, and M. Flores-Moreno, *Una especie nueva de alacrán del género Centruroides de importancia médica (Scorpiones: Buthidae) del estado de Guerrero, México.* Revista mexicana de biodiversidad, 2013. **84**(1): p. 100-116.
164. Riaño-Umbarila, L., et al., *Updating knowledge on new medically important scorpion species in Mexico.* Toxicon, 2017. **138**: p. 130-137.

165. Olamendi-Portugal, T., et al., *Isolation, chemical and functional characterization of several new K+-channel blocking peptides from the venom of the scorpion Centruroides tecomanus.* Toxicon, 2016. **115**: p. 1-12.
166. Marinkelle, C. and H. Stahnke, *Toxicological and clinical studies on Centruroides margaritatus (Gervais), a common scorpion in western Colombia.* Journal of medical entomology, 1965. **2**(2): p. 197-199.
167. Beltrán-Vidal, J., et al., *Colombian scorpion Centruroides margaritatus: Purification and characterization of a gamma potassium toxin with full-block activity on the hERG1 channel.* Toxins, 2021. **13**(6): p. 407.
168. Rodrigues, A.R.A., et al., *Tityustoxin-K (alpha) blockade of the voltage-gated potassium channel Kv1. 3.* British journal of pharmacology, 2003. **139**(6): p. 1180-1186.
169. D'Suze, G., et al., *A novel K+ channel blocking toxin from Tityus discrepans scorpion venom.* FEBS letters, 1999. **456**(1): p. 146-148.
170. Batista, C.V., et al., *Two novel toxins from the Amazonian scorpion Tityus cambridgei that block Kv1. 3 and Shaker B K+-channels with distinctly different affinities.* Biochimica et Biophysica Acta (BBA)-Proteins and Proteomics, 2002. **1601**(2): p. 123-131.
171. Ravell, A.F.Q., R. Teruel, and J.P. Saavedra, *A new Centruroides Marx, 1890 (Scorpiones: Buthidae), from southern Guerrero State, Mexico.* Revista ibérica de aracnología, 2016(28): p. 25-34.
172. Selisko, B., et al., *Cobatoxins 1 and 2 from Centruroides noxius Hoffmann constitute a subfamily of potassium-channel-blocking scorpion toxins.* European journal of biochemistry, 1998. **254**(3): p. 468-479.
173. Jouirou, B., et al., *Cobatoxin 1 from Centruroides noxius scorpion venom: chemical synthesis, three-dimensional structure in solution, pharmacology and docking on K+ channels.* Biochem J, 2004. **377**(Pt 1): p. 37-49.
174. Stocker, M. and C. Miller, *Electrostatic distance geometry in a K+ channel vestibule.* Proceedings of the National Academy of Sciences, 1994. **91**(20): p. 9509-9513.
175. Borrego, J., et al., *Recombinant expression in Pichia pastoris system of three potent Kv1. 3 channel blockers: Vm24, Anuroctoxin, and Ts6.* Journal of Fungi, 2022. **8**(11): p. 1215.
176. Bartok, A., et al., *An engineered scorpion toxin analogue with improved Kv1. 3 selectivity displays reduced conformational flexibility.* Scientific reports, 2015. **5**(1): p. 18397.
177. Wai, D.C., et al., *A Fluorescent Peptide Toxin for Selective Visualization of the Voltage-Gated Potassium Channel Kv1. 3.* Bioconjugate Chemistry, 2022. **33**(11): p. 2197-2212.
178. Mouhat, S., M. De Waard, and J.M. Sabatier, *Contribution of the functional dyad of animal toxins acting on voltage-gated Kv1-type channels.* Journal of peptide science: an official publication of the European Peptide Society, 2005. **11**(2): p. 65-68.
179. Martin, B., et al., *Novel K+-channel-blocking toxins from the venom of the scorpion Centruroides limpidus limpidus Karsch.* Biochemical Journal, 1994. **304**(1): p. 51-56.
180. Valdez-Velázquez, L.L., et al., *Mass fingerprinting of the venom and transcriptome of venom gland of scorpion Centruroides tecomanus.* PloS one, 2013. **8**(6): p. e66486.
181. Selvakumar, P., et al., *Structures of the T cell potassium channel Kv1. 3 with immunoglobulin modulators.* Nature Communications, 2022. **13**(1): p. 3854.
182. Koschak, A., et al., *Subunit Composition of Brain Voltage-gated Potassium Channels Determined by Hongotoxin-1, a Novel Peptide Derived fromCentruroides limbatus Venom.* Journal of Biological Chemistry, 1998. **273**(5): p. 2639-2644.

183. Fajloun, Z., et al., *Chemical synthesis and characterization of Pi1, a scorpion toxin from Pandinus imperator active on K+ channels.* European journal of biochemistry, 2000. **267**(16): p. 5149-5155.
184. Mouhat, S., et al., *The functional dyad of scorpion toxin Pi1 is not itself a prerequisite for toxin binding to the voltage-gated Kv1. 2 potassium channels.* Biochemical Journal, 2004. **377**(1): p. 25-36.
185. Castle, N., et al., *Maurotoxin: a potent inhibitor of intermediate conductance Ca2+-activated potassium channels.* Molecular pharmacology, 2003. **63**(2): p. 409-418.
186. Kharrat, R., et al., *Maurotoxin, a four disulfide bridge toxin from Scorpio maurus venom: purification, structure and action on potassium channels.* FEBS letters, 1997. **406**(3): p. 284-290.
187. Choe, S., A. Kreusch, and P.J. Pfaffinger, *Towards the three-dimensional structure of voltage-gated potassium channels.* Trends in biochemical sciences, 1999. **24**(9): p. 345-349.
188. Chen, X., et al., *Structure of the full-length Shaker potassium channel Kv1. 2 by normal-mode-based X-ray crystallographic refinement.* Proceedings of the National Academy of Sciences, 2010. **107**(25): p. 11352-11357.
189. Lange, A., et al., *Toxin-induced conformational changes in a potassium channel revealed by solid-state NMR.* Nature, 2006. **440**(7086): p. 959-962.
190. Possani, L.D., B. Selisko, and G.B. Gurrola, *Structure and function of scorpion toxins affecting K+-channels.* Perspectives in drug discovery and design, 1999. **15**: p. 15-40.
191. Luna-Ramírez, K., et al., *Structure, molecular modeling, and function of the novel potassium channel blocker urotoxin isolated from the venom of the Australian scorpion Urodacus yaschenkoi.* Molecular pharmacology, 2014. **86**(1): p. 28-41.
192. Corbett, M.A., et al., *Dominant KCNA2 mutation causes episodic ataxia and pharmacoresponsive epilepsy.* Neurology, 2016. **87**(19): p. 1975-1984.
193. Stühmer, W., et al., *Molecular basis of functional diversity of voltage-gated potassium channels in mammalian brain.* The EMBO journal, 1989. **8**(11): p. 3235-3244.
194. Pandit, R., L. Chen, and J. Götz, *The blood-brain barrier: Physiology and strategies for drug delivery.* Advanced drug delivery reviews, 2020. **165**: p. 1-14.
195. Demeule, M., et al., *Identification and design of peptides as a new drug delivery system for the brain.* The Journal of pharmacology and experimental therapeutics, 2008. **324**(3): p. 1064-1072.
196. Oller-Salvia, B., et al., *Blood–brain barrier shuttle peptides: an emerging paradigm for brain delivery.* Chemical Society Reviews, 2016. **45**(17): p. 4690-4707.
197. Adessi, C. and C. Soto, *Strategies to improve stability and bioavailability of peptide drugs.* Frontiers in Medicinal Chemistry-Online, 2004. **1**(1): p. 513-528.
198. Craik, D.J., et al., *The future of peptide-based drugs.* Chemical biology & drug design, 2013. **81**(1): p. 136-147.
199. Fosgerau, K. and T. Hoffmann, *Peptide therapeutics: current status and future directions.* Drug discovery today, 2015. **20**(1): p. 122-128.
200. Diao, L. and B. Meibohm, *Pharmacokinetics and pharmacokinetic–pharmacodynamic correlations of therapeutic peptides.* Clinical pharmacokinetics, 2013. **52**: p. 855-868.
201. Wang, L., et al., *Therapeutic peptides: current applications and future directions.* Signal transduction and targeted therapy, 2022. **7**(1): p. 48.
202. Richards, K.L., et al., *Selective NaV1. 1 activation rescues Dravet syndrome mice from seizures and premature death.* Proceedings of the National Academy of Sciences, 2018. **115**(34): p. E8077-E8085.

203. Olivera, B.M., et al., *Neuronal calcium channel antagonists. Discrimination between calcium channel subtypes using. omega.-conotoxin from Conus magus venom.* Biochemistry, 1987. **26**(8): p. 2086-2090.
204. Williams, J.A., M. Day, and J.E. Heavner, *Ziconotide: an update and review.* Expert opinion on pharmacotherapy, 2008. **9**(9): p. 1575-1583.
205. McGivern, J.G., *Ziconotide: a review of its pharmacology and use in the treatment of pain.* Neuropsychiatric disease and treatment, 2007. **3**(1): p. 69-85.
206. Lin, J., Z. Yu, and X. Gao, *Advanced Noninvasive Strategies for the Brain Delivery of Therapeutic Proteins and Peptides.* ACS nano, 2024. **18**(34): p. 22752-22779.
207. Zou, L., et al., *Progress in research and application of HIV-1 TAT-derived cell-penetrating peptide.* The Journal of membrane biology, 2017. **250**: p. 115-122.
208. Singh, C.S., et al., *Discovery of a highly conserved peptide in the iron transporter melanotransferrin that traverses an intact blood brain barrier and localizes in neural cells.* Frontiers in neuroscience, 2021. **15**: p. 596976.
209. Ji, X., et al., *Recombinant expressing angiopep-2 fused anti-VEGF single chain Fab (scFab) could cross blood–brain barrier and target glioma.* AMB Express, 2019. **9**: p. 1-12.
210. Yu, S., et al., *TAT-modified ω-conotoxin MVIIA for crossing the blood-brain barrier.* Marine Drugs, 2019. **17**(5): p. 286.

9. KEY WORDS

Voltage-gated potassium channel

Kv1.2

Kv1.2-related gain of function mutations

Scorpion toxins

CboK toxins

Cvill toxins

sCm39

Patch-clamp electrophysiology

10. ACKNOWLEDGEMENT

Read! And your Lord is the Most Generous, who has taught by the pen. Has taught man that which he knew not. (96:3-5)

All praise and gratitude to Allah Almighty, who has blessed me with clarity of mind and strength. to complete my PhD dissertation.

I am deeply grateful to my supervisor, Prof. Dr. György Panyi, for his support throughout the four years of my doctoral studies. I sincerely appreciate the time, expertise, and guidance he invested in this scientific work. I am especially thankful for the opportunities he provided and the skills I gained in his lab.

My heartfelt thanks go to all the kind and collaborative colleagues in our lab. Special thanks to Dr. Muhammad Umair Naseem and Dr. Szántó Tibor for his guidance in learning patch-clamp electrophysiology and to Dr. Jesus Borrego for his helpful discussions and support. I am also grateful to our amazing technical lab assistants Cecilia Nagy, Adrienn Bagosi, and Amna Sami, for their dedicated efforts in maintaining a productive and well-organized laboratory environment.

I would like to express my sincere thanks to our collaborators at UNAM, Mexico, Prof. Lourival D. Possani and his laboratory members, for providing us with peptide toxins.

I am grateful to my colleagues and friends Gabriela Serrano and Ghofrane Medyouni for their emotional support and companionship during the challenging phases of my PhD.

My deepest appreciation goes to my beloved husband, whose unwavering support and belief in me have been my greatest strength, and to my precious daughter, who has filled my life with purpose and joy. All my accomplishments are dedicated to my parents, whose love, encouragement, and sacrifices shaped me into the woman I am today.

In the end I would like to thank *Richter Gedeon Talentum Foundation* for supporting my PhD. My PhD has also been supported by Project no. 2024-1.2.3-HU-RIZONT-2024-00099 has been implemented with the support provided by the Ministry of Culture and Innovation of Hungary from the National Research, Development and Innovation Fund, financed under the 2024-1.2.3-HU-RIZONT funding scheme.

11. APPENDIX

UNIVERSITY AND NATIONAL LIBRARY
UNIVERSITY OF DEBRECEN
H-4002 Egyetem tér 1, Debrecen
Phone: +3652/410-443, email: publikaciok@lib.unideb.hu

Registry number: DEENK/306/2025.PL
Subject: PhD Publication List

Candidate: Kashmala Shakeel
Doctoral School: Doctoral School of Molecular Medicine

List of publications related to the dissertation

1. Naseem, M. U., Gurrola-Briones, G., Romero-Imbachi, M. R., Borrego, J., Carcamo-Noriega, E., Beltrán-Vidal, J., Zamudio, F. Z., **Shakeel, K.**, Possani, L. D., Panyi, G.: Characterization and Chemical Synthesis of Cm39 (α-KTx 4.8): a Scorpion Toxin That Inhibits Voltage-Gated K+ Channel KV1.2 and Small- and Intermediate-Conductance Ca2+-Activated K+ Channels KCa2.2 and KCa3.1.
   Toxins. 15 (1), 1-21, 2023.
   DOI: http://dx.doi.org/10.3390/toxins15010041
   IF: 3.9

2. **Shakeel, K.**, Olamendi-Portugal, T., Naseem, M. U., Becerril, B., Zamudio, F. Z., Delgado-Prudencio, G., Possani, L. D., Panyi, G.: Of Seven New K^+ Channel Inhibitor Peptides of Centruroides bonito, α-KTx 2.24 Has a Picomolar Affinity for Kv1.2.
   Toxins. 15 (8), 1-20, 2023.
   DOI: http://dx.doi.org/10.3390/toxins15080506
   IF: 3.9

List of other publications

3. Sanches, K., Ashwood, L. M., Olushola-Siedoks, A. A. M., Wai, D. C. C., Rahman, A., **Shakeel, K.**, Naseem, M. U., Panyi, G., Prentis, P., Norton, R. S.: Structure-function relationships in domain peptides: from the sea anemone.
   Proteins. 92 (2), 192-205, 2024.
   DOI: http://dx.doi.org/10.1002/prot.26594
   IF: 3.2 (2023)

UNIVERSITY AND NATIONAL LIBRARY
UNIVERSITY OF DEBRECEN
H-4002 Egyetem tér 1, Debrecen
Phone: +3652/410-443, email: publikaciok@lib.unideb.hu

4. Borrego, J., Naseem, M. U., Sehgal, A. N. A., Panda, L. R., **Shakeel, K.**, Gáspár, A., Nagy, C., Varga, Z., Panyi, G.: Recombinant Expression in Pichia pastoris System of Three Potent Kv1.3 Channel Blockers: Vm24, Anuroctoxin, and Ts6.
J. Fungi. 8 (11), 1-15, 2022.
DOI: http://dx.doi.org/10.3390/jof8111215
IF: 4.7

Total IF of journals (all publications): 15,7
Total IF of journals (publications related to the dissertation): 7,8

The Candidate's publication data submitted to the Tudóstér have been validated by DEENK on the basis of the Journal Citation Report (Impact Factor) database.

22 May, 2025

DEBRECENI EGYETEM
Egyetemi és Nemzeti Könyvtár